Piperazine-based pyrido[1,2-*a*]benzimidazoles: synthesis and pharmacological evaluation as potential antimalarial and antischistosomal agents

Dissertation Presented for the Degree of

Master of Science

In the Department of Chemistry

University of Cape Town

by

Consolata Nsanzimpaka Nsanzubuhoro

Supervisor: Prof. Kelly Chibale

Department of Chemistry

University of Cape Town

Rondebosch, 7700

Cape Town

South Africa

November 2018

DECLARATION

I declare that the project titled: ***Piperazine-based pyrido[1,2-a]benzimidazoles: synthesis and pharmacological evaluation as potential antimalarial and antischistosomal agents*** is my original work and has not been presented for the award of any degree at any university. I know the meaning of plagiarism and declare that the work in this dissertation, except for that which is properly acknowledged, is my own.

Signed by candidate

.....

Consolata Nsanzimpaka Nsanzubuhoro

November 2018

ACKNOWLEDGEMENTS

I would like to thank my supervisor, Professor Kelly Chibale, who steered me in the right direction when I needed it. I appreciate the opportunity, the guidance and the advice throughout my years of study and research.

I would like to also thank everyone who was involved in the various assays that were conducted in this research project including the administrative staff whose great work ethic and diligence contributed to the completion of this work. I am grateful to the members of Kelly Chibale's research group, especially Godfrey Mayoka, for his mentorship and invaluable support on this project.

I must express my very profound gratitude to my family: my parents, Emmanuel and Martha; my twin sister, Christa; and my brothers, René and Rémy, for their unwavering support and continuous encouragement throughout my journey. This accomplishment would not have been possible without them.

Above all, thanks be to God for protecting me and providing me with the strength that I needed to overcome the challenges that I was faced with to see this project to completion.

CONFERENCES

1. **Gordon Research Seminar (GRS) and Gordon Research Conference (GRC)**: Biology of Host-Parasite Interactions held on 09 – 10 June and 10 - 15 June 2018, respectively, at Salve Regina University in Newport, Rhode Island, United States. Poster presentation entitled: *Potency and Physicochemical Optimisation of Piperazine-based Antimalarial 3-trifluoromethyl Pyrido [1,2-a] benzimidazole derivatives.*

2. **4th Malaria Research Conference** held on 30 July - 01 August 2018, in Johannesburg, South Africa. Poster presentation entitled: *Potency and Physicochemical Optimisation of Piperazine-based Antimalarial 3-trifluoromethyl Pyrido [1,2-a] benzimidazole derivatives.*

ABSTRACT

The emergence and spread of parasites resistant to first-line antimalarial drugs comprising artemisinin combination therapies (ACTs) threaten malaria control. There is therefore a need to develop novel and chemically diverse alternatives that are safe, efficacious, and able to circumvent drug resistance.

Schistosomiasis is the second most prevalent tropical disease in the world after malaria, and treatment relies on a single drug: praziquantel. Although praziquantel shows multiple benefits over drugs previously used to treat schistosomiasis, dependence on it will result in therapeutic limitations and drug resistance threats. Therefore, there is a dire need to develop novel antischistosomal drugs that are effective and affordable.

One attractive approach to accelerate the drug discovery and development process is the exploration of current drugs and drug leads as probable therapies for other diseases. This strategy is known as drug repurposing or drug repositioning, of which the latter is applied in this research project. The cytological similarities in the degradation of haemoglobin performed by *Plasmodium* parasites and *Schistosoma* blood flukes in malaria and schistosomiasis, respectively, suggest an opportunity for the repositioning of antimalarial scaffolds as antischistosomal agents.

Pyrido[1,2-*a*]benzimidazoles (PBIs) demonstrate various biological and pharmacological properties such as anti-inflammatory, analgesic, antimicrobial, antiviral, and antineoplastic activities. More recently, PBI derivatives showed favourable *in vitro* activities against both *Plasmodium falciparum* and adult *Schistosoma mansoni,* but modest i*n vivo* potencies. Pharmacokinetic analysis suggests that the sub-optimal *in vivo* efficacy of PBIs is related to solubility-limited absorption and poor metabolic stability. With the aim of circumventing these challenges, structural modifications have been employed to explore structure-activity and structure-property relationships to produce target compounds with improved drug-likeness (**Figure A**).

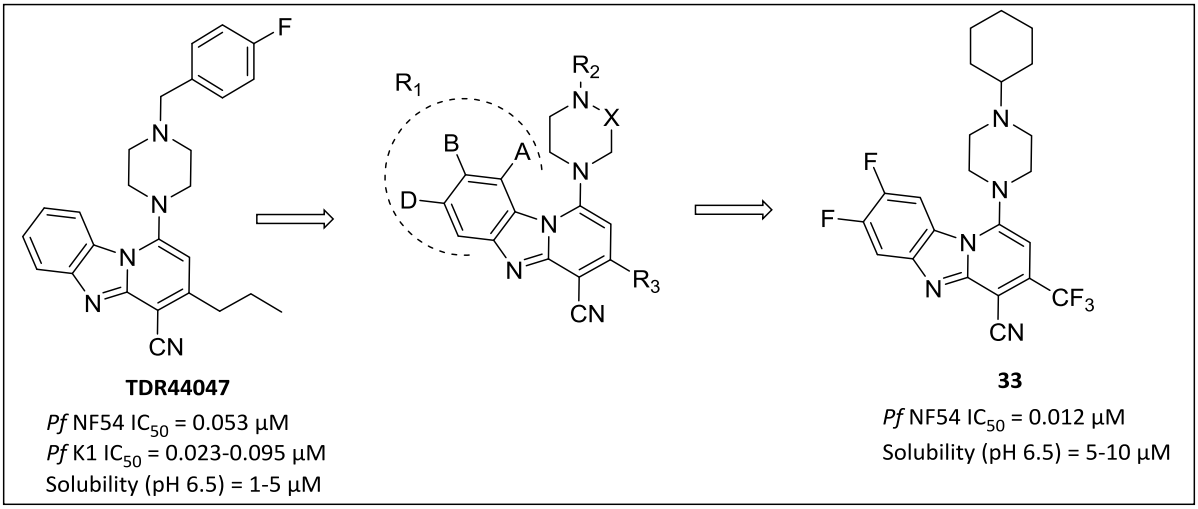

TDR44047
Pf NF54 IC_{50} = 0.053 µM
Pf K1 IC_{50} = 0.023-0.095 µM
Solubility (pH 6.5) = 1-5 µM

33
Pf NF54 IC_{50} = 0.012 µM
Solubility (pH 6.5) = 5-10 µM

Figure A: Structure-activity explorations around lead compound **TDR44047**, resulting in compound **33**, which showed improved solubility and antiplasmodium activity against *Plasmodium falciparum (Pf)* NF54

This study aimed to expand the SAR by performing chemical modifications on the PBI scaffold with the purpose of maintaining or improving biological activity, and to address solubility-limited absorption challenges with this series of compounds (**Figure A**). The synthesized derivatives were tested against the chloroquine-sensitive (NF54) strain of *P. falciparum* and against adult *S. mansoni* concurrently. The most active compound in this PBI series, a di-fluoro-substituted derivative composed of a cyclohexyl piperazine side-chain (**33**), showed improved *in vitro* activity against the NF54 strain of *P. falciparum* (IC_{50} = 0.012 µM) and enhanced solubility (**Figure A**). Compounds with methylene or ethylene linkers at the R_1 position (**Figure A**) showed comparable potency, although the directly linked phenyl piperazine analogue showed poor antiplasmodium activity. Compounds containing hydrophobic electron-withdrawing fluoro, chloro, and trifluoromethyl Craig plot substituents at the *para* position of the phenyl group showed enhanced antiplasmodium activity compared to those containing hydrophobic electron-releasing methyl groups and hydrophilic electron-withdrawing cyano groups. In the LHS-unsubstituted series of compounds, regio-isomerism at substituent R_2 (**Figure A**) resulted in comparable antiplasmodium activity, and this observation was maintained with LHS-substituted PBI derivatives. Notably, unsubstituted derivatives and di-substituted groups displayed moderate to high antiplasmodium potency. Mechanistic evaluations of the compounds

revealed non-existent to weak correlations between antiplasmodium activities and their potential to inhibit hemozoin (Hz) formation. This suggests that Hz inhibition is not the sole target of this class of compounds, although it may be a contributory mode of action.

Compounds were also screened at 10 µM against newly transformed schistosomula and adult *S. mansoni*. Two compounds showed high antischistosomal activity against both larval and adult parasites, resulting in > 70% inhibition of worm viability.

A turbidimetric assay was carried out to assess the solubility of target PBI compounds. In most cases, the synthesized compounds displayed high *in vitro* activities and slight improvements in solubility. This therefore encourages further optimization of piperazinyl PBI compounds to improve efficacy and solubility.

TABLE OF CONTENTS

LIST OF ABBREVIATIONS AND SYMBOLS

Å	Angström
ºC	Degrees Celsius
δ	Delta (NMR chemical shift)
µM	Micromolar
ACT	Artemisinin Combination Therapy
APCI	Atmospheric Pressure Chemical Ionization
BHIA	Beta-hematin Inhibition Activity
CL	Clearance
C Log P	Calculated Logarithm of n-octanol/water Partition Coefficient
CHO	Chinese Hamster Ovarian (Cells)
CQ	Chloroquine
DCM	Dichloromethane
DHA	Dihydroartemisinin
DMF	N,N-Dimethylformamide
DMSO	Dimethyl Sulfoxide
DMSO-d_6	Deuterated Dimethyl Sulfoxide
EG	Early Gametocyte
ESI	Electron Spray Ionization
ERG	Electron Releasing Group
Et_3N	Triethylamine
EtOAc	Ethyl Acetate

EWG	Electron Withdrawing Group
F	Bioavailability
FWR	Female Worm Reduction
h	Hour/s
HBA	Hydrogen-bond Acceptor
HBD	Hydrogen-bond Donor
HLM	Human Liver Microsomes
$T_{1/2}$	Half-life
HTS	High-throughput Screening
HPLC	High Performance Liquid Chromatography
Hz	Hemozoin
IC_{50}	Half-maximal Inhibitory Concentration
ip	Intraperitoneal
LG	Late Gametocyte
LHS	Left-Hand Side
MeOH	Methanol
Met. Stab.	Metabolic Stability
mg/kg	Milligram per Kilogram
MLM	Mouse Liver Microsomes
MSD	Mean Survival Days
MMV	Medicines for Malaria Venture
Mwt	Molecular Weight
m/z	Mass-to-Charge ratio
$NaHCO_3$	Sodium Bicarbonate

NMR	Nuclear Magnetic Resonance
NTD	Neglected Tropical Disease
NTS	Newly Transformed Schistosomula
Pf	*Plasmodium falciparum*
PBI	Pyrido[1,2-*a*]benzimidazole
PBS	Phosphate-Buffered Saline
PD	Pharmacodynamic
PK	Pharmacokinetic
p.o.	Per Oral
POC	Proof-of-Concept
$POCl_3$	Phosphorus (V) Oxychloride
R_f	Retardation Factor
RLM	Rat Liver Microsomes
SAR	Structure-Activity Relationship
SEC	Single-Exposure Chemoprotection
SERC	Single-Exposure Radical Cure
SI	Selectivity Index
THF	Tetrahydrofuran
TLC	Thin-Layer Chromatography
TWR	Total Worm Reduction

LIST OF FIGURES

LIST OF TABLES

LIST OF SCHEMES

CHAPTER 1: INTRODUCTION AND LITERATURE REVIEW

1.1 Malaria

1.1.1 Etiology and epidemiology

In 2016, the World Health Organization reported approximately 216 million malaria cases and over 440 000 malaria deaths worldwide.[1] The mosquitoes responsible for malaria in humans are the 40 species of infected female Anopheles mosquitoes, which through a bite, transmit protozoa of the genus, *Plasmodium*.[2] These parasitic protozoans are of the sporozoan sub-class *Coccidia*. They infect red blood cells in humans and survive best in tropical and temperate zones.[2]

The 1907 Nobel Prize winner Charles Louis Alphonse Laveran was the first person to discover the malaria parasite in the blood sample of a malaria infected patient.[2,3] Six years after this discovery, Camillo Golgi, a neurophysiologist 1906 Nobel Prize winner established that two species of malaria parasites existed and hence two forms of the disease.[3,4] In the one form of the disease, patients experienced fever every other day (tertian periodicity) and the other was associated with fever every third day (quartan periodicity). These two forms also produced different numbers of merozoites upon maturity and the fever was as a result of the rupture and release of merozoites into the blood stream of the infected host.[3]

To date, there are five known *plasmodium* species that cause the disease: *P. falciparum, P. vivax, P. ovale*, *P. malariae* and *P. knowlesi.* These species are distributed in various regions, dependent on ecological and behavioural parameters that affect the infected mosquito's ability to transmit the *plasmodium* parasite. *Plasmodium falciparum* is common in the tropical regions of Sub-Saharan Africa, South East Asia, Oceania and certain areas of South America (**Figure 1**). It is responsible for majority of infections and causes the most severe form of malaria.

Plasmodium vivax, another virulent protozoa, is widespread primarily in Asia, America, certain areas of Eastern Europe and North Africa. This species has a broader geographical

distribution compared to *P. falciparum*, because of its ability to withstand low temperatures and high altitudes. Despite this wide geographical distribution, majority of cases occur in Ethiopia, India and Pakistan. *Plasmodium ovale* is found mainly in tropical western and central Africa and islands in the West Pacific. It is similar to *P. vivax* in that it also has a dormant liver stage which can reactivate, resulting in relapse (recurrence of infection from hypnozoites). *Plasmodium malariae* and *P. knowlesi* are found in areas where *P. falciparum* is distributed, however, they are less prevalent.[5]

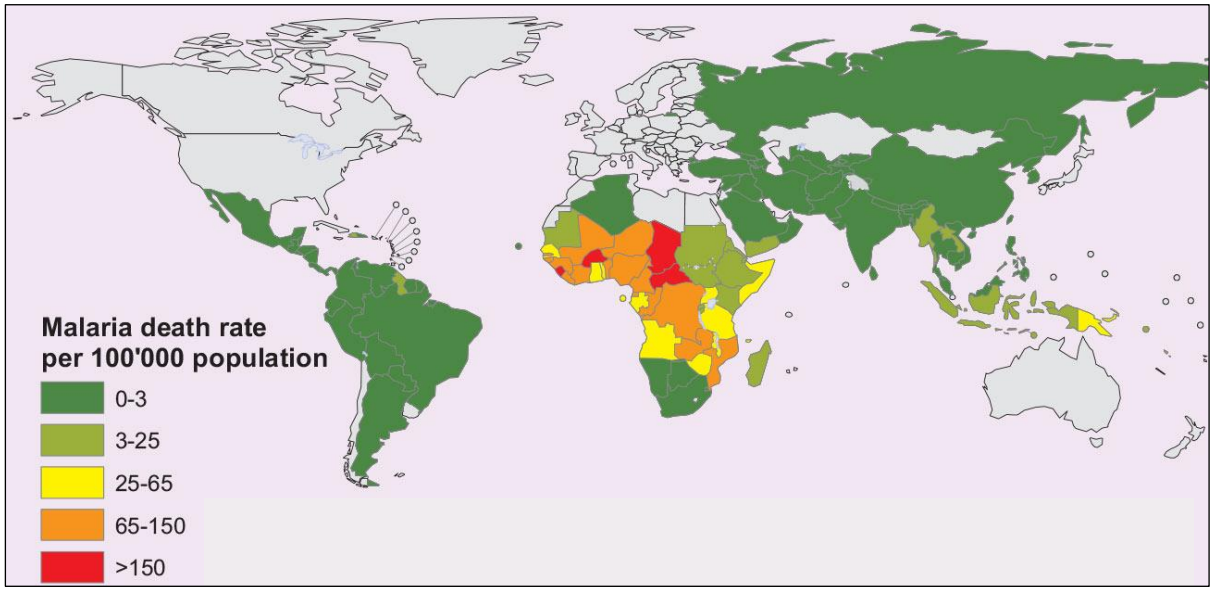

Figure 1: World map showing malaria hotspots[6]

There are several risk factors for infection including: travel to malaria endemic regions; poor malaria chemoprevention measures; settled migrants relocating to their country of origin-where malaria is endemic; low host-immunity individuals (majorly affecting those who live in non-endemic regions) and immunocompromised patients with weakened immune systems. In regions with high malaria transmission rates, pregnant women and young children (especially under the age of 5 years) are the most vulnerable groups.[1,7]

1.1.2 Life cycle and pathogenesis

The malaria transmission cycle involves two types of hosts: humans and female Anopheles mosquitoes. The female Anopheles mosquito acts as a vector and harbors the *plasmodium* parasite, which, via biting a human, injects plasmodial sporozoites, which rapidly make their way to the human host liver and infect hepatocytes.[2] The sporozoites develop into liver

schizonts and further rupture to release thousands of merozoites into the human blood. In the case of *P. vivax* and *P. ovale,* a dormant stage (hypnozoites) may occur in the liver and results in relapses. After replication of the parasite in the liver, asexual multiplication occurs in the erythrocytes and the released merozoites invade red blood cells. The parasite progresses through the ring stage, develops into trophozoites and later mature into schizonts, which burst to release more merozoites, thereby repeating the erythrocytic infection cycle[2,8] (**Figure 2**).

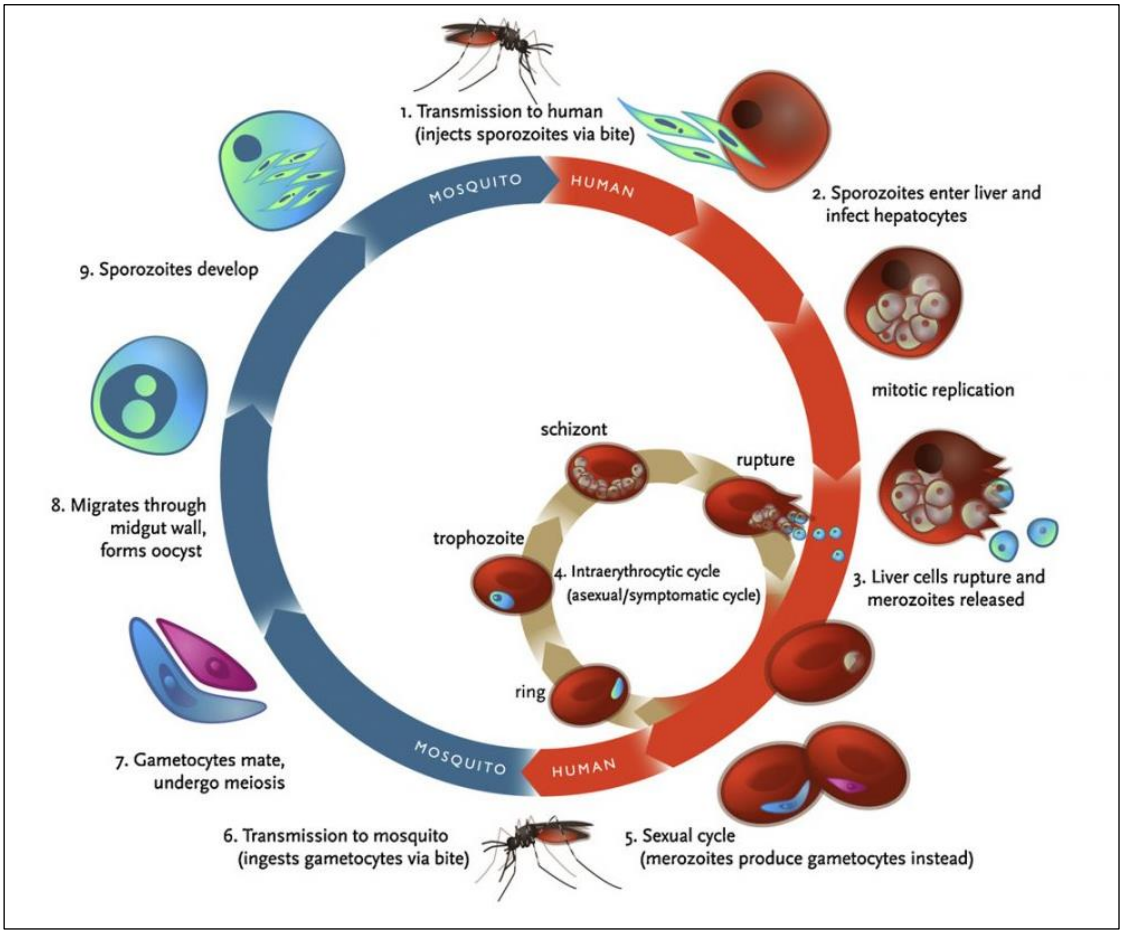

Figure 2: Malaria life cycle of *plasmodium* parasites[9]

The blood stage parasites are responsible for the clinical symptoms of malaria. During the erythrocytic cycle, some parasites differentiate into male microgametocytes and female macrogametocytes (the sexual forms of the parasite). Once taken up by the mosquito, the gametocytes fertilize within the mosquito's gut, undergoes meiosis and then migrates through the midgut wall to form an oocyst, within which sporozoites develop and are inoculated into the human host, continuing the transmission cycle[2,8] (**Figure 2**).

1.1.3 Chemotherapy and challenges in malaria treatment

Malaria is preventable and if contracted, with timely diagnosis, is also curable. The treatment prescribed to a malaria infected patient is usually based on several factors including: the *Plasmodium* parasite species causing the infection; the health status of the patient and severity of the disease; the drug susceptibility of the *Plasmodium* parasite subject to local and regional resistance patterns; and lastly the risk groups, which include children under the age of 5, pregnant women and non-immune travelers.[10,11]

Despite the availability of malaria treatment, there has been the major concern of drug resistance where previously effective antimalarial drugs such as chloroquine and pyrimethamine/sulfadoxine (**Figure 3**) are compromised by the development of drug resistant parasites.[12]

Novel drug regimens such as artemisinin-combination therapies (ACTs) have been remarkably effective in treating malaria forms resistant to the aforementioned drugs.[5] Artemisinin analogs are fast-acting and potent antimalarial drugs that perform poorly as single agents against *P. falciparum* due to their rapid elimination. However, in combination with other antimalarial agents, artemisinin derivatives have shown impressive efficacy. ACTs consist of an artemisinin derivative (fast-acting), e.g., artemether in combination with a longer-acting blood schizonticide e.g., lumefantrine, amodiaquine, sulfadoxine/pyrimethamine, piperaquine and are, at present, the first line treatment for most malaria infections.[13] However, recent reports have shown signs of emerging parasite resistance to ACTs in South-East Asia.[14,15] As a result, research and development is necessary to develop antimalarial drugs that are safe, potent against drug resistant strains of the *Plasmodium* parasite and affordable to benefit the affected larger deprived community.

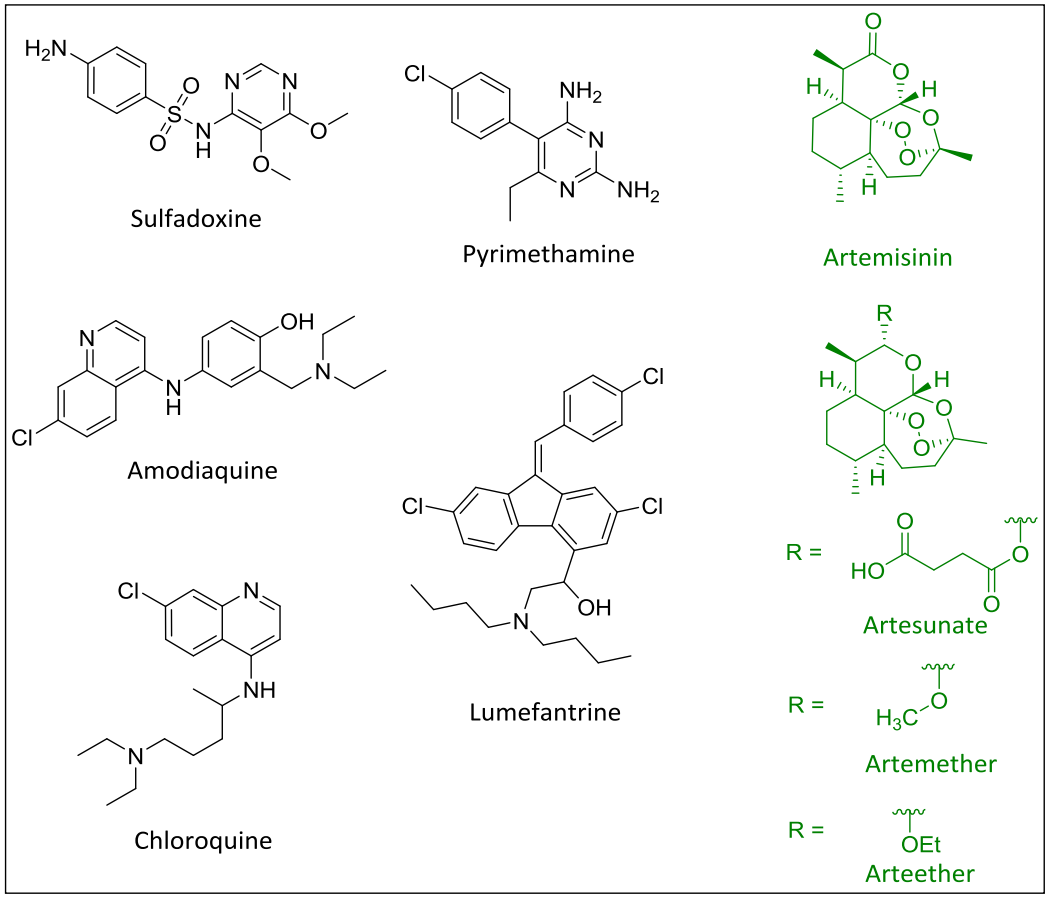

Figure 3: Artemisinin and its various semi-synthetic derivatives and other examples of antimalarial drugs in clinical use

The optimization and improvement of existing drugs through chemical modification approaches have shown various successes in malaria drug development and this strategy is responsible for many existing antimalarial agents.[16,17]

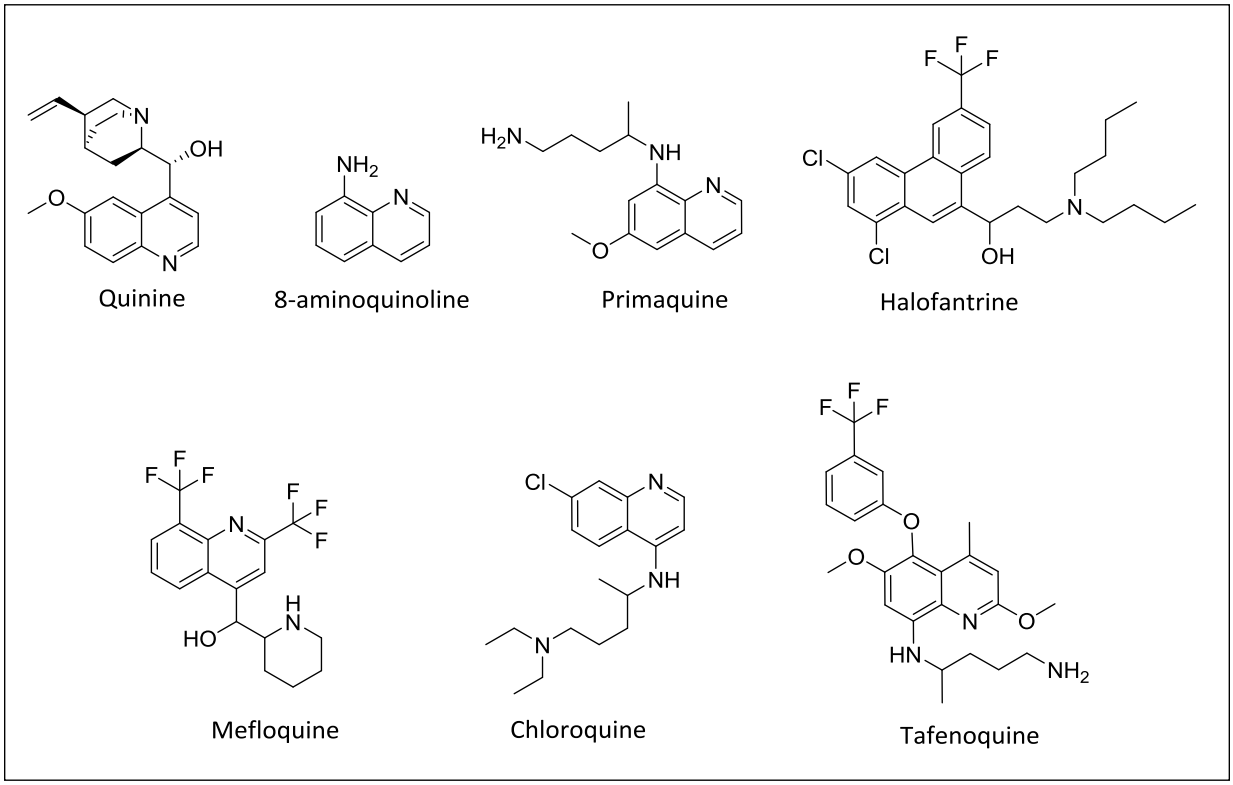

Figure 4: Examples of some successful chemical modifications

Quinine is a good example of a drug that was improved by employing chemical modification in a malarial context. Chloroquine, primaquine and mefloquine were optimized from quinine through chemical modification strategies[18] (**Figure 4**). Another good example is tafenoquine, an 8-aminoquinoline which, compared to the parent compound primaquine, showed enhanced activity against hepatic-stage parasites. Lumefantrine, a drug used in combination with artemether was adapted from halofantrine, which was linked to fatal cardiotoxicity.[16,17]

1.1.4 Current Drug Pipeline

Drug candidates undergo different phases of development in the pipeline before they can be approved. Pre-clinical assessment involves the examination of the potential drug in non-humans to study the efficacy, toxicity of the candidate drug as well as the pharmacokinetics (oral bioavailability and half-life) of the drug. If the drug candidate successfully passes through this stage, it undergoes phase 1 clinical trials. During Phase 1 trials, the promising drug is investigated on normal healthy volunteers for dose-range finding. After the drug has progressed from phase 1, it is examined in phase 2 on patients (approximately 100-300) to carefully study the efficacy and side effects of the candidate drug. During phase 3 clinical

trials, the efficacy and safety of the potential drug candidate is assessed on a larger group of patients (about 300-1000). Candidate drugs may fail at different stages of the drug development pipeline, however, drugs that progress successfully past phase III clinical trials, are approved.[19,20]

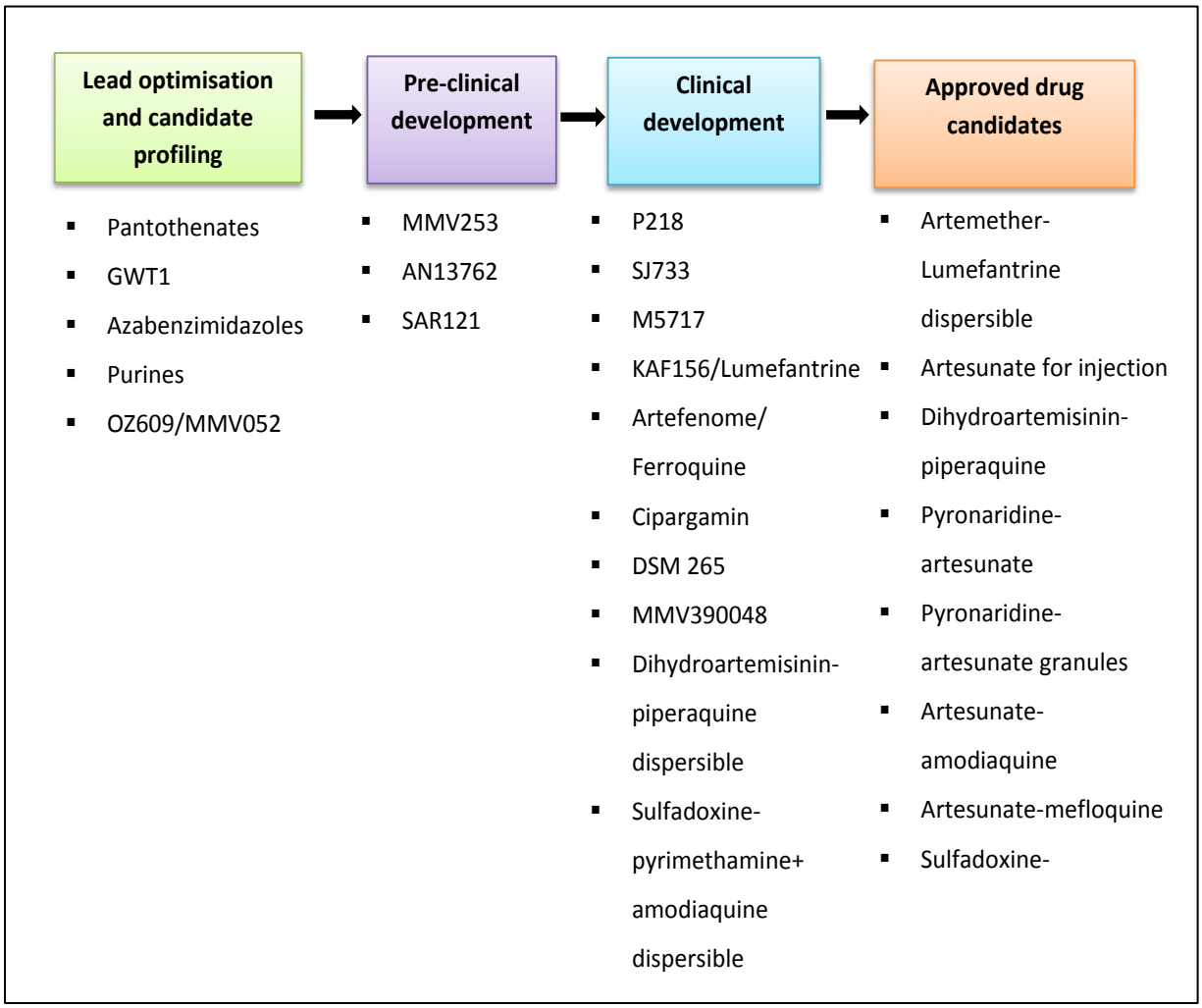

Figure 5: Current Malaria Drug Pipeline (Medicines for Malaria Venture, MMV) highlighting the various drug candidates at different stages of development[21]

The drug development pipeline includes projects focused on developing novel drugs or drug regimens for different patient populations. A good example is the development of a pediatric formulation of coartem (artemether-lumefantrine combination), the first example of a child-friendly taste-masked dispersible ACT[22] (**Figure 5**). Pyronaridine-artesunate and dispersible dihydroartemisinin (DHA)-piperaquine (**Figure 6**) are approved antimalarial ACT

drug candidates (**Figure 5**). These are aimed at delivering child-friendly formulations to cater for the extremely high malaria cases in children under the age of five.[23,24]

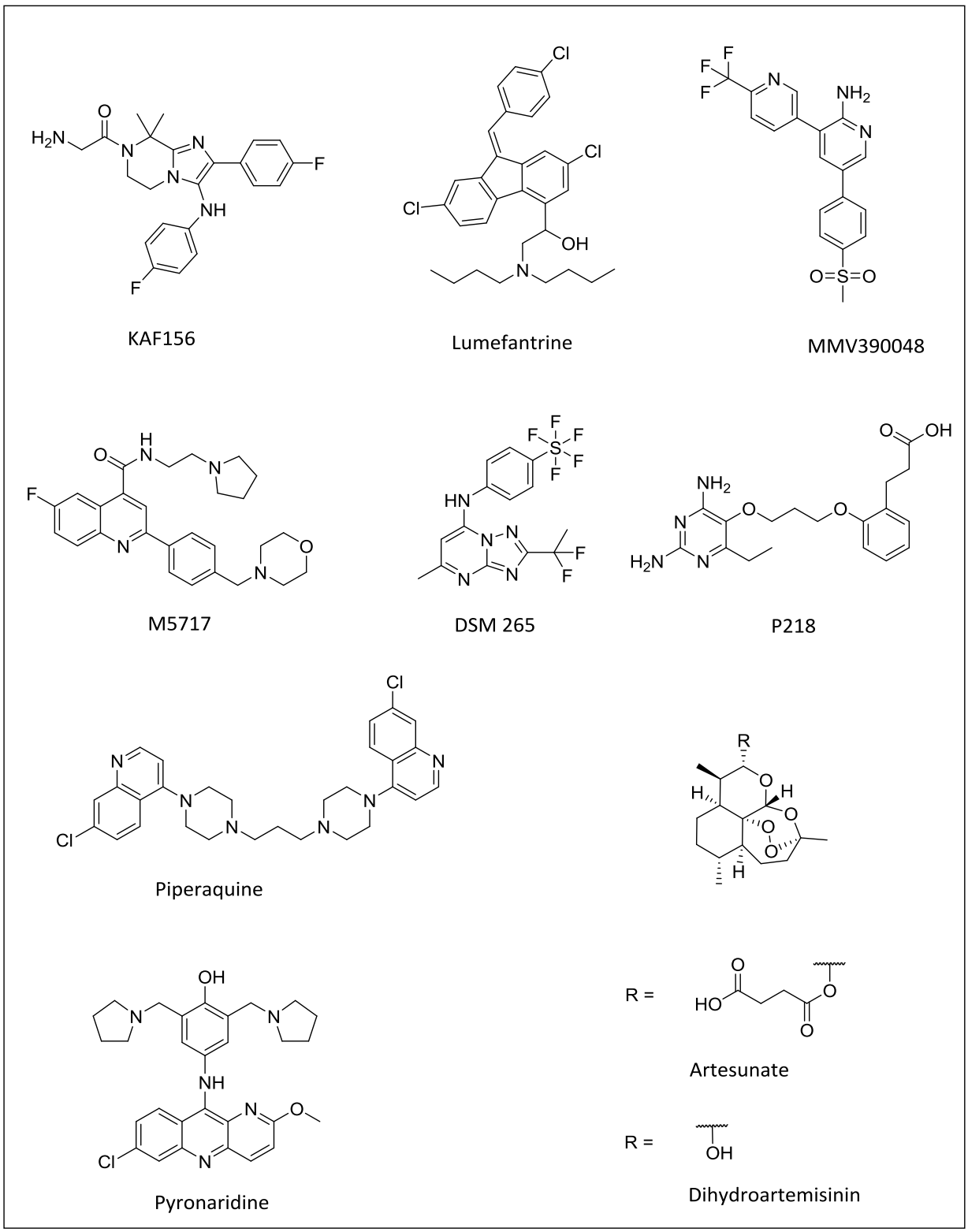

Figure 6: Structures of some phase I, phase II and approved drug candidates in the MMV Malaria Drug Development Pipeline

The Global Malaria Agenda aims to control, eliminate and eradicate the malaria burden[25] via various strategies: optimization of current chemotherapy, single-exposure radical cure (SERC) and single-exposure chemoprotection (SEC).[26,27] These strategies aim to reduce mortality and morbidity rates in endemic settings, block transmission from symptomatic and asymptomatic individuals in order to protect uninfected individuals and consequently reduce malaria incidences. These aims can be achieved through the development of antimalarial agents that are effective against resistant *Plasmodium* parasites and inventing drugs that cater for the vulnerable populations.[28] The SERC agenda targets improving the convenience of administration, making the antimalarial drug affordable so that it benefits the highly affected communities in resource-poor settings. The SEC program focuses on the development of new antimalarial drugs that target novel pathophysiology in order to forestall development of resistance and ensure that the antimalarials are safe and effective with minimal adverse effects.[26,27]

The MMV manages a portfolio of many malaria related projects and currently includes nine new drug candidates in clinical development. This portfolio focuses on the development of new drugs aimed at addressing unmet medical needs in malaria treatment for the vulnerable young children, pregnant women and for relapsing malaria and relevant projects whose objective is to eliminate malaria.[20,25,28] Cipargamin, currently in phase II clinical development (**Figure 5**) is hoped to function in severe malaria cases.[29,30] The KAF156/Lumefantrine combination drug candidate (**Figure 6**) for malaria treatment has an unknown mechanism of action, however, has also demonstrated desired potency against parasites that are resistant to current drugs.[31] Although DSM265 has reduced activity against *P. vivax* and due to its single enzyme target, is likely to suffer resistance, DSM265 is a potential chemoprotective agent[32,33] (**Figure 6**). The MMV390048, an inhibitor of *Plasmodium* phosphatidylinositol 4-kinase is an aminopyridine derivative (**Figure 6**) that has undergone preclinical development, completed phase 1 human trials and has shown potency against multiple parasite life cycle stages.[34] The *P. falciparum* EF2 inhibitor, M5717 is undergoing clinical development and has demonstrated desirable potential to address various clinical needs, for example: single-dose treatment, transmission blocking and chemoprotection.[35] P218 is a *P. falciparum* dihydrofolate reductase inhibitor that has recently completed its first-in-human study[36,37] (**Figure 6**).

Advances in antimalarial research and development are important for the world's future ability to treat and control malaria. Unfortunately, malaria being a disease of poverty, the business-driven industrial antimalarial drug research due to the inadequate market incentive, is not competitive and, therefore, efforts into research in this disease area are minimal. [38] However, some mechanisms of partnering with industry have been implemented for improvement and the enhancement of scientific research into better chemotherapy. [5]

1.1.5 Chemoprophylaxis

The use of antimalarials as chemoprophylactic agents is useful for tourists visiting malaria endemic areas - mefloquine, doxycycline and primaquine (**Figure 7**) are the common drugs taken for this effect. Chloroquine also has potential to serve as a malaria prophylactic drug, but can only be effective in regions that are unaffected by *P. falciparum* and in regions where this species is not yet resistant to the drug.[39,40]

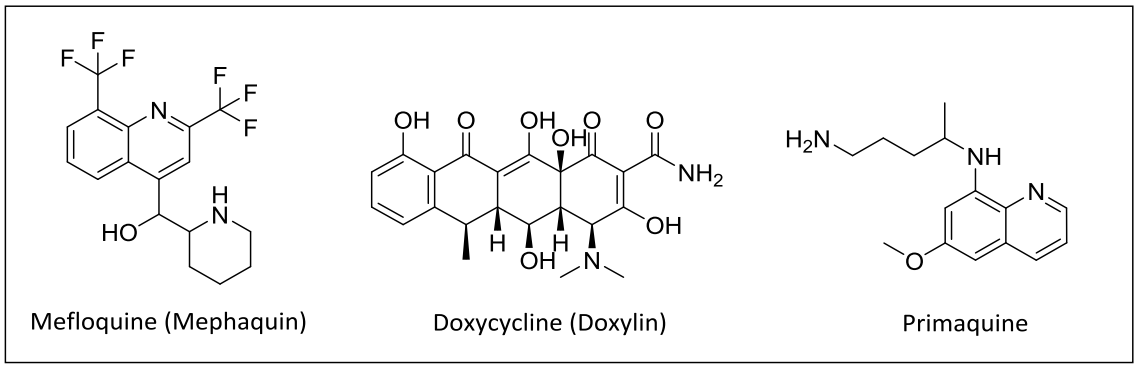

Figure 7: Examples of malaria chemoprophylactic agents

Although malaria is common in developing countries, it has a global impact in that about half of the world's population are at risk of being infected. This raises the need for global attention to reduce the prevalence and impact of malaria by implementing approaches such as vector control, chemoprophylaxis, and chemotherapy.[41]

1.2 Schistosomiasis

1.2.1 Etiology and epidemiology

Schistosomiasis also known as bilharzia or snail fever is a water-borne parasitic disease caused by trematode flatworms of the genus *Schistosoma* species. *S. haematobium*, *S. mansoni*, *S. intercalatum*, *S. guineensis*, *S. japonicum*, and *S. mekongi* species infect humans and cause illness.[42]

After malaria, schistosomiasis is the second most prevalent tropical disease in the world, a major source of morbidity and mortality for many developing countries in Africa, South America, the Caribbean, the Middle East and Asia[43] (**Figure 8**). Schistosomiasis affects over 200 million people and over 700 million are at risk of infection. The endemic areas are commonly in tropical and sub-tropical regions and in communities that lack proper sanitation.[44,45]

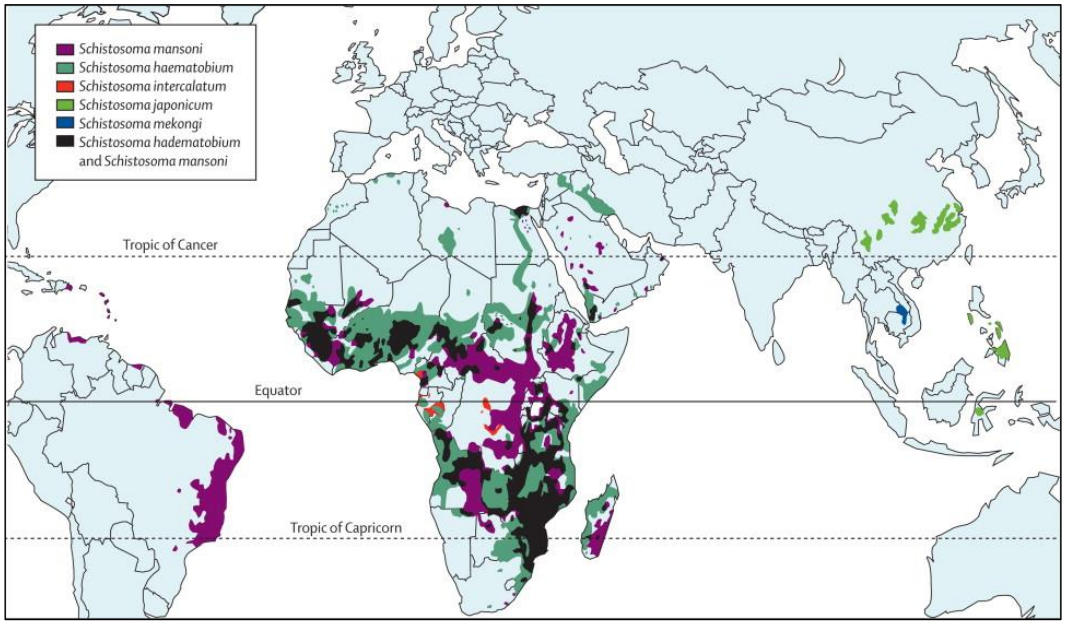

Figure 8: World Map showing schistosomiasis hotspots[46]

There are two main types of schistosomiasis: genitourinary and intestinal, whose occurrence is dependent on the *Schistosoma* parasitic species causing the infection.[47] **Table 1** shows the two types of shistosomiasis that exist, the form that each *schistosoma* species causes and the geographical distribution of schistosomiasis in each category.

Table 1: Geographical distribution of *Schistosoma* species.

***Schistosoma* species**	**Type of schistosomiasis**	**Geographical distribution**
S. haematobium	Urogenital	Africa, the Middle-East, India, and Turkey
S. mansoni	Intestinal	Africa, the Middle-East, the Caribbean, South-America
S. japonicum	Intestinal	South-east and East Africa
S. mekongi	Intestinal	Cambodia and Laos
S. intercalatum	Intestinal	Central and West Africa
S. guineensis	Intestinal	Central and West Africa

A human is infected with schistosomiasis when the cercariae of parasite blood flukes (schistosomes), released by freshwater snails penetrate the human skin during exposure to contaminated freshwater. In the body of the infected hosts, the larval forms develop into adult schistosomes.[45,48] These male and female worms reside in various locations in the mesenteric venules and is in some way species-specific. For instance, *S. japonicum* and *S. mekongi* are frequently found in the mesenteric venules of the small intestines whereas *S. mansoni* and *S. intercalatum* are commonly found in the mesenteric venules of the large intestines. *S. haematobium* on the other hand, resides in the vesical venous plexus of the bladder or the rectal venules and is the reason it causes urogenital schistosomiasis (**Table 1**).[43,48]

1.2.2 Life cycle and pathogenesis

Similar to other trematodes, schistosomiasis has a very complex life-cycle, which involves two hosts: the intermediate (snail) and the definitive (mammalian) hosts. It is acquired via skin exposure to contaminated water infested with cercariae (parasitic larvae). The cercariae are free-living in contaminated freshwater and are released by the specific snail intermediate host which then with the aid of proteolytic enzymes swim and penetrate the human skin.[43,45] Upon penetration, the cercariae sheds off its tail and transform into

schistosomulae, which via portal blood circulation to the liver mature into male and female worms. During the hosts circulation, the thread-like female worm attaches to the gynecophoric canal (a ventral groove) of the male schistosome fluke, migrate to the venous plexus or the mesenteric venules in various locations, where the female schistosomes begin egg production. The eggs circulate and penetrate the wall of the lumen of the intestine or the bladder and are then expelled in the faeces or urine of the definitive host. The miracidium, liberated from the eggs then seek out the intermediate snail host, bringing the transmission cycle full circle[43,45,48,49] (**Figure 9**).

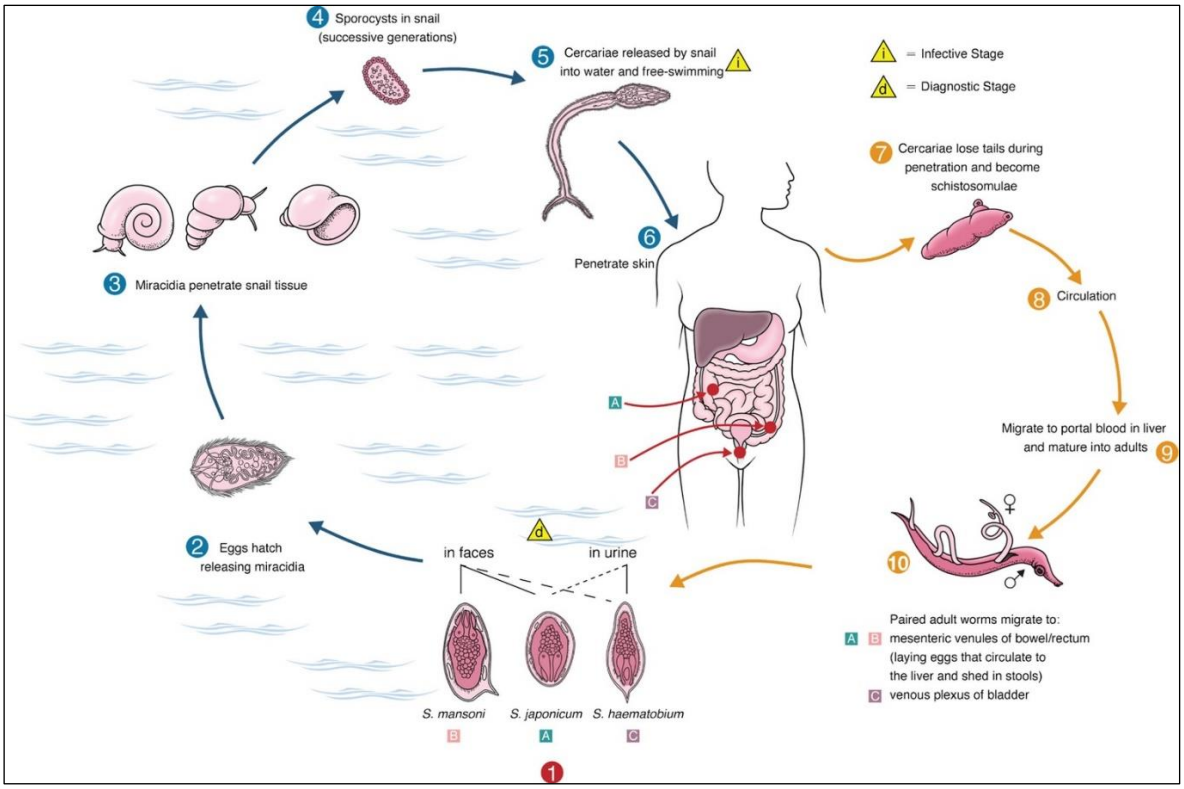

Figure 9: Schistosomiasis life cycle[50]

1.2.3 Chemotherapy and challenges in schistosomiasis treatment

Schistosomiasis is a neglected tropical disease (NTD). The NTDs are infectious diseases that, even though are treatable and preventable, still cause high rates of morbidity and mortality. These diseases are more prevalent in developing countries, affecting the poor, and causing significant health and financial burdens.

The development of drugs against these diseases to clinical stages is heavily neglected: out of the many potential drugs that register for clinical trials only a few are focused on NTDs. This is due to the very low research investment for NTDs compared to first world diseases such as cardiovascular and central nervous system diseases. Fortunately, the situation is changing, having more pharmaceutical companies and other development partners commit to contributing to the eradication and control of NTD researches.

Most patients suffering from schistosomiasis rely on one drug, praziquantel, for treatment and because of this; there are therapeutic limitations and drug resistance threats. This highlights the urgent need to discover and develop novel antischistosomal drugs. In one example of a drug discovery effort, a diverse compound with *in vitro* activity against *Plasmodium falciparum* discovered by the MMV were tested against schistosomula and adult *S. mansoni in vitro*.[51] Based on the obtained *in vitro* results, favourable compounds were further investigated *in vivo*. This work identified two potential leads: N,N'-diarylurea (MMV665852) and 2,3-dianilinoquinoxaline (MMV007224) derivatives (**Figure 10**), that were found active against *S. mansoni*, reducing worm burden by 52.5% and 40.8%, respectively. The two leads displayed satisfactory pharmacokinetic profiles, low cytotoxic potential and thus are a good foundation for further antischistosomal drug discovery and development studies.[42,51]

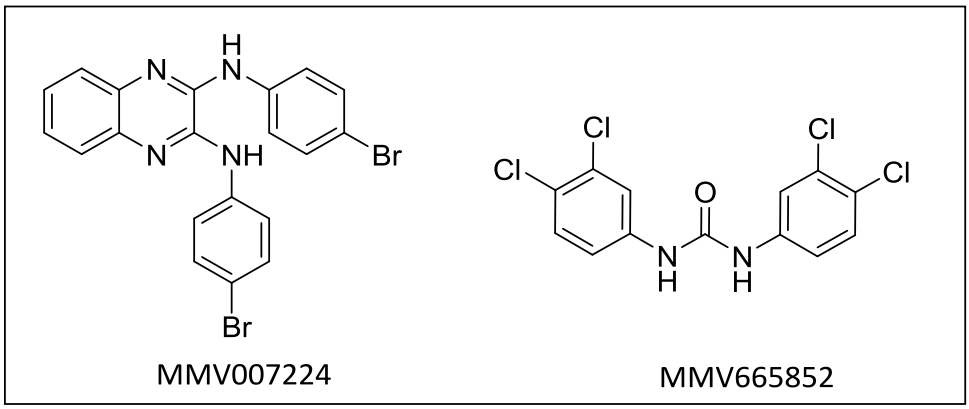

Figure 10: Potential antischistosomal early leads identified from the open access MMV malaria box

Praziquantel (**Figure 11**) is the preferred drug prescription for the treatment of schistosomiasis. There are other drugs (oxamniquine and metrifonate; **Figure 11**) that can

be used for treatment. However, unlike praziquantel that cures all forms of schistosomiasis, these drug options have exclusive efficacy and are limited to specific *Schistosoma* species (*S. mansoni* and *S. haematobium*, respectively). The dependence on only one drug, praziquantel, for its ability to treat all forms of the disease may potentially result in drug resistance, highlighting the need to develop new drugs that are as effective and affordable as praziquantel.[52,53]

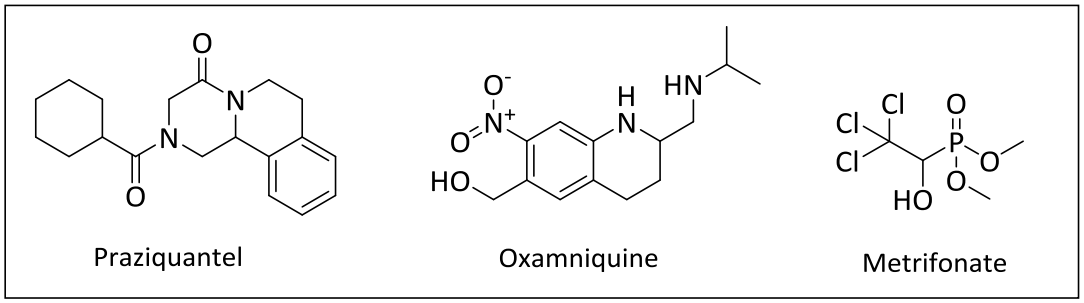

Figure 11: Drugs currently used to treat schistosomiasis

Despite the success of praziquantel as an antichistosomal agent, it also has several shortcomings. Firstly, it is commercially available as a racemic mixture of the L and D isomers and yet only the L-isomer is active.[53] Secondly, praziquantel has a bitter taste which may affect medical compliance. Lastly, the biggest problem is its limited activity against adult schistosomes only and its failure to treat the juvenile stages of the flukes.[54]

1.3 Approaches to Antimalarial and Antischistosomal Drug Discovery

1.3.1 Introduction

As already mentioned, malaria is an infectious disease killing hundreds of thousands of people every year. The increasing resistance of malaria parasites to current chemotherapy is a major contributor to malarial mortality and morbidity. Also, in the case of schistosomiasis, the reliance on praziquantel for treatment for its ability to treat all forms of the disease raises legitimate resistance concerns. Resistance is a major challenge and is addressed by various drug development strategies.[55,56]

Common to many drug development programs, antimalarial and antischistosomal drug development programs aim to introduce new agents with improved efficacy and safety.[57] More specific to malaria and schistosomiasis, is the need for widespread treatment in developing countries considering the lack of resources in these affected areas, oral drugs and more specifically single daily dosing. These efforts are crucial in this setting to make these novel drugs widely useful, affordable and routinely available to majority of the affected population.[16]

Approaches to drug discovery and development range from strategies that benefit from understanding specific aspects of the biology of parasites to making chemical modifications to generate new compounds.[16,58]

1.3.2 Target-based screening versus Phenotypic whole-cell screening

Target-based screening and phenotypic screening are competing strategies for drug discovery. Target-based screening is a molecular hypothesis-driven approach. It makes use of known drug targets (e.g. enzymes) against which compounds are screened for hit compound identification. A requirement for this procedure is that the known parasitic drug target needs to be validated.[59] There are four levels of validation. First, target essentiality must be validated by determining the effect of disrupting function or diminishing expression in an organism on proliferation in culture or in the host. Second, phenotypic validation, defined as a chemical compound inhibiting an enzyme target and also demonstrating an effect on the organism (most often cell kill), must be demonstrated. Third, *in vivo* validation, also known as *in vivo* proof-of-concept (POC), which refers to the capability of a compound to create the intended pharmacodynamic (PD) effect in an animal model, must be achieved. For an antimalarial drug, this most often is the reduction of parasitemia in a mouse model of infection. To show efficacy, the compound needs favourable *in vivo* pharmacokinetic (PK) properties for sufficient exposure in the blood to produce the intended PD response. Fourth, clinical validation represents the most important level of validation. To achieve clinical validation, the human PK must be favourable, whether it would be exposure in the blood for asexual stages of the malaria parasite or in the liver for liver stage disease.[59,60]

Advances in recombinant technology, genetics and molecular biology have improved target-based drug discovery significantly: genes can be expressed and examined against large compound libraries via high-throughput screening (HTS). However, hit compounds obtained from this approach often result in poor *in vivo* efficacy, likely due to the expected physiological differences between the identified target and the biological system.[61,62]

Unlike target-based approaches, phenotypic whole-cell screening empirical approaches may operate without knowledge of a drugs molecular target but rely on phenotypic measures. This approach benefits from the removal of target bias, taking into account the uncertainty of complex multifaceted biological systems.[61] The disadvantage, however, are that these assays generally require more resources, time and effort as further studies are necessary to understand the mechanism(s) of action for lead optimization.[59,61,63]

1.3.3 Drug Repurposing and Repositioning

The progression of drug discovery and development is accompanied by various challenges. Some of the major challenges stem from the high cost associated with drug development and discovery. Large investments are pumped into drug discovery and development projects. Unfortunately, these projects yield low returns owing to the number of drugs that make it to the market-a major economic loss.[12,42]

One attractive approach that is recommended to possibly overcome this obstacle and accelerate the drug discovery and development process is the exploration of current drugs and drug leads as probable therapies for other diseases. This strategy is known as drug repositioning or drug repurposing.[42]

Drug repurposing refers to a strategy where an existing drug, currently in use in a certain disease area, is investigated for use in another disease indication. Drug repositioning, however, involves the use of a drug active in one disease indication as a chemical modification template to generate derivatives that are employed in another disease area.[64] This strategy can also be applied to rescue drug candidates that have failed or have been abandoned during the development process. This shortens the drug discovery process

significantly as, in many cases, these drugs have undergone many stages of clinical development and, presumably, have known pharmacokinetic and safety profiles.[64]

Drug repurposing and repositioning approaches have been used and are currently in use. Examples of generic approaches used are exploring: similarities of the drug target and genome information; *in silico* approaches; non-hypothesis driven screening; and as in the case of malaria and schistosomiasis similarities in their cell biology. The degradation of haemoglobin by the *plasmodium* parasite and the blood fluke *schistosoma* suggests an opportunity for the repurporsing and repositioning of antimalarial scaffolds/agents as antischistosomal agents.[42] There are also some successfully repurposed/rescued/repositioned drugs that are currently in use such as bupropion, repurposed from an antidepressant to smoking cessation; pyrimethamine and other antimalarial sulfur-based drugs, which have been repositioned from sulfur-based antibacterials. Thalidomide has also been rescued to multiple myeloma[64,65] (**Figure 12**).

Antimalarial chemotherapy has also benefited from drug repurposing. Folate antagonists and tetracyclines were initially developed for their impressive antibacterial activity and were found to also possess antimalarial activity. These examples suggest the need to screen new antimicrobial drugs and other available developed or marketed drugs as potential treatments for malaria.[16]

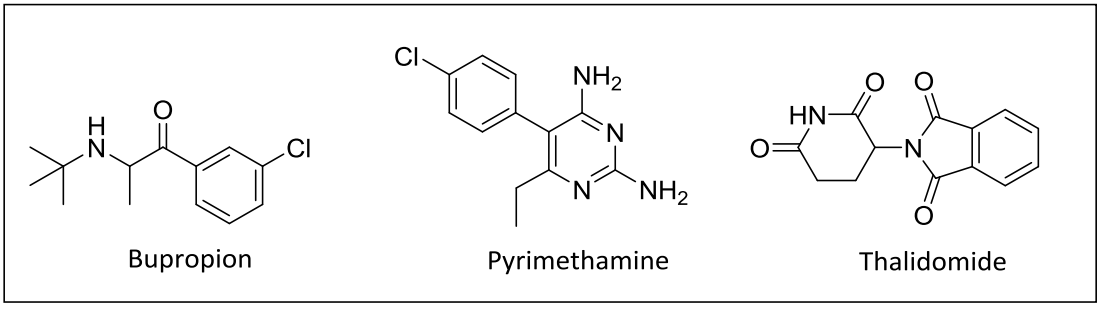

Figure 12: Successful repurposed/repositioned/rescued drugs

Previous research work have shown that the reliance of drug discovery efforts in other disease areas and the use of these approaches have the potential to improve drug discovery in neglected diseases.[42]

1.3.4 Hemoglobin Degradation

Malarial parasites have limited potential to synthesize their own amino acids. Consequently, the parasite degrades hemoglobin of the infected host to liberate amino acids as a source of its nutrition.[66,67] This is followed by the release of toxic heme, ferriprotoporphyrin IX. Since free heme is toxic to the parasite, the parasite polymerizes the heme to insoluble hemozoin (non-toxic polymer form of heme) and globin and is then further hydrolyzed to amino acids for its nutrition (**Figure 13**).[68]

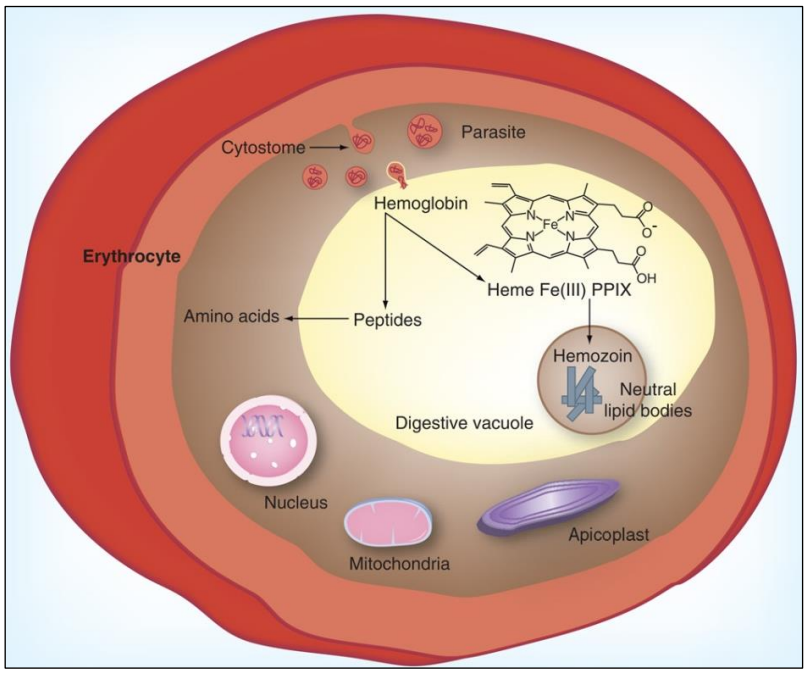

Figure 13: Haemoglobin degradation pathway[69]

Chloroquine, mepacrine and pyronaridine shown in **Figure 14** are examples of antimalarial agents that have been shown to target hemozoin formation. The inhibition of hemozoin formation from heme is an important therapeutic strategy in antimalarial drug discovery[16,67] and was carried out in this research project.

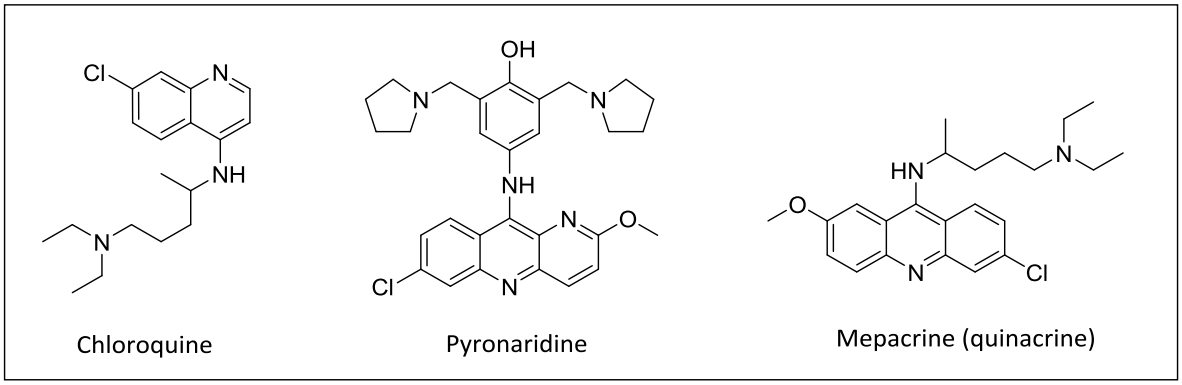

Figure 14: Structures of chloroquine, pyronaridine and mepacrine

The β-hematin Inhibition Activity (BHIA) assay is used to screen compounds for their inhibitory effect against β-hematin (the synthetic equivalent of hemozoin) formation. Novel antimalarial β-hematin inhibitors can form strong complexes with heme (toxic to the parasite), to prevent the formation of β-hematin. Improvements in high-throughput screening methods and a good understanding of the interaction of drugs with this target have been essential in drug discovery. This allows for the exploration of heme-targeting drug candidates and provides opportunities for target-based structural design for the development of novel drugs.[68]

The discovery that *Schistosoma* also convert heme to the non-toxic form (hemozoin) suggests that new heme-targeting novel drugs are not only essential for malaria but are potential chemotherapeutic agents for schistosomiasis.[42]

1.4 The Role of Solubility in Drug Discovery

Solubility is an important factor in drug discovery and needs to be carefully considered in order to reduce chances of failure later on in the drug development process.[70] Compounds with poor solubility profiles result in numerous drawbacks such as poor absorption, hence poor bioavailability, inaccurate and unreliable bioassay results arising from compound precipitation from solution during the experimental procedure. This, therefore, calls for the need to prioritize the optimization of solubility in the early stages of drug discovery. Developing drugs with desirable aqueous solubility and permeability, which are the two most important physicochemical properties, results in favourable oral bioavailability.

Subsequently, the degree of absorption will have an impact on the fraction of the administered dose that reaches systemic circulation, hence bioavailability. Therefore, it is vital that solubility is optimized in lead molecules.[70]

In the context of oral drug administration, the drug needs to dissolve in intestinal media prior to absorption into systemic circulation. Poor absorption is one of the major reasons that prevent many drug candidates from reaching the market. It is therefore economically desirable to ensure that sub-optimal solubility profiles of drug candidates are addressed during the early development stages.[70]

The solubility of compounds can be improved using various methods which include physical, chemical and supramolecular methods.[70] The use of solid dispersions, micronization and the selection of polymorphs with optimum solubility are examples of physical methods. The micronization method lowers the size of the drug particles, which, in turn, increases its surface area to volume ratio thus increasing the dissolution rate. Solid dispersions are mixtures of non-polar drugs with hydrophilic carrier polymers that enhance solubility.[71]

Conversely, supramolecular approaches involve the use of either cyclodextrin inclusion complexes or co-crystals. Co-crystal formation between the lipophilic active pharmaceutical ingredient (API) and more hydrophilic co-formers enhances both the compound's solubility and oral bioavailability, which is desirable.[72]

Cyclodextrins can be classified into three main groups: α-, β- or γ, where the number of sugars in the cyclic ring determines the category (**Figure 15**). The cyclic oligosaccharide is made up of non-polar interior cavities and polar groups on its exterior. Due to the hydrophobic nature of the inner cavities, when in aqueous solution, the interior is occupied by water at high enthalpy. This, together with hydrophobic guest molecules, form cyclodextrin inclusion complexes.[73]

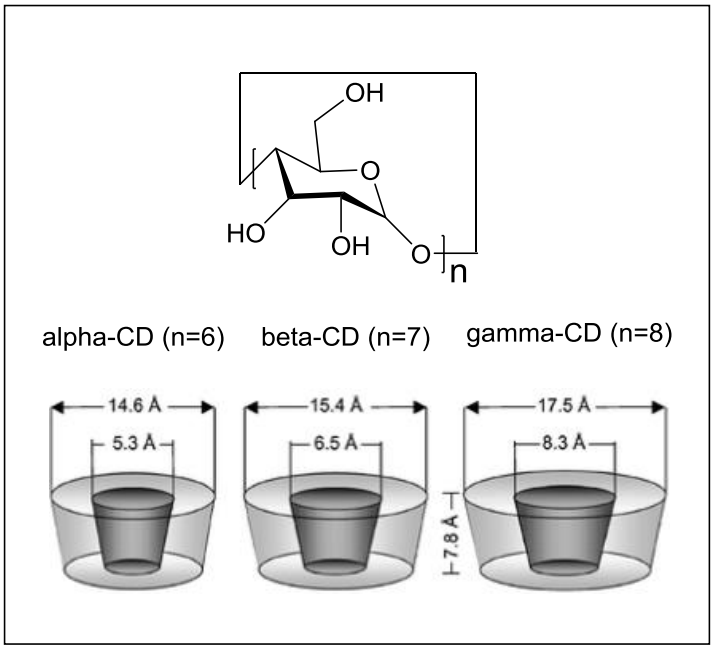

Figure 15: The structures of alpha (α), beta (β) and gamma (γ) cyclodextrins[74]

Chemical methods were explored in this research project and involved the chemical modification of a given compound template to improve its aqueous solubility. Approaches that are used for chemical modifications in order to improve solubility include introducing ionizable groups; introducing polar groups; and using other hydrogen-bonding groups such as hydroxyl, amino, amides and carboxylic acids.[75] The goal is to reduce both the lipophilicity of molecules and improve interactions with aqueous media which can be achieved by introducing hydrophilic functional groups (**Figure 16** and **Figure 17**).[70]

Solubility affects oral bioavailability which is well illustrated in **Figure 16**. L-685,434 and indinavir are protease inhibitors that have potent activity *in vitro* in both enzyme and cell-based assays. However, the early lead compound, L685,434 demonstrated poor *in vivo* efficacy possibly due to poor solubility and therefore low bioavailability. To overcome this hurdle, indinavir was optimized from L-685,434 by introducing ionizable centers to improve the oral bioavailability of the compound (**Figure 16**).[76]

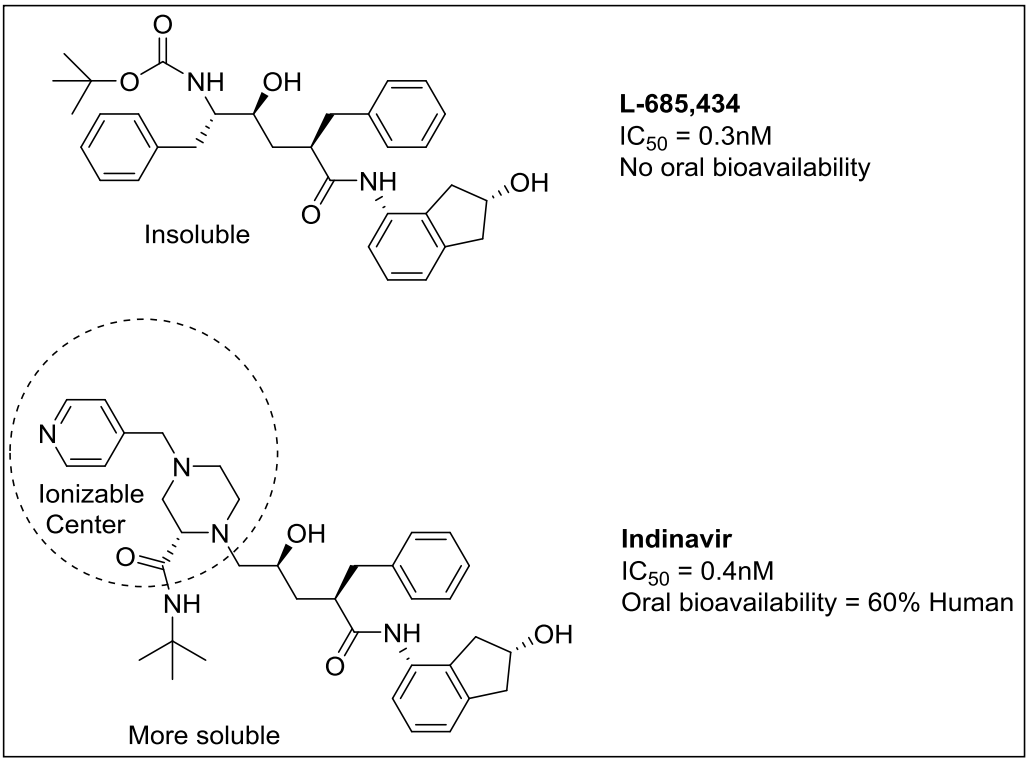

Figure 16: Influence of solubility on oral bioavailability[76]

Reducing the lipophilicity of a molecule improves its solubility because lowering lipophilicity in some cases involves decreasing the size of the molecule. This can be done by first identifying lipophilic components in the molecule that can be replaced with smaller or polar groups.[70,75]

Addition of hydrogen bond donors and acceptors can improve aqueous solubility. **Figure 17** shows nystatin, a poorly soluble but potent antifungal agent. To address this pharmacokinetic liability, structural modifications via the addition of hydrogen bonds were employed to improve solubility. Introducing hydroxyl groups at positions **31** in compound **C17.1** and **33** in compound C17.2 displayed a 2000-fold increase in solubility (**Figure 17**).[76]

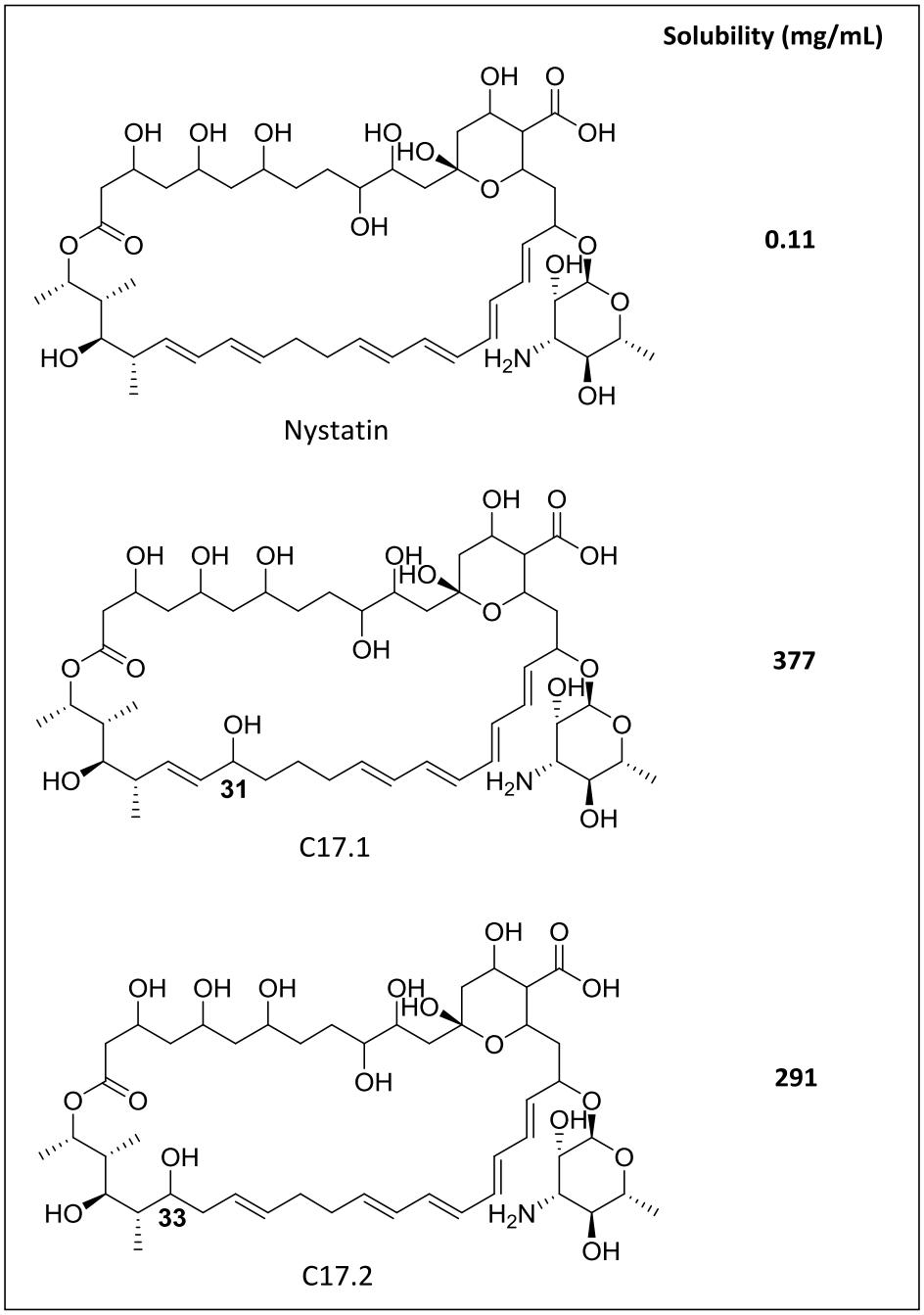

Figure 17: Effect of the addition of hydrogen bonding on aqueous solubility[76]

Intermolecular interactions involving pi-pi stacking contribute to poor solubility. This is because molecules with this type of interaction are capable of forming crystals that require high energy to disrupt. However, such molecular interactions can be substantially discouraged by incorporating molecular features that disrupt molecular planarity (removal of aromaticity or introduction of saturation) and symmetry as well as increase the dihedral angle for biaryl systems. Substitution of benzylic positions and twisting of fused rings can

also disrupt pi-pi intermolecular interactions. These strategies can discourage crystal packing and therefore improve solubility.[75,76] **Figure 18** illustrates an example of this strategy using vanilloid receptor 1 antagonists.

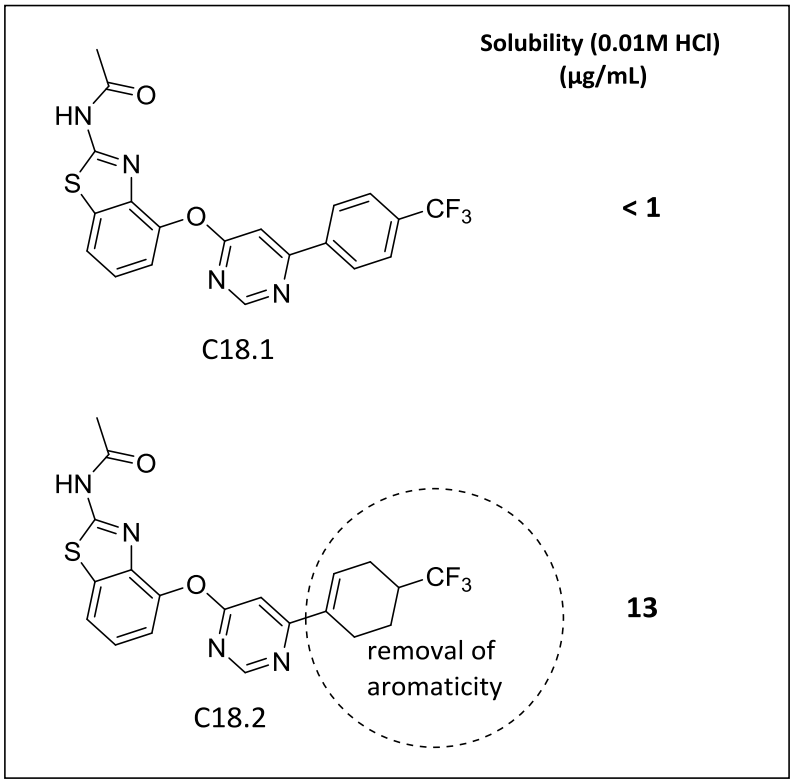

Figure 18: Enhanced solubility via the removal of aromaticity[75]

Compound **C18.1** displayed poor thermodynamic aqueous solubility. In an effort to improve this, a second-generation clinical candidate was developed by the removal of aromaticity to form the more soluble saturated compound **C18.2** (**Figure 18**).

1.5 References

1. World Health Organization. *World Malaria Report 2017*; **2017**.
2. Cox, F. E. History of the Discovery of the Malaria Parasites and Their Vectors. *Parasites and Vectors* **2010**, *3* (1), 1–9.
3. Bruce-Chuvatt, L. J. Alphonse Laveran's discovery 100 years ago and today's global fight against malaria. *J. R. Soc. Med.* **1981**, *74*, 531–536.
4. Berlucchi, G. British Roots of Italian Neurophysiology in the Early 20th Century. *Curr. Biol.* **2008**, *18* (2), 51–56.
5. Ridley, R. G. Medical Need, Scientific Opportunity and the Drive for Antimalarial Drugs. *Nature* **2002**, *415*, 686–693.
6. WHO Global Malaria Programme. World Malaria Report. *World Heal. Organ.* **2012**.
7. Killeen, G. F.; Smith, T. A.; Ferguson, H. M.; Mshinda, H.; Abdulla, S.; Lengeler, C.; Kachur, S. P. Preventing Childhood Malaria in Africa by Protecting Adults from Mosquitoes with Insecticide-Treated Nets. *PLoS Med.* **2007,** *4* (7), e229.
8. Soulard, V.; Bosson-Vanga, H.; Lorthiois, A.; Roucher, C.; Franetich, J. F.; Zanghi, G.; Bordessoulles, M.; Tefit, M.; Thellier, M.; Morosan, S.; Le Naour, G.; Capron, F.; Suemizu, H.; Snounou, G.; Moreno-Sabater, A.; Mazier, D. Plasmodium Falciparum Full Life Cycle and Plasmodium Ovale Liver Stages in Humanized Mice. *Nat. Commun.* **2015**, *24* (6), 7690.
9. Klein, E. Y. Antimalarial Drug Resistance: A Review of the Biology and Strategies to Delay Emergence and Spread. *International Journal of Antimicrobial Agents* **2013**, *41* (4), 311-317.
10. del Prado, G. R. L.; García, C. H.; Cea, L. M.; Espinilla, V. F.; Moreno, M. F. M.; Márquez, A. D.; Polo, M. J. P.; García, I. A. Malaria in Developing Countries. *Journal of Infection in Developing Countries* **2014**, *8* (1), 1-4.
11. Takem, E. N.; D'Alessandro, U. Malaria in Pregnancy. *Mediterranean Journal of Hematology and Infectious Diseases* **2013**, *5* (1), e2013010.
12. Pink, R.; Hudson, A.; Mouriès, M.-A.; Bendig, M. Opportunities and Challenges in Antiparasitic Drug Discovery. *Nat. Rev. Drug Discov.* **2005**, *4*, 727–740.

13. O'Neill, P. M.; Barton, V. E.; Ward, S. A. The Molecular Mechanism of Action of Artemisinin--the Debate Continues. *Molecules* **2010**, *15*, 1705–1721.
14. Paloque, L.; Ramadani, A. P.; Mercereau-puijalon, O.; Augereau, J.; Benoit-vical, F. Plasmodium Falciparum: Multifaceted Resistance to Artemisinins. *Malar. J.* **2016**, *15*, 1–12.
15. Ashley, E.; Dhorda, M.; Fairhurst, R. M.; Amaratunga, C.; Lim, P.; Suon, S.; Sreng, S.; Anderson, J. M.; Mao, S.; Sam, B.; Sopha, C.; Chuor, C. M.; Nguon, C.; Sovannaroth, S.; Pukrittayakamee, S.; Jittamala, P.; Chotivanich, K.; Chutasmit, K.; Suchatsoonthorn, C.; Runcharoen, R.; Hien, T. T.; Thuy-Nhien, N. T.; Thanh, N. V.; Phu, N. H.; Htut, Y.; Han, K.-T.; Aye, K. H.; Mokuolu, O. a.; Olaosebikan, R. R.; Folaranmi, O. O.; Mayxay, M.; Khanthavong, M.; Hongvanthong, B.; Newton, P. N.; Onyamboko, M. a.; Fanello, C. I.; Tshefu, A. K.; Mishra, N.; Valecha, N.; Phyo, A. P.; Nosten, F.; Yi, P.; Tripura, R.; Borrmann, S.; Bashraheil, M.; Peshu, J.; Faiz, M. A.; Ghose, A.; Hossain, M. A.; Samad, R.; Rahman, M. R.; Hasan, M. M.; Islam, A.; Miotto, O.; Amato, R.; MacInnis, B.; Stalker, J.; Kwiatkowski, D. P.; Bozdech, Z.; Jeeyapant, A.; Cheah, P. Y.; Sakulthaew, T.; Chalk, J.; Intharabut, B.; Silamut, K.; Lee, S. J.; Vihokhern, B.; Kunasol, C.; Imwong, M.; Tarning, J.; Taylor, W. J.; Yeung, S.; Woodrow, C. J.; Flegg, J. a.; Das, D.; Smith, J.; Venkatesan, M.; Plowe, C. V.; Stepniewska, K.; Guerin, P. J.; Dondorp, A. M.; Day, N. P.; White, N. J. Spread of Artemisinin Resistance in Plasmodium Falciparum Malaria. *N. Engl. J. Med.* **2014**, *371*, 411–423.
16. Rosenthal, P. J. Antimalarial Drug Discovery: Old and New Approaches. *J. Exp. Biol.* **2003**, *206*, 3735-3744.
17. ter Kuile, F. O.; Nosten, F.; Chongsuphajaisiddhi, T.; White, N. J.; Dolan, G.; Luxemburger, C.; Phaipun, L.; Edstein, M. D.; Webster, H. K. Halofantrine versus Mefloquine in Treatment of Multidrug-Resistant Falciparum Malaria. *Lancet* **1993,** *341* (8852), 1044-1049.
18. Kaur, K.; Jain, M.; Reddy, R. P.; Jain, R. Quinolines and Structurally Related Heterocycles as Antimalarials. *European Journal of Medicinal Chemistry* **2010**, *45* (8), 3245-3264.
19. Biamonte, M. A.; Wanner, J.; Le Roch, K. G. Recent Advances in Malaria Drug Discovery. *Bioorganic and Medicinal Chemistry Letters* **2013**, *23* (10), 2829-2843.

20. Bathurst, I.; Hentschel, C. Medicines for Malaria Venture: Sustaining Antimalarial Drug Development. *Trends in Parasitology* **2006**, *22* (7), 301-307.
21. Medicines for Malaria Venture, MMV Annual Report 2017; **2017**.
22. Abdulla, S.; Sagara, I. Dispersible Formulation of Artemether/Lumefantrine: Specifically Developed for Infants and Young Children. *Malar. J.* **2009**, ***8*** **(1), 1-**7.
23. Djimdé, A.; Lefèvre, G. Understanding the Pharmacokinetics of Coartem. *Malar. J.* **2009**, *8* (1), 1-4.
24. Djimdé, A. A.; Tekete, M.; Abdulla, S.; Lyimo, J.; Bassat, Q.; Mandomando, I.; Lefèvre, G.; Borrmann, S. Pharmacokinetic and Pharmacodynamic Characteristics of a New Pediatric Formulation of Artemether-Lumefantrine in African Children with Uncomplicated Plasmodium Falciparum Malaria. *Antimicrob. Agents Chemother.* **2011**, *55* (9), 3994-3999.
25. Alonso, P. L.; Brown, G.; Arevalo-Herrera, M.; Binka, F.; Chitnis, C.; Collins, F.; Doumbo, O. K.; Greenwood, B.; Hall, B. F.; Levine, M. M.; Mendis, K.; Newman, R. D.; Plowe, C. V.; Rodríguez, M. H.; Sinden, R.; Slutsker, L.; Tanner, M. A Research Agenda to Underpin Malaria Eradication. *PLoS Medicine* **2011**, *8* (1), e1000406.
26. Price, R. N.; Nosten, F. Single-Dose Radical Cure of Plasmodium Vivax: A Step Closer. *The Lancet* **2014**, *383* (9922), 1020-1021.
27. Anthony, M. P.; Burrows, J. N.; Duparc, S.; Moehrle, J. J.; Wells, T. N. C. The Global Pipeline of New Medicines for the Control and Elimination of Malaria. *Malar. J.* **2012**, *11*, 316.
28. WHO. *Global Technical Strategy for Malaria 2016-2030*; **2015**.
29. Huskey, S. E. W.; Zhu, C. Q.; Fredenhagen, A.; Kühnöl, J.; Luneau, A.; Jian, Z.; Yang, Z.; Miao, Z.; Yang, F.; Jain, J. P.; Sunkara, G.; Mangold, J. B.; Stein, D. S. KAE609 (Cipargamin), a New Spiroindolone Agent for the Treatment of Malaria: Evaluation of the Absorption, Distribution, Metabolism, and Excretion of a Single Oral 300-mg Dose of [14C]KAE609 in Healthy Male Subjects. *Drug Metab. Dispos.* **2016**, *44* (5), 672-682.
30. White, N. J.; Pukrittayakamee, S.; Phyo, A. P.; Rueangweerayut, R.; Nosten, F.; Jittamala, P.; Jeeyapant, A.; Jain, J. P.; Lefèvre, G.; Li, R.; Magnusson, B.; Diagana, T. T.; Leong, F. J. Spiroindolone KAE609 for Falciparum and Vivax Malaria. *N. Engl. J. Med.* **2014**, *371* (5), 403-410.

31. White, N. J.; Duong, T. T.; Uthaisin, C.; Nosten, F.; Phyo, A. P.; Hanboonkunupakarn, B.; Pukrittayakamee, S.; Jittamala, P.; Chuthasmit, K.; Cheung, M. S.; Feng, Y.; Li, R.; Magnusson, B.; Sultan, M.; Wieser, D.; Xun, X.; Zhao, R.; Diagana, T. T.; Pertel, P.; Leong, F. J. Antimalarial Activity of KAF156 in Falciparum and Vivax Malaria. *N. Engl. J. Med.* **2016**, *375* (12), 1152-1160.
32. Sulyok, M.; Rückle, T.; Roth, A.; Mürbeth, R. E.; Chalon, S.; Kerr, N.; Samec, S. S.; Gobeau, N.; Calle, C. L.; Ibáñez, J.; Sulyok, Z.; Held, J.; Gebru, T.; Granados, P.; Brückner, S.; Nguetse, C.; Mengue, J.; Lalremruata, A.; Sim, B. K. L.; Hoffman, S. L.; Möhrle, J. J.; Kremsner, P. G.; Mordmüller, B. DSM265 for Plasmodium Falciparum Chemoprophylaxis: A Randomised, Double Blinded, Phase 1 Trial with Controlled Human Malaria Infection. *Lancet Infect. Dis.* **2017**, *7* (6), 636-644.
33. Phillips, M. A.; Lotharius, J.; Marsh, K.; White, J.; Dayan, A.; White, K. L.; Njoroge, J. W.; El Mazouni, F.; Lao, Y.; Kokkonda, S.; Tomchick, D. R.; Deng, X.; Laird, T.; Bhatia, S. N.; March, S.; Ng, C. L.; Fidock, D. A.; Wittlin, S.; Lafuente-Monasterio, M.; Benito, F. J. G.; Alonso, L. M. S.; Martinez, M. S.; Jimenez-Diaz, M. B.; Bazaga, S. F.; Angulo-Barturen, I.; Haselden, J. N.; Louttit, J.; Cui, Y.; Sridhar, A.; Zeeman, A. M.; Kocken, C.; Sauerwein, R.; Dechering, K.; Avery, V. M.; Duffy, S.; Delves, M.; Sinden, R.; Ruecker, A.; Wickham, K. S.; Rochford, R.; Gahagen, J.; Iyer, L.; Riccio, E.; Mirsalis, J.; Bathhurst, I.; Rueckle, T.; Ding, X.; Campo, B.; Leroy, D.; Rogers, M. J.; Rathod, P. K.; Burrows, J. N.; Charman, S. A. A Long-Duration Dihydroorotate Dehydrogenase Inhibitor (DSM265) for Prevention and Treatment of Malaria. *Sci. Transl. Med.* **2015**, *7* (296), 296ra111.
34. Paquet, T.; Le Manach, C.; Cabrera, D. G.; Younis, Y.; Henrich, P. P.; Abraham, T. S.; Lee, M. C. S.; Basak, R.; Ghidelli-Disse, S.; Lafuente-Monasterio, M. J.; Bantscheff, M.; Ruecker, A.; Blagborough, A. M.; Zakutansky, S. E.; Zeeman, A. M.; White, K. L.; Shackleford, D. M.; Mannila, J.; Morizzi, J.; Scheurer, C.; Angulo-Barturen, I.; Santosmartínez, M.; Ferrer, S.; Sanz, L. M.; Gamo, F. J.; Reader, J.; Botha, M.; Dechering, K. J.; Sauerwein, R. W.; Tungtaeng, A.; Vanachayangkul, P.; Lim, C. S.; Burrows, J.; Witty, M. J.; Marsh, K. C.; Bodenreider, C.; Rochford, R.; Solapure, S. M.; Jiménez-Díaz, M. B.; Wittlin, S.; Charman, S. A.; Donini, C.; Campo, B.; Birkholtz, L. M.; Khanson, K.; Drewes, G.; Kocken, C. M.; Delves, M. J.; Leroy, D.; Fidock, D. A.; Waterson, D.; Street, L. J.; Chibale, K. Antimalarial Efficacy of MMV390048, an

Inhibitor of Plasmodium Phosphatidylinositol 4-Kinase. *Sci. Transl. Med.* **2017**, *9* (387), eaad9735.

35. Baragaña, B.; Hallyburton, I.; Lee, M. C. S.; Norcross, N. R.; Grimaldi, R.; Otto, T. D.; Proto, W. R.; Blagborough, A. M.; Meister, S.; Wirjanata, G.; Ruecker, A.; Upton, L. M.; Abraham, T. S.; Almeida, M. J.; Pradhan, A.; Porzelle, A.; Martínez, M. S.; Bolscher, J. M.; Woodland, A.; Norval, S.; Zuccotto, F.; Thomas, J.; Simeons, F.; Stojanovski, L.; Osuna-Cabello, M.; Brock, P. M.; Churcher, T. S.; Sala, K. A.; Zakutansky, S. E.; Jiménez-Díaz, M. B.; Sanz, L. M.; Riley, J.; Basak, R.; Campbell, M.; Avery, V. M.; Sauerwein, R. W.; Dechering, K. J.; Noviyanti, R.; Campo, B.; Frearson, J. A.; Angulo-Barturen, I.; Ferrer-Bazaga, S.; Gamo, F. J.; Wyatt, P. G.; Leroy, D.; Siegl, P.; Delves, M. J.; Kyle, D. E.; Wittlin, S.; Marfurt, J.; Price, R. N.; Sinden, R. E.; Winzeler, E. A.; Charman, S. A.; Bebrevska, L.; Gray, D. W.; Campbell, S.; Fairlamb, A. H.; Willis, P. A.; Rayner, J. C.; Fidock, D. A.; Read, K. D.; Gilbert, I. H. A Novel Multiple-Stage Antimalarial Agent That Inhibits Protein Synthesis. *Nature* **2015**, *522* (7556), 315-320.
36. Yuthavong, Y.; Tarnchompoo, B.; Vilaivan, T.; Chitnumsub, P.; Kamchonwongpaisan, S.; Charman, S. A.; McLennan, D. N.; White, K. L.; Vivas, L.; Bongard, E.; Thongphanchang, C.; Taweechai, S.; Vanichtanankul, J.; Rattanajak, R.; Arwon, U.; Fantauzzi, P.; Yuvaniyama, J.; Charman, W. N.; Matthews, D. Malarial Dihydrofolate Reductase as a Paradigm for Drug Development against a Resistance-Compromised Target. *Proc. Natl. Acad. Sci.* **2012**, *109* (42), 16823-16828.
37. Abbat, S.; Jain, V.; Bharatam, P. V. Origins of the Specificity of Inhibitor P218 toward Wild-Type and Mutant PfDHFR: A Molecular Dynamics Analysis. *J. Biomol. Struct. Dyn.* **2015**, *33* (9), 1913-1928.
38. Vangapandu, S.; Jain, M.; Kaur, K.; Patil, P.; Patel, S. R.; Jain, R. Recent Advances in Antimalarial Drug Development. *Medicinal Research Reviews* **2007,** *27* (1), 65-107.
39. Bloechliger, M.; Schlagenhauf, P.; Toovey, S.; Schnetzler, G.; Tatt, I.; Tomianovic, D.; Jick, S. S.; Meier, C. R. Malaria Chemoprophylaxis Regimens: A Descriptive Drug Utilization Study. *Travel Med. Infect. Dis.* **2014**, *12*, 718-725.
40. Freedman, D. O. Malaria Prevention in Short-Term Travelers. *N Engl J Med.* **2008**, *359*, 603–612.

41. Lee, V. J.; Ow, S.; Heah, H.; Tan, M. Y.; Lam, P.; Ng, L. C.; Lam-Phua, S. G.; Imran, A. Q.; Seet, B. Elimination of Malaria Risk through Integrated Combination Strategies in a Tropical Military Training Island. *Am. J. Trop. Med. Hyg.* **2010,** *82* (6), 1024-1029.
42. Njoroge, M.; Njuguna, N. M.; Mutai, P.; Ongarora, D. S. B.; Smith, P. W.; Chibale, K. Recent Approaches to Chemical Discovery and Development against Malaria and the Neglected Tropical Diseases Human African Trypanosomiasis and Schistosomiasis. *Chem. Rev.* **2014**, *114*, 11138–11163.
43. Jong, E. C. Schistosomiasis. In *Netter's Infectious Disease* **2011**, *85*, 516-521.
44. Chitsulo, L.; Engels, D.; Montresor, A.; Savioli, L. The Global Status of Schistosomiasis and Its Control. *Acta Trop.* **2000**, *77* (1), 41–51.Ross, A. G. P.; Bartley, P. B.; Sleigh, A. C.; Olds, G. R.; Li, Y.; Williams, G. M.; McManus, D. P. Schistosomiasis. *N. Engl. J. Med.* **2002**, *346* (16), 1212-1220.
45. Ross, A. G. P.; Bartley, P. B.; Sleigh, A. C.; Olds, G. R.; Li, Y.; Williams, G. M.; McManus, D. P. Schistosomiasis. *N. Engl. J. Med.* **2002**, *346* (16), 1212-1220.
46. Ferrari, T. C. A.; Moreira, P. R. R. Neuroschistosomiasis: Clinical Symptoms and Pathogenesis. *The Lancet Neurology* **2011**, *10* (9), 853-864.
47. Shebel, H. M.; Elsayes, K. M.; Abou El Atta, H. M.; Elguindy, Y. M.; El-Diasty, T. A. Genitourinary Schistosomiasis: Life Cycle and Radiologic-Pathologic Findings. *RadioGraphics* **2012**, *32* (4), 1035-1044.
48. Gryseels, B. Schistosomiasis. *Infectious Disease Clinics of North America* **2012**, *26* (2), 383-397.
49. Gryseels, B.; Polman, K.; Clerinx, J.; Kestens, L. Human Schistosomiasis. *Lancet* **2006**, *368* (9541), 1106-1118.
50. Center for Disease Control and Prevention. *Parasites - Schistosomiasis*. **2012**.
51. Ingram-Sieber, K.; Cowan, N.; Panic, G.; Vargas, M.; Mansour, N. R.; Bickle, Q. D.; Wells, T. N. C.; Spangenberg, T.; Keiser, J. Orally Active Antischistosomal Early Leads Identified from the Open Access Malaria Box. *PLoS Negl. Trop. Dis.* **2014**, *8*, 1–30.
52. Cioli, D.; Pica-Mattoccia, L. Praziquantel. *Parasitol. Res.* **2003,** *90*, 3–9.
53. Keiser, J.; Utzinger, J. Antimalarials in the Treatment of Schistosomiasis. *Curr. Pharm. Des.* **2012**, *18*, 3531–3538.

54. Olliaro, P.; Delgado-Romero, P.; Keiser, J. The Little We Know about the Pharmacokinetics and Pharmacodynamics of Praziquantel (Racemate and R-Enantiomer). *Journal of Antimicrobial Chemotherapy* **2014**, *69* (4), 863-870.
55. White, N. J. Artemisinin Resistance--the Clock Is Ticking. *Lancet* **2010**, *376* (9758), 2051-2052.
56. Hanboonkunupakarn, B.; White, N. J. The Threat of Antimalarial Drug Resistance. *Trop. Dis. Travel Med. Vaccines* **2016**, *14* (6), 548-550.
57. Ray, S.; Madrid, P. B.; Catz, P.; Levalley, S. E.; Furniss, M. J.; Rausch, L. L.; Guy, R. K.; Derisi, J. L.; Iyer, L. V.; Green, C. E.; Mirsalis, J. C. Development of a New Generation of 4-Aminoquinoline Antimalarial Compounds Using Predictive Pharmacokinetic and Toxicology Models. *J. Med. Chem.* **2010**, *53*, 3685-3695.
58. Keseru, G. M.; Makara, G. M. Hit Discovery and Hit-to-Lead Approaches. *Drug Discovery Today* **2006**, *11* (15-16), 741-748.
59. Swinney, D. C.; Anthony, J. How Were New Medicines Discovered? *Nat. Rev. Drug Discov.* **2011**, *10* (7), 507-519.
60. Chen, X. P.; Du, G. H. Target Validation: A Door to Drug Discovery. *Drug Discov. Ther.* **2007**, *1* (1), 23-29.
61. Swinney, D. C. Phenotypic vs. Target-Based Drug Discovery for First-in-Class Medicines. *Clinical Pharmacology and Therapeutics* **2013**, *93* (4), 299-301.
62. Mamanova, L.; Coffey, A. J.; Scott, C. E.; Kozarewa, I.; Turner, E. H.; Kumar, A.; Howard, E.; Shendure, J.; Turner, D. J. Target-Enrichment Strategies for next-Generation Sequencing. *Nature Methods* **2010**, *7*, 111–118.
63. Zheng, W.; Thorne, N.; McKew, J. C. Phenotypic Screens as a Renewed Approach for Drug Discovery. *Drug Discovery Today* **2013**, 18 (21-22),1067-1073.
64. Ashburn, T. T.; Thor, K. B. Drug Repositioning: Identifying and Developing New Uses for Existing Drugs. *Nat. Rev. Drug Discov.* **2004**, *3*, 673–683.
65. Nzila, A.; Ma, Z.; Chibale, K. Drug Repositioning in the Treatment of Malaria and TB. *Future Med. Chem.* **2011**, *3*, 1413–1426.
66. Goldberg, D. E.; Slater, A. F.; Cerami, A.; Henderson, G. B. Hemoglobin Degradation in the Malaria Parasite Plasmodium Falciparum: An Ordered Process in a Unique Organelle. *Proc. Natl. Acad. Sci.* **1990**, *87* (8), 2931-2935.

67. Francis, S. E.; Sullivan, D. J.; Goldberg, D. E. Hemoglobin Metabolism in the Malaria Parasite Plasmodium Falciparum. *Annu. Rev. Microbiol.* **1997**, *51*, *97*-123.
68. Basilico, N.; Pagani, E.; Monti, D.; Olliaro, P.; Taramelli, D. A Microtitre-Based Method for Measuring the Haem Polymerization Inhibitory Activity (HPIA) of Antimalarial Drugs. *J. Antimicrob. Chemother.* **1998**, *42* (1), 55-60.
69. Fong, K. Y.; Wright, D. W. Hemozoin and Antimalarial Drug Discovery. *Future Medicinal Chemistry* **2013**, *5* (12), 1437-1450.
70. Savjani, K. T.; Gajjar, A. K.; Savjani, J. K. Drug Solubility: Importance and Enhancement Techniques. *ISRN Pharm.* **2012**, *2012*, 1–10.
71. Vasconcelos, T.; Sarmento, B.; Costa, P. Solid Dispersions as Strategy to Improve Oral Bioavailability of Poor Water Soluble Drugs. *Drug Discov Today* **2007**, *12*, 1068–1075.
72. Sekhon, B. Pharmaceutical Co-Crystals-a Review. *ARS Pharm.* **2009**, *50*, 99–117.
73. Brewster, M. E.; Loftsson, T. Cyclodextrins as Pharmaceutical Solubilizers. *Adv. Drug Deliv. Rev.* **2007**, *59*, 645–666.
74. Chierotti, M. R.; Gobetto, R. Solid-State NMR Studies of Weak Interactions in Supramolecular Systems. *Chemical Commun.* **2008**, *14*, 1621-1634.
75. Ishikawa, M.; Hashimoto, Y. Improvement in Aqueous Solubility in Small Molecule Drug Discovery Programs by Disruption of Molecular Planarity and Symmetry. *J. Med. Chem.* **2011**, *54* (6), 1539–1554.
76. Di, L.; Kerns, E. H. *Drug-Like Properties: Concepts, Structure Design and Methods from ADME to Toxicity Optimization*, 1st Ed.; Elsevier Inc, **2008**.

CHAPTER 2: PYRIDO[1,2-*a*]BENZIMIDAZOLES

2.1 Introduction

This chapter covers the design, synthesis, and characterization of the synthesized pyrido[1,2-*a*]benzimidazole (PBI) compounds. Various amine groups were introduced at the R_6 position of the PBI scaffold (**Figure 19**) in an attempt to maintain/ improve biological activity and enhance aqueous solubility. The modifications on the LHS portion of the PBI at positions R_1, R_2 and R_3 were aimed at improving both potency and metabolic stability.

A multistep protocol was employed to synthesize the target compounds using a synthetic route reported in literature.[1] The synthesized PBI derivatives were further characterized and tested for biological activity and their physicochemical properties analyzed.

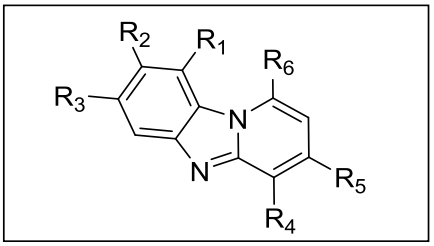

Figure 19: Generic pyrido[1,2-*a*]benzimidazole scaffold

2.1.1 Background

The chemical structure of benzimidazoles consists of two fused rings: a benzene and an imidazole (**Figure 20**). Benzimidazoles have shown favourable biological properties desirable in drug discovery.[2,3,4]

Pyrido[1,2-*a*]benzimidazoles are compounds composed of three fused rings: a pyridine, an imidazole and a benzene ring (**Figure 20**).

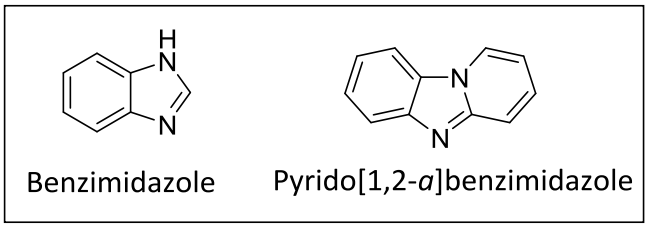

Figure 20: Chemical structures of benzimidazole and pyrido[1,2-*a*]benzimidazole.

2.1.2 Pharmacological activity

The benzimidazole and pyrido[1,2-*a*]benzimidazole class of molecules have shown a diverse range of pharmacological activities, including antifungal,[5] antioxidative,[6] and antiproliferative properties.[7]

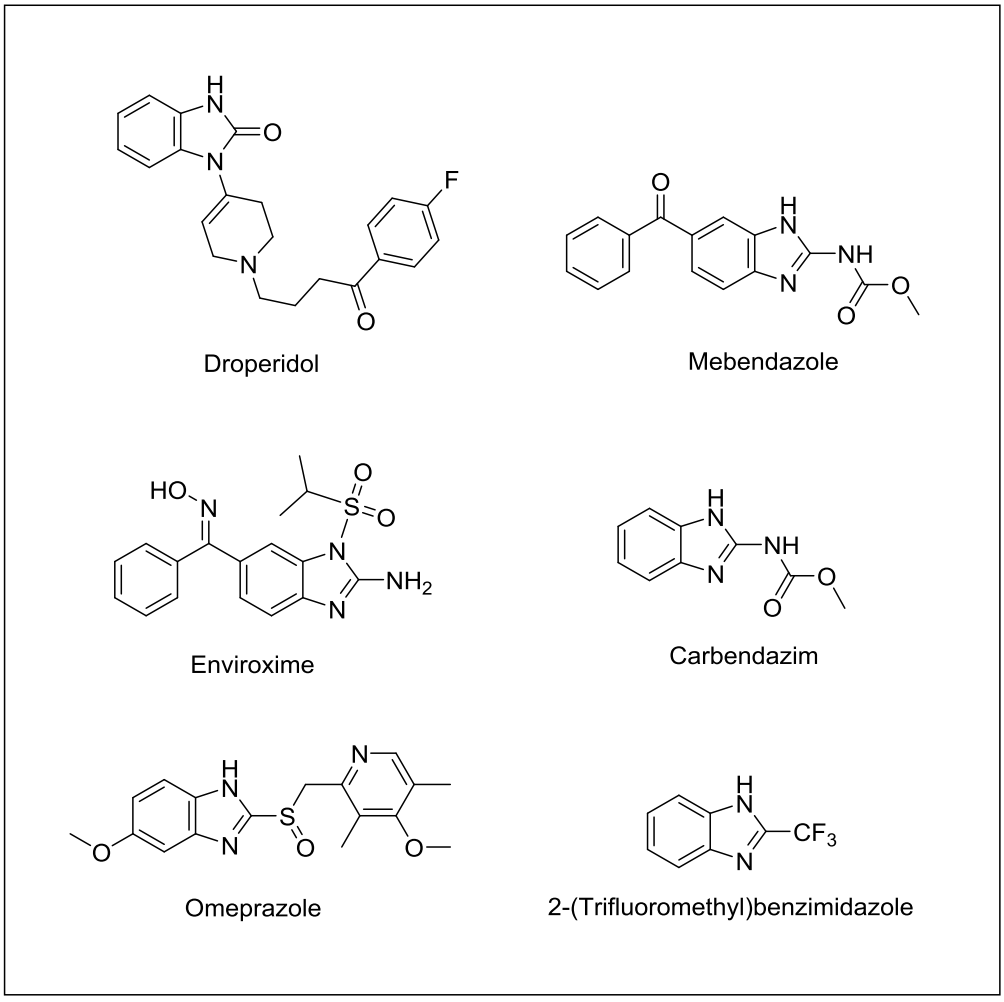

Figure 21: Examples of current drugs with benzimidazoles

There are compounds currently available for therapeutic uses that are composed of these heterocyclic fused ring systems. On the basis of their bicyclic structure, benzimidazole derivatives have been optimized in various disciplines and have led to the generation of various pharmacologically active drugs, for example: mebendazole used to treat parasitic worm infestations,[8,9] droperidol (an antidopaminergic drug), and omeprazole (used to treat gastroesophageal reflux) (**Figure 21**).[3,10,11] Methyl 2-benzimidazolecarbamate (carbendazim) is a potential anticancer agent; enviroxime possesses enhanced antiviral activity; and 2-(trifluoromethyl)benzimidazole derivatives have potent anti-protozoal activity.

Pyrido[1,2-*a*]benzimidazoles also possess a diverse range of pharmacological properties. **Figure 22** below shows various biologically active pyrido[1,2-*a*]benzimidazoles that demonstrate antifungal[12] and anticancer[13] properties.

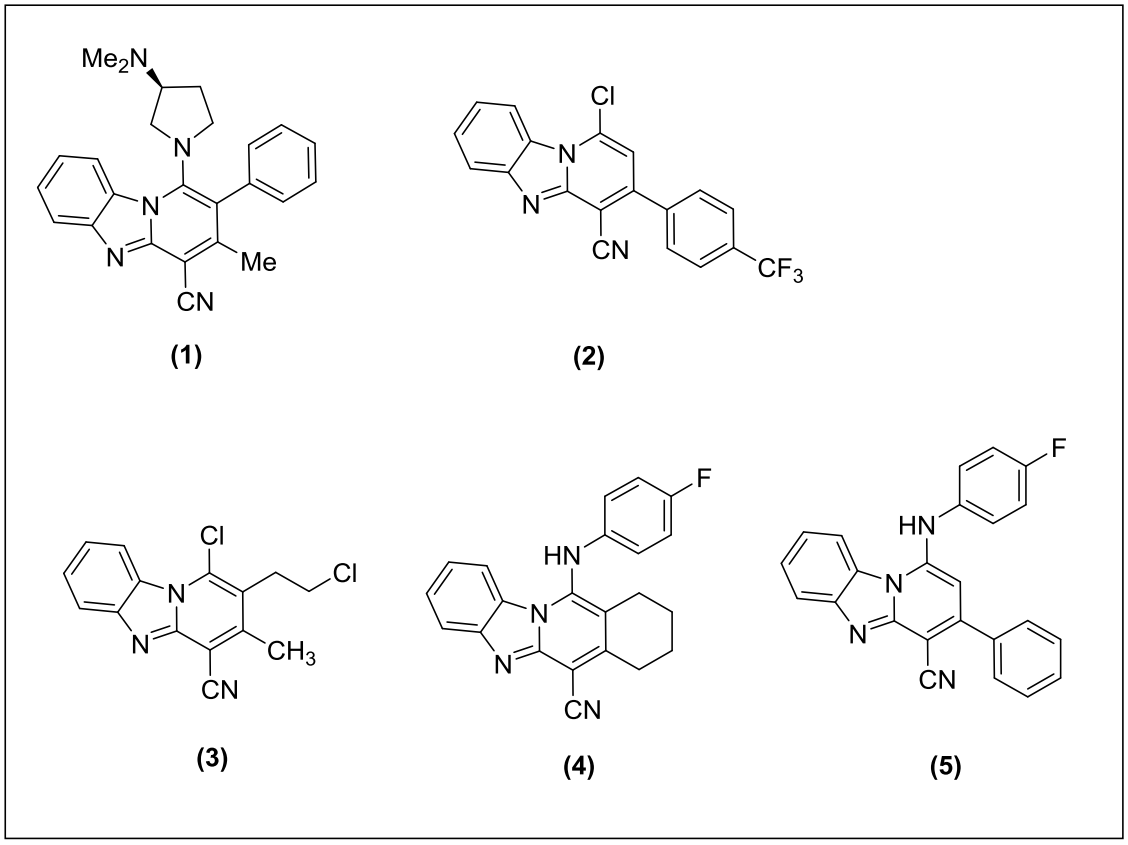

Figure 22: Pyrido[1,2-*a*]benzimidazole derivatives as antifungal **(1)** and anticancer **(2)**, **(3)**, **(4)**, **(5)** agents

2.1.3 Antimalarial activity

In 2000, a library of 1440 diverse non-proprietary compounds underwent *in vitro* screening against protozoa. Through this screen, a pyrido[1,2-*a*]benzimidazole (PBI) derivative, TDR15087 (**Figure 23**), was identified as moderately active against *Plasmodium falciparum* GHA and W2 strains (IC_{50} = 0.17 - 0.37 µM). As a result, the various *in vitro* antiplasmodium structure-activity relationships (SARs) of 535 PBI analogues were explored. These compounds were evaluated against the chloroquine-resistant *Pf* strain K1, and cytotoxicity was assessed against the mammalian L-6 cell-line. From this screen, over 7% of the compounds were identified as active (*Pf* IC_{50} < 0.1 µg/mL), including the *N*-benzylpiperazine analogs TDR35885 (*Pf* K1 IC_{50} = 0.050 - 0.078 µM) and TDR44047 (*Pf* K1 IC_{50} = 0.023 - 0.095 µM; **Figure 23**), which displayed both high selectivity and improved *in vitro* activity compared to that of TDR15087 (*Pf* K1 IC_{50} = 0.17 - 0.36 µM; **Figure 23**).[1]

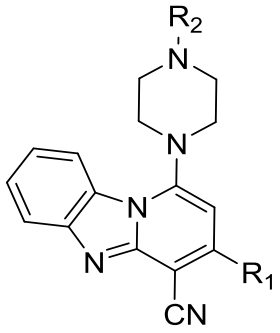

Code	R_1	R_2	*Pf* K1 IC_{50} (µM)
TDR15087	Ph	H	0.17 - 0.36
TDR35885	Me	CH_2Ph	0.050 - 0.078
TDR44047	n-Pr	$CH_2Ph(4\text{-}F)$	0.023 - 0.095

Figure 23: Pyrido[1,2-*a*]benzimidazole screening hits showing *in vitro* activity against *Plasmodium falciparum (Pf)*

Despite their *in vitro* antiplasmodium activity, these piperazinyl-based derivatives (**Figure 23**) showed poor *in vivo* activity in a *Plasmodium berghei*-infected mouse model at doses up to 4 x 100 mg/kg following intraperitoneal (ip) administration, presumably because of their low solubility and poor metabolic stability.[1] To address these challenges, SAR studies were

conducted, resulting in the synthesis of frontrunner PBIs with alkylamino side-chains as shown in **Figure 24**.[1]

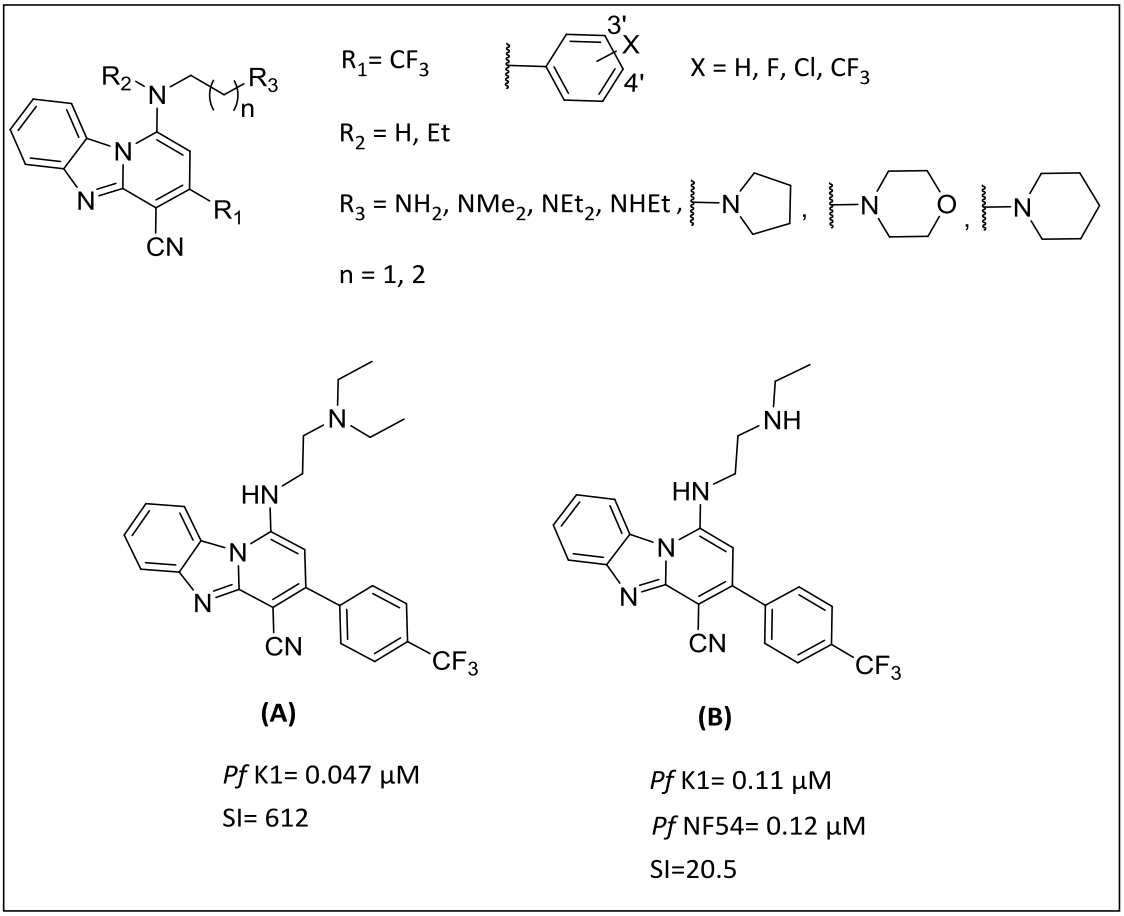

Figure 24: Structure-activity relationship study around the pyrido[1,2-*a*]benzimidazole core, showing potencies (IC_{50}) against the *Plasmodium falciparum (Pf)* strains NF54 (chloroquine-sensitive) and K1 (chloroquine-resistant), and the selectivity Index (SI) of lead compounds **A** and **B**

Lead compound **A** displayed sub-micromolar activity against the chloroquine-resistant *P. falciparum* strain K1 (IC_{50} = 0.047 µM; **Figure 24**) and negligible cytotoxicity against the mammalian cell-line L-6 (SI = 612). Compound **B**, the mono-desethyl metabolite of **A**, showed *in vitro* antiplasmodium activity against the chloroquine-sensitive *P. falciparum* strain NF54 (0.12 µM) and the chloroquine-resistant strain K1 (0.11 µM), and a SI of 20.5 when considering its cytotoxicity against the mammalian cell-line L-6.[1]

After evaluation of the compounds' *in vitro* microsomal metabolic stabilities in human, rat, and mouse liver microsomes (HLM, RLM, and MLM, respectively), compound **A** displayed a shorter degradation half-life (13.7 min in HLM, 24.8 min in RLM, and 24.1 min in MLM) compared to compound **B**, which exhibited a moderate half-life (136.8 min in HLM, 284.4 min in RLM, and 321.2 min in MLM).[1]

Single-dose oral efficacy studies were carried out in a *P. berghei*-infected mouse model using the hydrochloride salts of the most active compounds (**Table 2**). These compounds showed significant potency (**Table 2**) when administered at a dose of 25 mg/kg (compound **A** caused a 70.33% reduction in parasitemia on day 5) and 50 mg/kg (compound **A** caused a 78.22% reduction in parasitemia on day 5). However, antimalarial activity did not improve significantly at the higher dose, presumably due to systemic exposure saturation attributable to solubility-limited absorption. The orally administered salt of compound **B** was evaluated in single- and multi-dose *in vivo* efficacy studies in a *P. berghei*-infected mouse model. This revealed that efficacy increased with doses greater than 25 mg/kg. Administration of a 50 mg/kg dose caused 50.24%, 71.22%, and 79.79% reductions in parasitemia on days 3, 4, and 5, respectively (**Table 2**). A similar result was observed after subcutaneous administration. Preliminary systemic exposure studies following both oral and subcutaneous administration of the compound **B** salt also showed saturation at oral doses > 25 mg/kg and subcutaneous doses of 50 mg/kg. This replicated observation led to the conclusion that solubility-limited absorption resulted in poor bioavailability of the compounds, and thus in limited systemic exposure and poor efficacy with increasing dosage.[1]

Table 2: Oral efficacy of dihydrochloride salts of selected pyrido[1,2-*a*]benzimidazole compounds in a *Plasmodium berghei*-infected mouse model

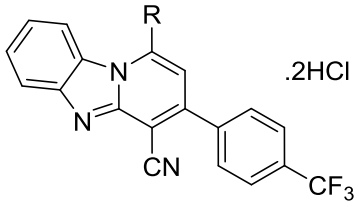

Compound	R	Dose (mg/kg)	% Reduction in parasitemia				MSD (days)
			Day 2	Day 3	Day 4	Day 5	
(A)	—$NH(CH_2)_2N(Et)_2$	1×50	5.15	29.76	59.97	78.22	8
(A)	—$NH(CH_2)_2N(Et)_2$	1×25	13.07	24.38	51.13	70.33	8
(B)	—$NH(CH_2)_2NHEt$	1×50	30.78	50.24	71.22	79.79	12.7
(B)	—$NH(CH_2)_2NHEt$	1×25	23.51	55.45	62.25	68.92	13.3
1.3	—$NH(CH_2)_2N$	1×50	14.04	47.92	73.01	88.53	8.7
1.3	—$NH(CH_2)_2N$	1×25	14.75	43.20	63.73	63.72	7.7
1.4	—$NH(CH_2)_2N$	1×50	23.38	9.30	0.00	0.00	5
1.4	—$NH(CH_2)_2N$	1×25	28.44	28.07	38.72	46.41	12.7
Chloroquine		1×10	99.99	-	-	-	9
Control		-	-	-	-	-	5

MSD, mean survival days

Further SAR investigations were carried out on the PBI frontrunner compound **B** (**Figure 24**) to generate other PBI derivatives with enhanced pharmacokinetic (PK) profiles, and to explore SARs by evaluating the effect of diverse changes around the scaffold on potency and

oral absorption in a mouse model. A summary of the various SAR studies of the PBI chemical series is shown in **Figure 25**.[14]

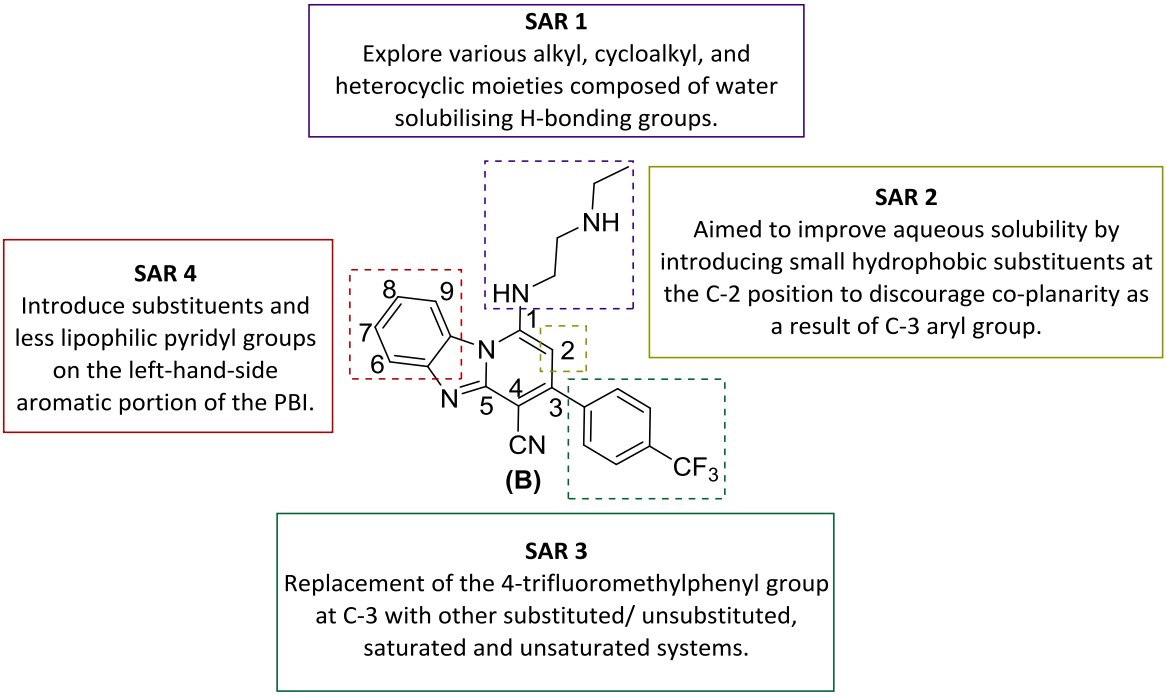

Figure 25: Summary of structure-activity relationship studies carried out on lead compound **B**, which showed activity against chloroquine-sensitive (NF54) and chloroquine-resistant (K1) *Plasmodium falciparum* strains

From this SAR study, compounds with favourable antiplasmodium activity, adequate solubility, and high microsomal stability were selected for further *in vivo* evaluation in a *P. berghei*-infected mouse model. The compounds' *in vitro* efficacy against the *Pf* NF54 strain and the *in vivo* oral efficacy of prioritized PBIs in *P. berghei*-infected mice are listed in **Table 3**. The test compounds were administered orally for 4 successive days at different time intervals (4, 24, 48, and 72 h) after infection with *P. berghei*.[14]

Table 3: Antiplasmodium activity against the chloroquine-sensitive *Plasmodium falciparum* strain NF54 and *in vivo* oral efficacy of prioritized pyrido[1,2-*a*]benzimidazoles in *Plasmodium berghei*-infected mice

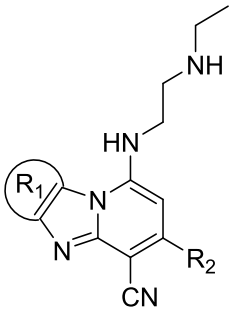

Compound	R_1	R_2	*Pf* NF54 IC_{50} (µM)	Oral dose (mg/kg)	% Reduction in parasitemia (MSD)[b]	Cured/ infected mice
(B)[a]	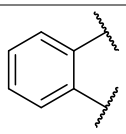	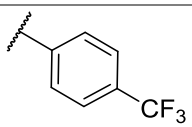	0.120	4 X 50 4 X 25 4 X 12.5 4 X 6 4 X 3	96.0 (14) 96.0 (14) 81.0 (14) 38.0 (7) 0(4)	0/3 0/3 0/3 0/3 0/3
2.1	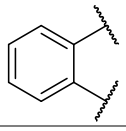	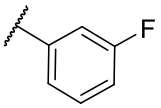	0.380	4 X 50	61.0 (24)	1/3
2.2	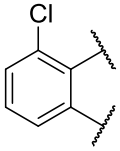	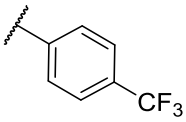	0.140	4 X 50	85.0 (7)	0/3
2.3	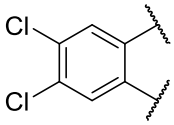	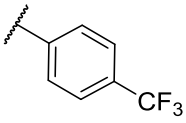	0.020	4 X 50 4 X 30 4 X 10 4 X 3	98.0 (30) 99.7 (30) 99.6 (18) 99.5 (17)	3/3 3/3 0/3 0/3
2.4	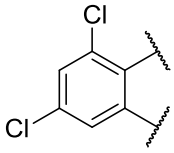	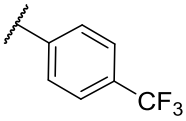	0.030	4 X 50 4 X 30 4 X 10 4 X 3	98.0 (30) 99.4 (30) 99.4 (18) 99.4 (16)	3/3 2/3 0/3 0/3
Chloroquine			0.016	4 X 30	99.9 (24)	0/10

MSD, mean survival days
a = HCl salt of compound was used

Although compound **2.1** (*Pf* NF54 IC_{50} = 0.38 µM) displayed lower *in vitro* antiplasmodium activity than compounds **B** (*Pf* NF54 IC_{50} = 0.12 µM) and **2.2** (*Pf* NF54 IC_{50} = 0.14µM), it displayed high microsomal stability (89% and 100% remaining in HLM and MLM, respectively, after 30 min) and improved *in vivo* efficacy (one mouse cured after administration of 4 x 50 mg/kg doses, **Table 3**). Compounds **2.3** (*Pf* NF54 IC_{50} = 0.02 µM) and **2.4** (*Pf* NF54 IC_{50} = 0.03 µM) showed improvement in *in vitro* antiplasmodium activity and retained microsomal stability (> 80% remaining in HLM and MLM after 30 min) compared to lead compound **B.** In the *in vivo* efficacy assessment, compounds **2.3** and **2.4** were completely curative after administration of 4 x 50 mg/kg doses. However, administration of lower dosages (4 x 10 mg/kg and 4 x 3 mg/kg), did not cure the infected mice. Subsequent PK studies were pursued for compounds **2.3** and **2.4**. The assay was carried out in mice receiving oral or intravenous doses of 10 mg/kg and 2.5 mg/kg, respectively. Both compounds showed slow rates of absorption (T_{max} ≥ 10 h) and elimination (CL < 30 mL/min/kg). Compounds **2.3** and **2.4** showed similar PK profiles as compound **B** in *P. berghei*-infected mice. This suggests that the improvement observed in the *in vivo* activities of compounds **2.3** and **2.4** is likely attributable to their improved antiplasmodium potencies rather than a result of their improved PK profiles.[14]

Mechanistic studies were also carried out to investigate the potential of PBIs to inhibit the formation of hemozoin (Hz). Results obtained from the β-hematin inhibitory activity (BHIA) assay showed that overall, this class of compounds are inhibitors of β-hematin formation (IC_{50} < 100 µM). This suggests that the hemoglobin degradation pathway is a potential contributory target of this set of compounds.[14]

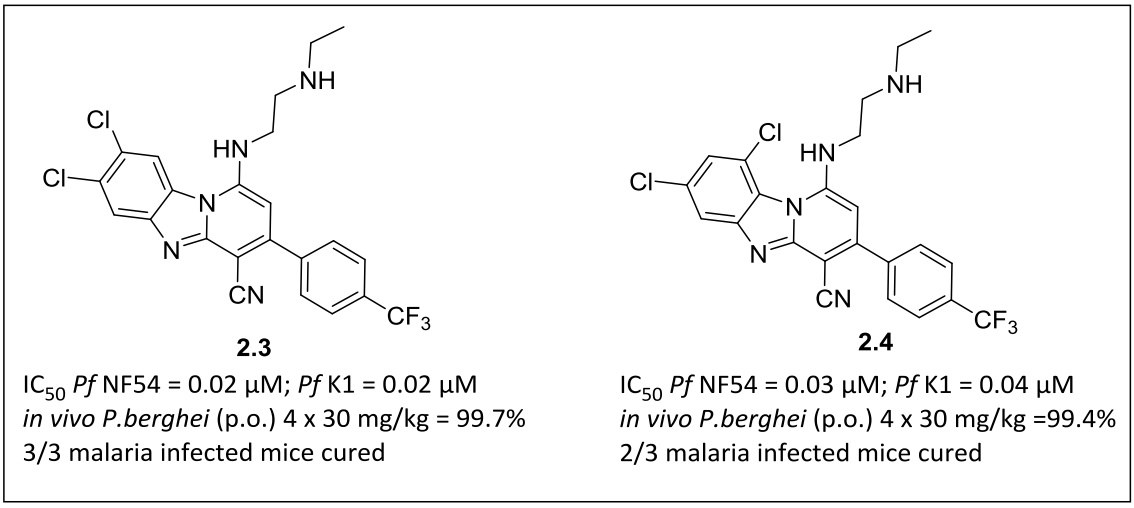

Figure 26: Structures of compounds **2.3** and **2.4**, which showed potent *in vitro* activity and improved *in vivo* oral efficacy in a *Plasmodium berghei*-infected mouse model

(Pf, Plasmodium falciparum; p.o., per oral)

The structures of compounds **2.3** and **2.4**, which showed improved potency, metabolic stability, and significantly better *in vivo* oral efficacy in a *P. berghei*-infected mouse model, are shown in **Figure 26**. These compounds also displayed high activity against the *P. berghei* liver and *P. falciparum* gametocyte stages, making them potential multistage-acting drug candidates.[14]

2.1.4 Antischistosomal activity

The *in vitro* and *in vivo* antischistosomal efficacies of PBIs explored in a recent study[15] are listed in **Table 4**. In this study, several compounds (10 µM) were screened against newly transformed schistosomula (NTS; **Table 4**). Compounds that caused > 70% inhibition of worm viability were further evaluated against adult *Schistosoma mansoni* at the same initial concentration of 10 µM. Subsequent studies to determine IC_{50} values were carried out against adult *S. mansoni*.[15]

Ten compounds were selected based on their potent *in vitro* activity against NTS and adult *S. mansoni*, favourable cytotoxicity, and moderate to good metabolic stability, and their *in vivo* efficacies against adult *S. mansoni* were further evaluated. Of these compounds, 70% possessed moderate *in vivo* activity, showing < 50% reduction in both total and female

worm (TW and FW, respectively) burden. In mice treated with 400 mg/kg compound **B**, no reduction in FW or TW burden was observed. However, compounds **3.1** and **3.2** (**Table 4**) showed significant TW and FW reduction, which, although lower than the parasite burden reduction caused by treatment with praziquantel,[16] is superior to that caused by other derivatives reported in the literature.[17–20]

Table 4: Percentage reduction and IC_{50} against adult *Schistosoma mansoni*, metabolic stability in mouse liver microsomes, and total and female worm burden reduction in 49-day-old adult *S. mansoni*-infected mice treated with a single 400 mg/kg oral dose

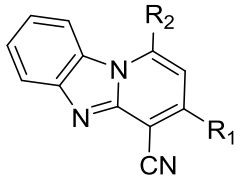

Compound	R_1	R_2	IC_{50} against adult *Schistosoma mansoni*	TWR (%)	FWR (%)	Met. Stab. (% remaining after 30 min of incubation in MLMs)
B	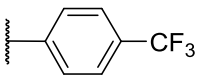	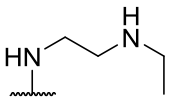	2.41	0.0	0.0	97 ± 8.3
3.1	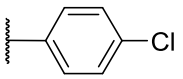	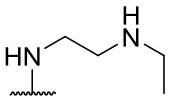	2.44	58.7	61.3	69 ± 10.8
3.2	CF_3	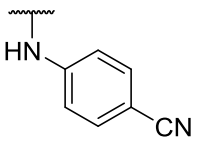	0.21	54.9	54.3	97 ± 6.1

TWR, total worm reduction; FWR, female worm reduction; Met. Stab., metabolic stability; MLM, mouse liver microsomes

PK analysis was carried out to evaluate the PK profile of compound **3.1** administered orally at a dose of 20 mg/kg and intravenously at a dose of 2 mg/kg in mice. The compound showed slow and incomplete absorption when administered orally (25% at a dose of 20 mg/kg), presumably because of low systemic exposure attributable to solubility-limited

absorption and a short half-life. Although the compounds in this study showed relatively low *in vivo* antischistosomal potency, significant efficacy was observed in *S. mansoni*-infected mice for compounds **3.1** (TWR = 58.7%, FWR = 61.3%) and **3.2** (TWR = 54.9%, FWR = 54.3%; **Table 4**). This suggests that further evaluation of this series of compounds is needed to expand SARs and to produce PBIs with improved *in vivo* antischistosomal efficacy. The structures of compounds **3.1** and **3.2**, which showed significant worm burden reduction efficacy, are shown in **Figure 27**.

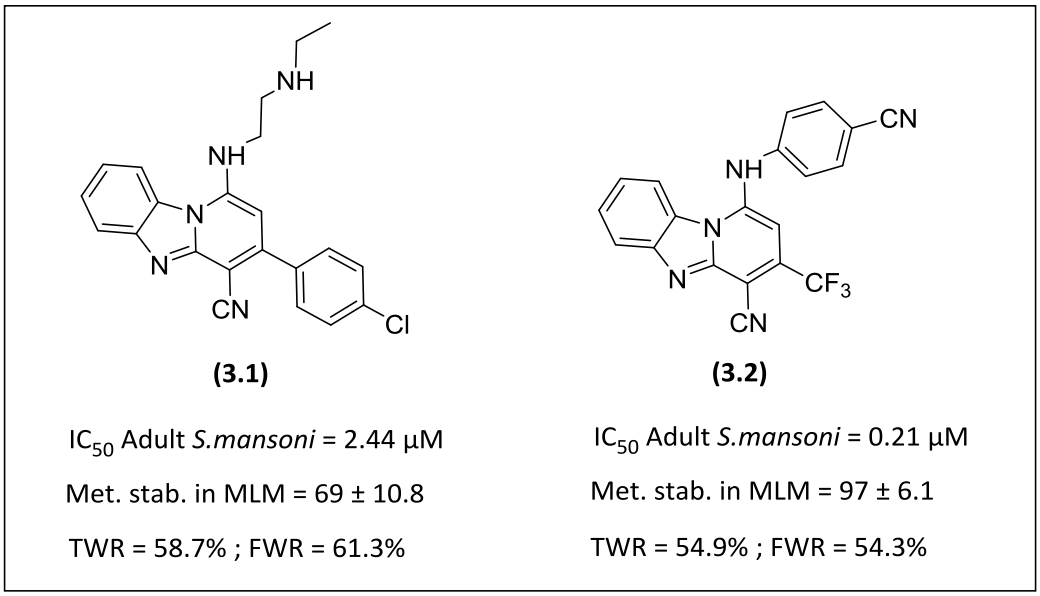

Figure 27: Structures of pyrido[1,2-*a*]benzimidazole derivatives and their potencies (IC_{50}) against adult *Schistosoma mansoni* (Met. stab., metabolic stability; MLM, mouse liver microsomes; TWR, total worm reduction; FWR, female worm reduction)

2.2 Aims and Objectives

2.2.1 Main Objective

The main objective of this project was to improve the potency and solubility profiles of antimalarial and antischistosomal piperazine-based pyrido[1,2-*a*]benzimidazoles.

2.2.2 Research Question/ Hypothesis

Is it possible to identify potential pyrido [1,2-*a*] benzimidazole-based antimalarial and antischistosomal drug leads with favourable solubility, cytotoxicity and *in vitro* potency?

2.2.3 Specific Aims

i) Synthesis and characterization of piperazine-based pyrido[1,2-*a*]benzimidazoles designed to improve pharmacological activity and/or solubility.

ii) Profiling of synthesized compounds with respect to antiplasmodium and antischistosomal activities as well as solubility.

iii) Derivation of antiplasmodium and antischistosomal structure-activity relationship (SAR) as well as solubility structure property relationship (SPR) profiles.

iv) Investigation of the factors (e.g. melting point, CLogP, and retention time on reversed-phase HPLC) affecting solubility and deduce relationships.

2.3 Rationale

This project aims to expand the SAR around the *N*-benzylpiperazine hit, TDR44047 (**Figure 23**) by executing medicinal chemistry modifications on the PBI core (**Figure 28**) with the aim of improving biological activity, solubility and metabolic stability.

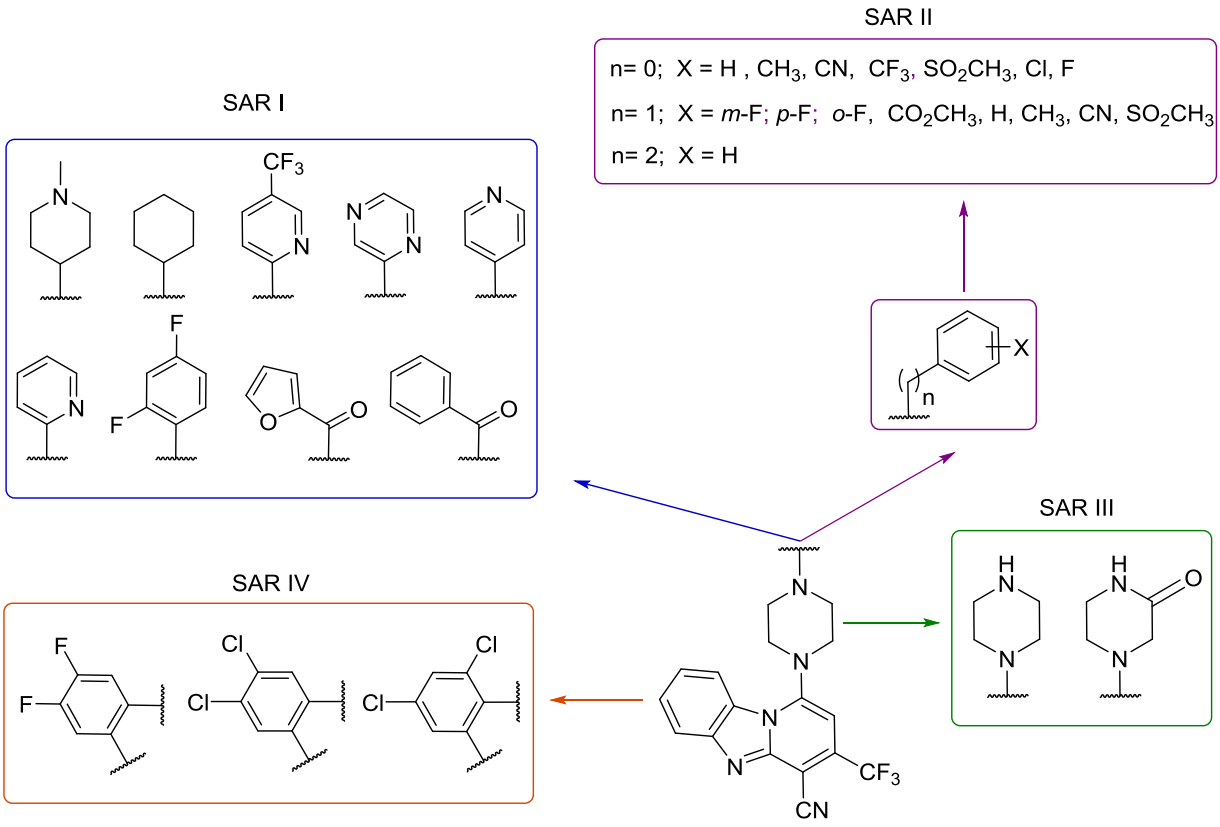

Figure 28: Chemistry SAR Plan for the synthesis of new piperazine-based pyrido[1,2-*a*]benzimidazole derivatives with four regions of diversity, incorporating various solubility enhancement strategies

In SAR I, aryl- and carboxamide-linked analogues as well as analogues containing saturated ring systems, were designed. SAR II was guided by the Craig Plot illustrated in **Figure 29** below. Craig plot X substituents were chosen from the various quadrants in order to synthesize target molecules with diverse lipophilic and electronic substituents. This SAR also included the exploration of various linkers: analogues were either directly linked, methylene-linked or ethylene linked to the piperazine moiety attached to the PBI core. Regioisomerism was also examined in SAR II, where positional isomers were synthesized, i.e. compounds with the same Craig plot X substituent at *ortho*, *meta*, and *para* positions (**Figure 28**). SAR III investigates the effect of introducing a carbonyl moiety on the piperazine ring to lower the lipophilicity of the compound and thereby potentially improve its solubility profile. SAR IV focuses on potentially improving the potency and metabolic stability of the generated compounds based on prior work already mentioned.

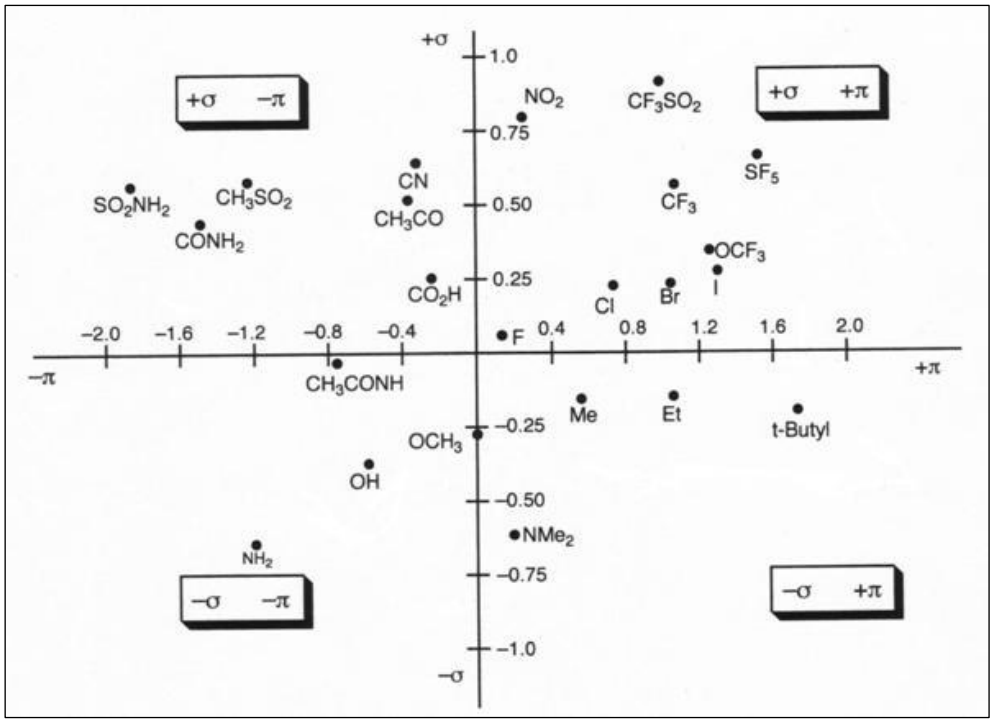

Figure 29: Craig plot substituents

The screening cascade summarizes the project work flow followed and the criterion required for progression through the flow chart (**Figure 30**). The work flow began with the synthesis and characterization of various PBI derivatives which were then subjected to *in vitro* antiplasmodium and antischistosomal testing. This exercise was conducted in parallel with solubility profiling, β-hematin inhibition activity, and gametocyte stage assays. Analogues that met the micromolar criterion in the *in vitro* antiplasmodium and antischistosomal activity assays were further evaluated for cytotoxicity against the mammalian Chinese Hamster Ovarian (CHO) cell line, aiming for a selectivity index (SI) of at least 10. Although not done in the context of this thesis work, compounds with an acceptable cytotoxicity profile would be assessed for *in vitro* metabolic stability. Analogues regarded as metabolically stable (i.e. 75% of its parent compound present after 30 minutes), would be further prioritized for *in vivo* pharmacokinetics (PK) to establish primary PK parameters such as bioavailability (F) and half-life ($T_{1/2}$) for the ultimate *in vivo* efficacy studies in a mouse model. Alternatively, *in vivo* efficacy studies on the *in vitro* metabolically stable compounds would be performed followed by *in vivo* PK (**Figure 30**).

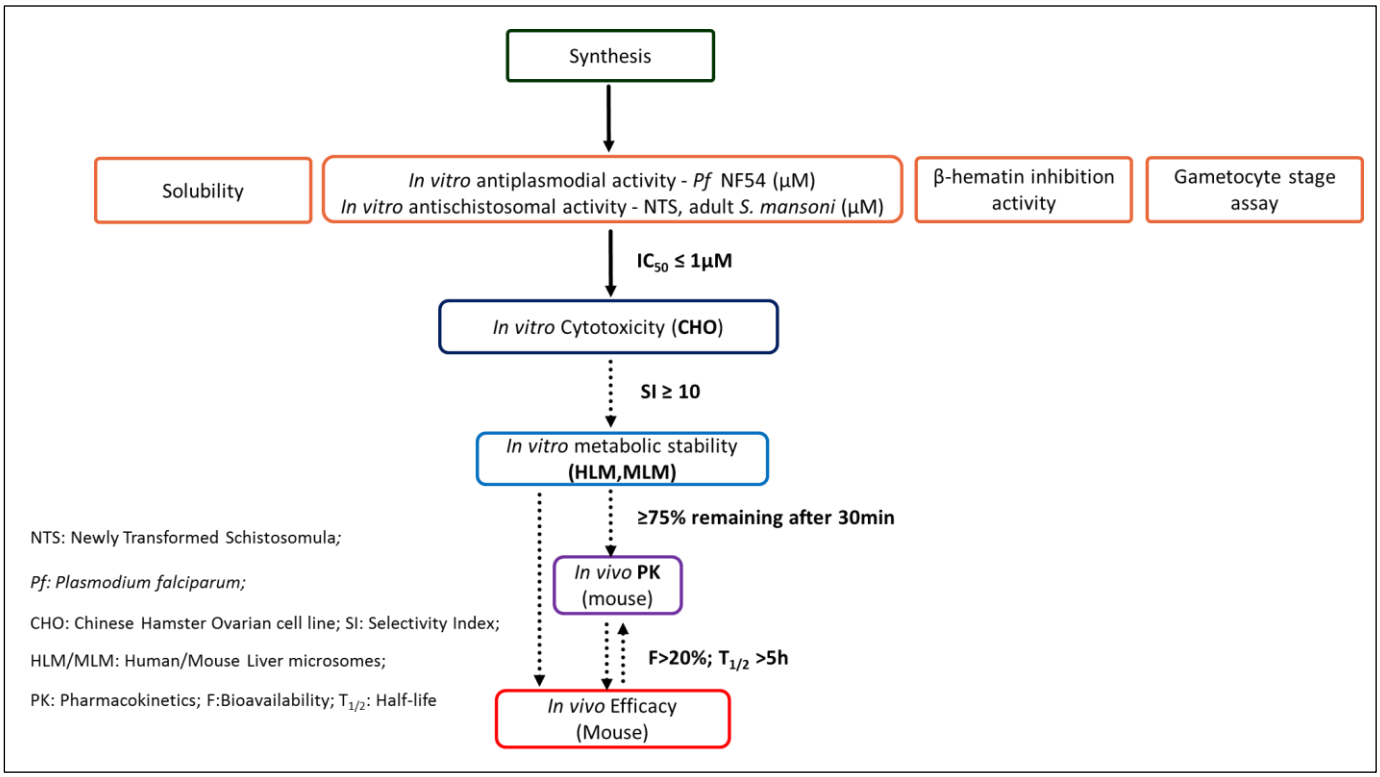

Figure 30: Screening cascade outlining the research programme from synthesis to *in vitro* cytotoxicity profiling

2.4 Synthesis and Characterization

2.4.1 Introduction

Structural modifications have been employed to explore structure-activity and structure-property relationships in order to furnish PBI analogues with potentially improved solubility, antiplasmodium and antischistosomal potencies.

The synthetic methodology that was employed by Ndakala *et al.,* was adopted to afford the various synthesized compounds (**Schemes 1 & 5**). **Scheme 1** shows the steps followed in the synthesis of the LHS-unsubstituted PBI target compounds, whereas **Scheme 5** depicts the approach followed to synthesize LHS-substituted PBI analogues. The latter includes an additional step, step (**i**), a cyclocondensation reaction using a commercially available appropriately substituted diaminobenzene with ethyl 2-cyanoacetate to afford intermediate **I**. The subsequent steps (**ii**) to (**iv**), however, are common in both schemes (**Schemes 1 & 5**).

The second step (**ii**) involves a cyclocondensation reaction using the appropriate benzimidazole acetonitrile **I** and reacting it with a β-ketoester in the presence of ammonium acetate to afford a tricyclic hydroxyl intermediate **II**. This intermediate is then subsequently chlorinated using phosphoryl chloride via a nucleophilic aromatic substitution reaction in the third step (**iii**). The fourth step (**iv**) involves amination of the chloro-intermediate using various amines *via* a nucleophilic aromatic substitution reaction in the presence of triethylamine to afford the PBI target derivatives in moderate to good yields.

2.4.2 Syntheses of left hand side-unsubstituted derivatives

The left hand side-substituted derivatives were synthesized via the scheme shown below (**Scheme 1**).

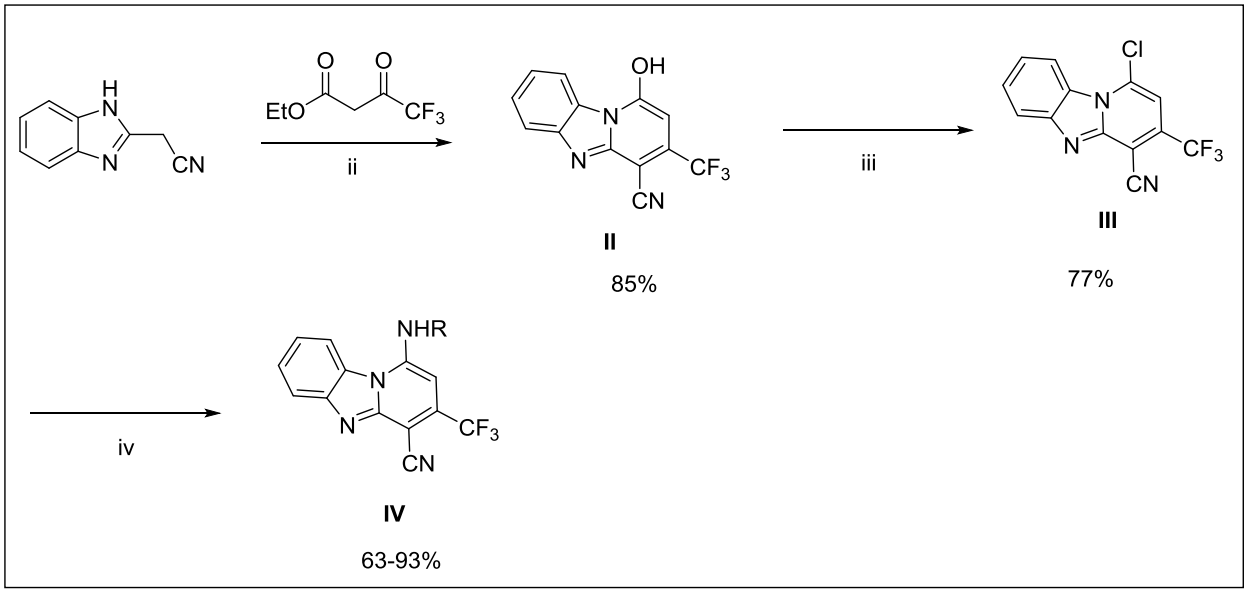

Scheme 1: Synthetic protocol towards LHS-unsubstituted PBI target compounds. Reagents and conditions: (ii) NH_4OAc, 140-150 °C, 10h; (iii) $POCl_3$, 130 °C, 8h; (iv) Appropriate amine, Et_3N, THF, 55-80 °C, 20-60 mins (microwave)

2.4.2.1 Mechanism for the formation of the cyclized hydroxyl intermediate II (Scheme 1&5, step (ii))

The second step (**ii**) involves a cyclisation condensation reaction between the appropriate benzimidazole acetonitrile and ethyl 4,4,4-trifluoro-3-oxobutanoate in the presence of ammonium acetate to afford a tricyclic hydroxyl intermediate (**Scheme 2**).

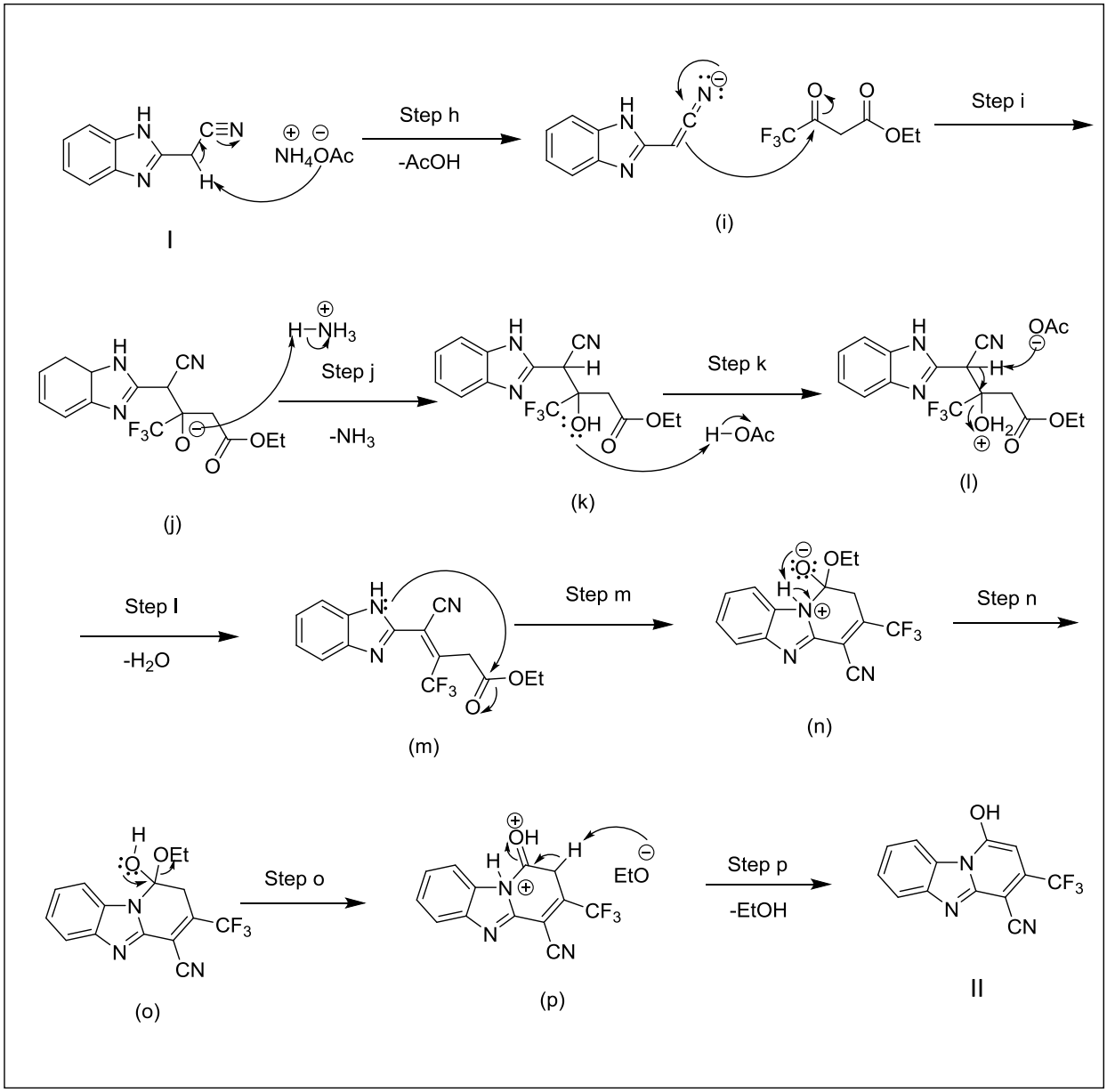

Scheme 2: Proposed reaction mechanism for the cyclisation step to form the tricyclic hydroxyl intermediate (**II**)

In this proposed mechanism, ammonium acetate abstracts the α–proton from 2-benzimidazole acetonitrile (**Step h**) to form the imine intermediate (**i**). This allows a nucleophilic attack of the more electrophilic carbonyl group (attached to the trifluoromethyl group) of the β-ketoester (**Step i**). This is followed by proton abstraction from ammonium ion leading to the release of ammonia (**Step j**). The hydroxyl oxygen abstracts the H-OAc proton (**Step k**), to form (**l**). Subsequently, the carbon-proton bond branching from the carbon-acetonitrile carbon forms a double bond (initiated *via* proton abstraction by the

acetate), resulting in the elimination of water (**Step l**). In the process of aromatization, the second electrophilic carbonyl group (attached to the alkoxyl group) is attacked by the nucleophilic nitrogen (**Step m**) to furnish intermediate (**n**). The amino proton is abstracted by the negatively charged oxygen (**Step n**) to afford intermediate (**o**). The eliminated alkoxyl group then abstracts the proton adjacent to the CF_3 group (**Step p**), and in the process, ethanol is lost to give the appropriately substituted tricyclic hydroxyl product (**II**).

2.4.2.2 Mechanism for the formation of the chloro intermediate III (Schemes 1&5, step (iii))

The third step (**iii**) involves the chlorination of the tricyclic hydroxyl intermediate *via* nucleophilic aromatic substitution using phosphoryl chloride ($POCl_3$) (**Scheme 3**).

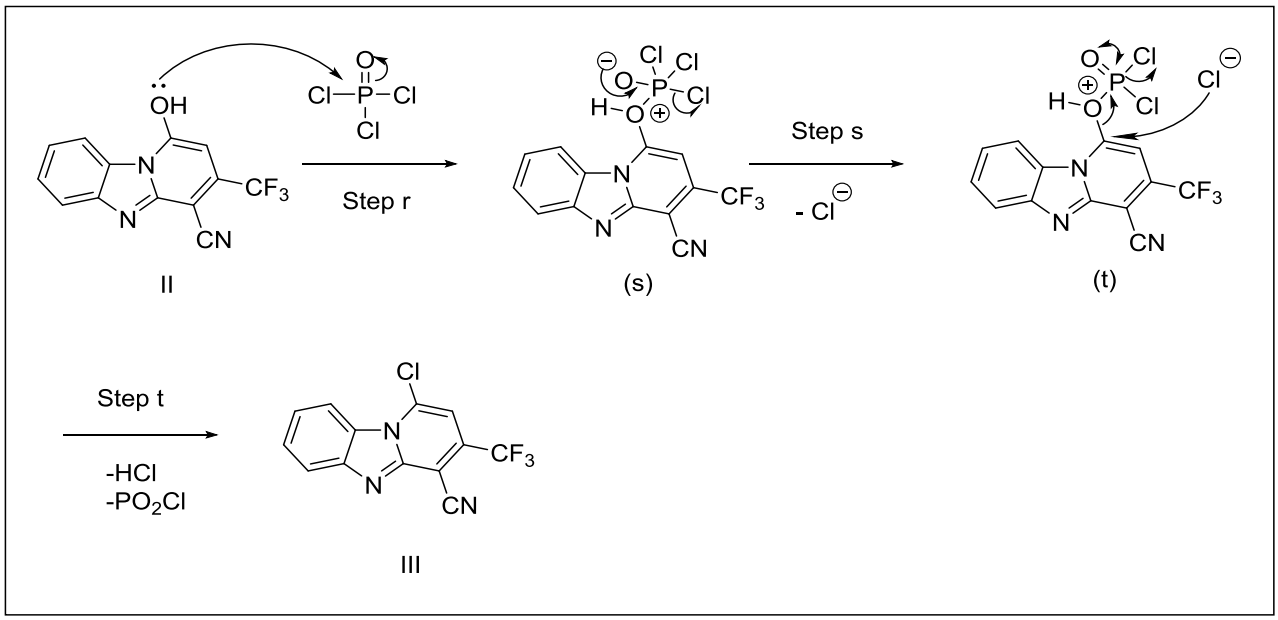

Scheme 3: Proposed reaction mechanism for the cyclisation step to form the tricyclic chlorinated intermediate (**III**)

The nucleophilic hydroxyl group attacks the electrophilic phosphorus centre, shifting electrons to the oxygen of the $POCl_3$ (**Step r**) to form intermediate (**s**). The reformation of the phosphorous oxygen double bond *via* rearrangement (**Step s**) leads to the loss of the chloride anion, giving intermediate (**t**). This intermediate undergoes a substitution reaction in which the nucleophilic chloride anion substitutes the phosphorus moiety, resulting in the

formation of $POCl_2$ and HCl to leave as side products (**Step t**) and further furnish the tricyclic choro-intermediate (**III**).

2.4.2.3 Mechanism for the formation of the aminated target molecule IV (Schemes 1&5, step (iv))

The penultimate step (**iv**) involves the amination of the chloro-intermediate using piperazine in the presence of triethylamine via nucleophilic aromatic substitution to yield the PBI target molecules (**Scheme 4**).

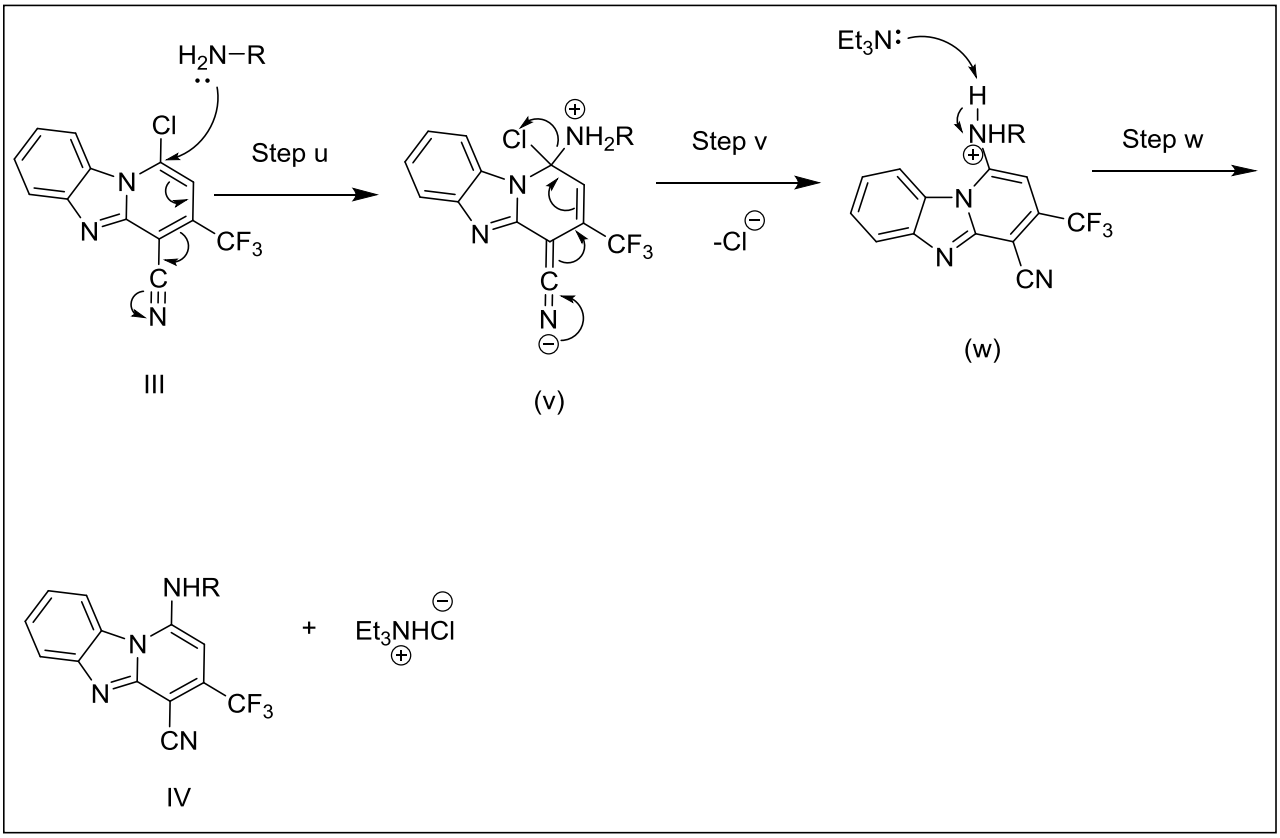

Scheme 4: Proposed reaction mechanism for the amination step to form target molecule (**IV**)

The formation of the target PBI molecules involves aromatic nucleophilic substitution of the chloro intermediate using various amines (**Step u**). This results in the rearrangement of bonds, making the cyano negatively charged, resulting in intermediate (**v**). The nucleophilic cyano group initiates another rearrangement which in turn leads to the loss of a chloride ion (**Step v**)**.** The triethylamine base abstracts the proton on the amine to mop up the acid

produced (**Step w**) in the form of a salt Et_3NHCl. This yields the aminated PBI target molecule (**IV**) and Et_3NHCl as a by-product.

2.4.3 Syntheses of left hand side-substituted derivatives

Left Hand Side-substituted derivatives were synthesized via the scheme shown below (**Scheme 5**).

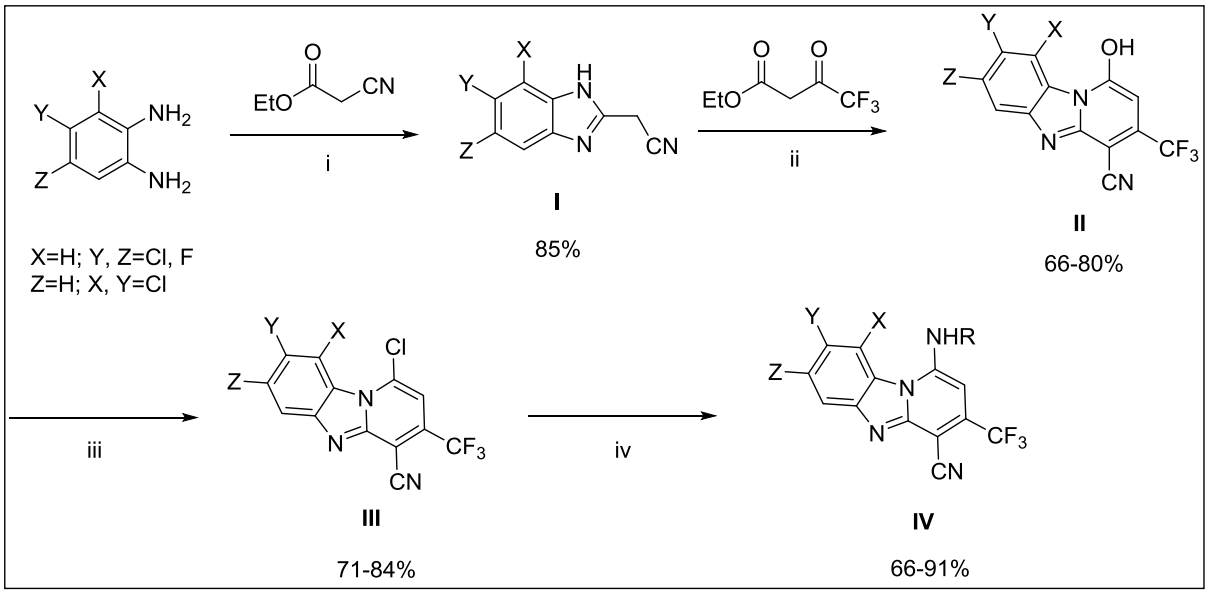

Scheme 5: Synthetic protocol towards LHS-substituted PBI target compounds. Reagents and conditions: (i) DMF, 160 °C, 9-12h; (ii) NH_4OAc, 140-150 °C, 10h; (iii) $POCl_3$, 130 °C, 8h; (iv) Appropriate amine, Et_3N, THF, 55-80 °C, 20-60 mins (microwave)

2.4.3.1 Mechanism for the formation of the intermediate I (Scheme 5, step (i))

The first step (**i**) involves a cyclisation reaction that forms a benzimidazole acetonitrile (**Scheme 6**).

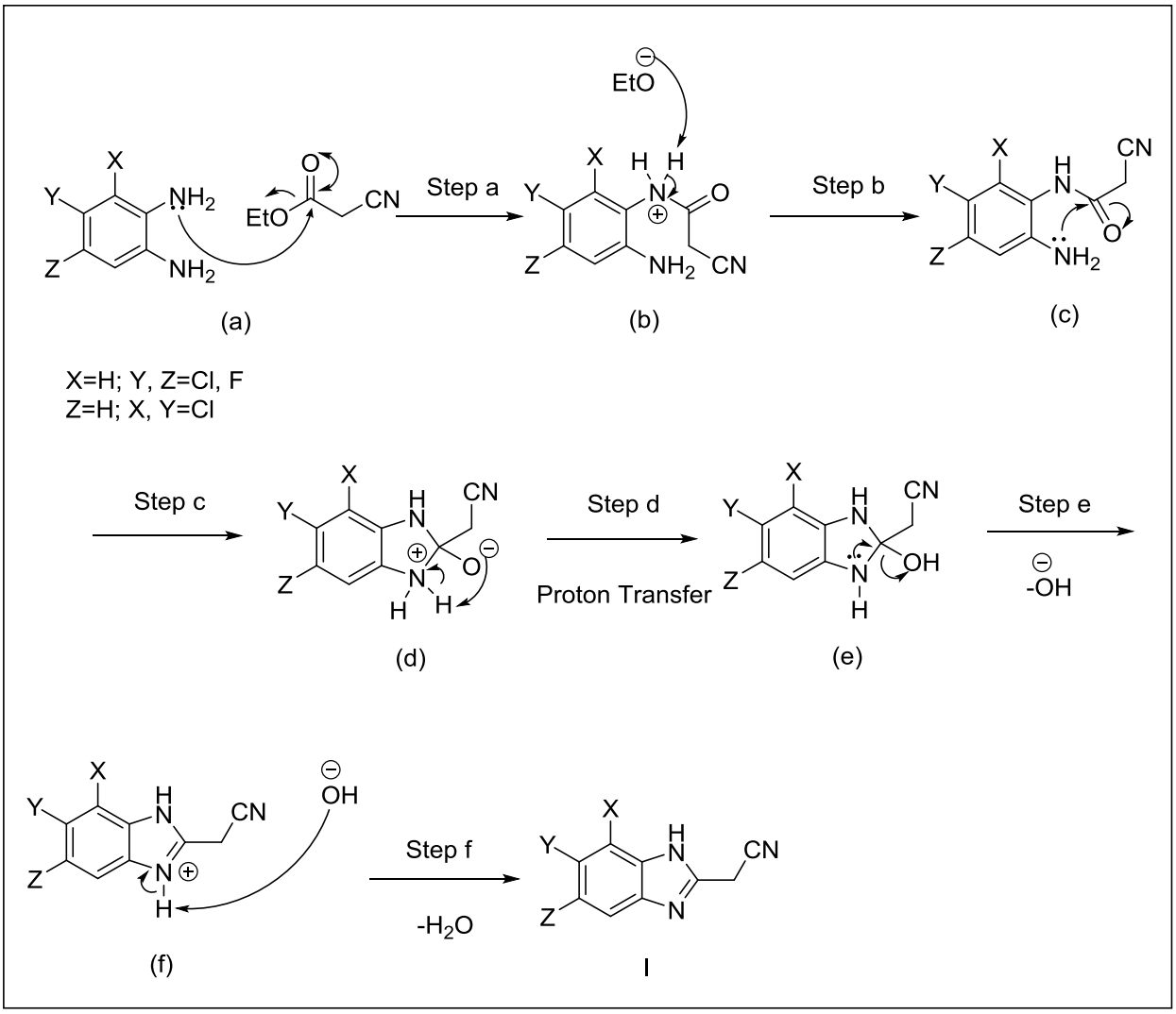

Scheme 6: Proposed reaction mechanism for the first cyclisation step to form intermediate (**I**)

The appropriate diaminobenzene reacts with ethyl cyanoacetate. The first step is initiated by nucleophilic attack of the electrophilic carbonyl carbon by one of the amino groups attached to the diaminobenzene, resulting in the loss of the ethoxyl group (**Step a**) to form intermediate (**b**). Abstraction of an amino proton by the eliminated ethoxyl group (**Step b**) results in attack of the electrophilic carbonyl centre by the nucleophilic lone pairs of the other amino group bonded to the diaminobenzene (**Step c**) to give intermediate (**c**). This leads to the initial formation of the second ring (**d**) which, via proton transfer, results in a cyclized carbinolamine intermediate (**e**). The double bond formed by the lone pair of electrons from the amino group leads to the loss of a hydroxide ion giving intermediate (**f**).

Finally, the loss of water via the abstraction of a proton by the hydroxide ion (**Step f**) furnishes the appropriately substituted benzimidazole acetonitrile (**I**).

2.5 Spectroscopic Analysis of Key Intermediates and Final Target Compounds.

2.5.1 Benzimidazole acetonitrile intermediate I

The characteristic ^{1}H NMR spectrum of intermediate **I** (**Scheme 2**) is shown in **Figure 31**.

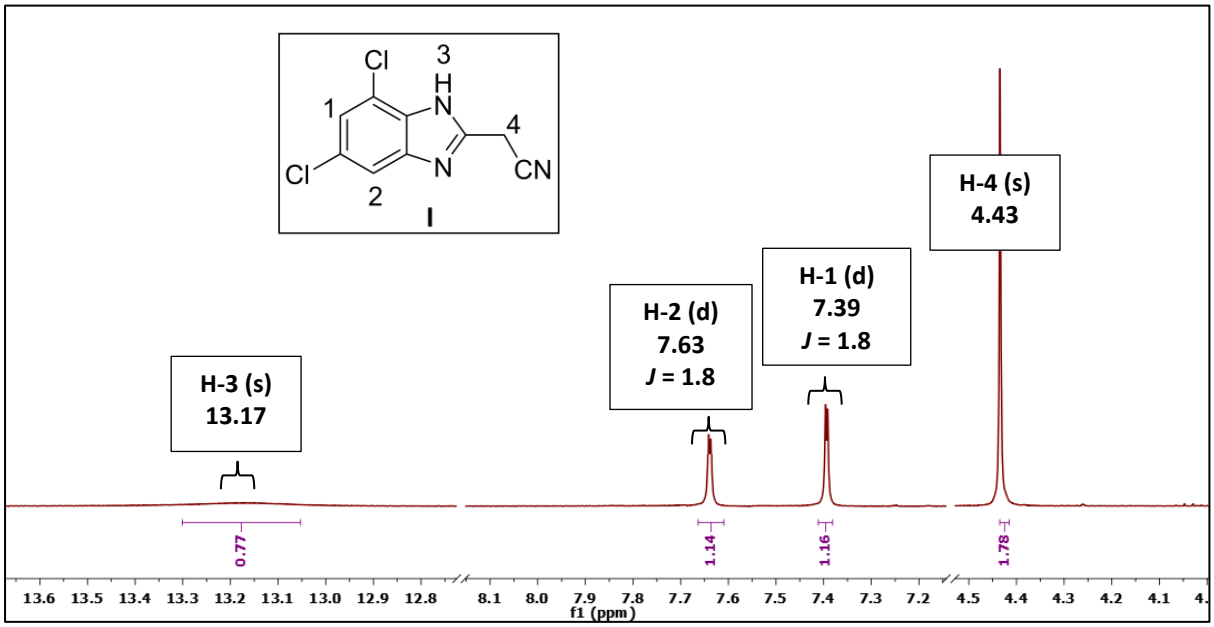

Figure 31: ^{1}H NMR spectrum of intermediate **I** in DMSO-d_6 at 300 MHz

The diagnostic broad singlet at δ 13.17 ppm, integrating for one proton, corresponds to the NH proton **H-3**. Another characteristic feature of compound **I** on the spectrum is the appearance of a singlet at δ 4.43 ppm, which integrated for two protons, and was assigned to the two **H-4** hydrogens. The signals due to protons **H-2** and **H-1** yielded two resolved doublets at δ 7.63 ppm and δ 7.39 ppm both with a small coupling constant (J = 1.7 Hz) due to a long-range coupling with proton **H-1** and **H-2** respectively.

2.5.2 Hydroxyl intermediate II

The ^{1}H NMR spectrum of intermediate **II** (**Scheme 1**) is shown in **Figure 32** below.

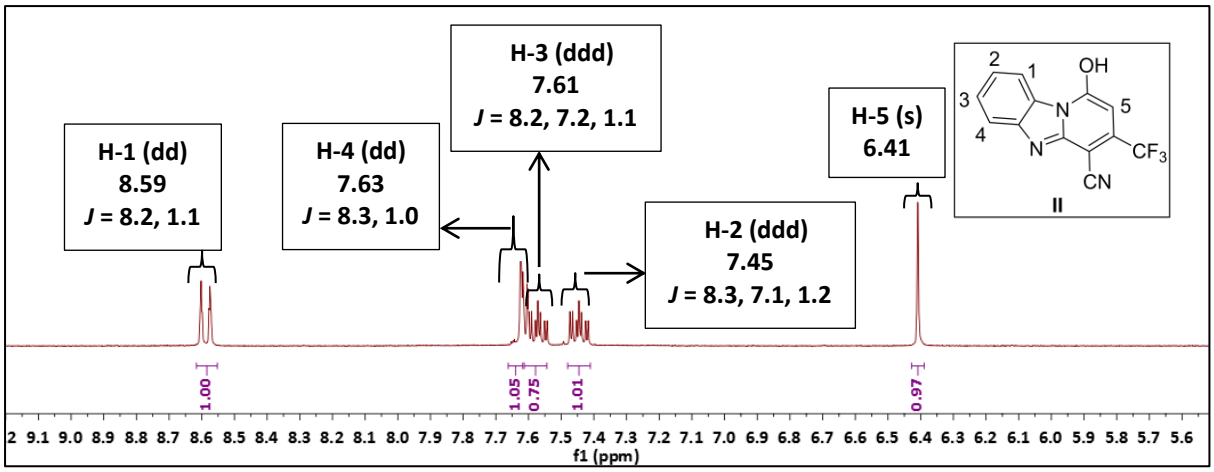

Figure 32: ^{1}H NMR spectrum of intermediate **II** in DMSO-d_6 at 400 MHz

The doublet of doublets observed in the aromatic region at δ 8.59 ppm can be allocated to proton **H-1**, as a result of the short-range coupling to **H-2** (*J* = 8.2 Hz), and the long-range coupling to **H-3** (*J* = 1.1 Hz). The signal at δ 7.63 ppm, integrating for one proton (**H-4**) appears as a doublet of doublets due to the adjacent short-range hydrogen **H-3** (*J* = 8.3 Hz), and the long-range **H-2** (*J* = 1.0 Hz) proton. The doublet of doublet of doublets at δ 7.61 ppm (**H-3**) appears as a result of the short-range protons **H-4** (*J* = 8.2 Hz), **H-2** (*J* = 7.2 Hz), and the long-range **H-1** (*J* = 1.1 Hz) proton. The signal at δ 7.45 ppm, integrating for one proton is associated with the aromatic proton **H-2**, and appears as a doublet of doublet of doublets due to the short-range hydrogens **H-1** (*J* = 8.3 Hz) and **H3** (*J* = 7.1 Hz), and the long-range **H4** (*J* = 1.2 Hz) proton. The sharp singlet, integrating for one proton at δ 6.41 ppm corresponds to proton **H5** which has no neighboring protons.

2.5.3 Chloro intermediate III

The ^{1}H NMR spectrum of intermediate **III** (**Scheme 1**) is shown in **Figure 33** below.

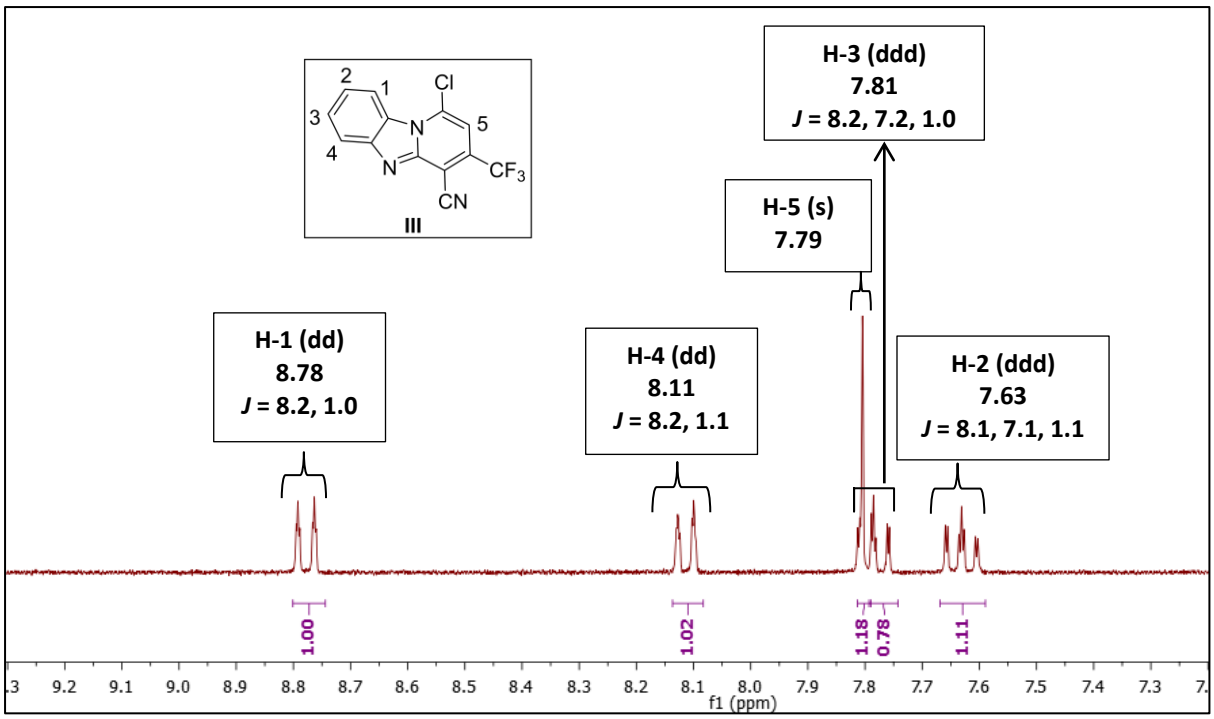

Figure 33: ^{1}H NMR spectrum of intermediate **III** in DMSO-d_6 at 600 MHz.

The ^{1}H-NMR spectrum of intermediate **III** (**Figure 33**) is characterized by the presence of a singlet at δ 7.79 ppm due to **H-5**, also present in the hydroxyl intermediate **II** (**Figure 32**). This singlet appears at a higher chemical shift compared to that of intermediate **II** (**Figure 32**), as a result of the deshielding effect of the chloro substituent. The two doublet of doublets, **H-1** and **H-4** each have one neigbouring hydrogen **H-2** (J = 8.2 Hz) and **H-3** (J = 8.2 Hz), a long-range coupling to **H-3** (J = 1.0 Hz) and **H-2** (J = 1.1 Hz) respectively, and both integrate for one proton. The signal corresponding to **H-3** yielded a doublet of doublet of doublets resonating at δ 7.81 ppm with a small coupling constant due to a long-range coupling with proton **H-1** (J = 1.0 Hz), and two large coupling constants due to the adjacent protons **H-4** (J = 8.2 Hz), and **H-2** (J = 7.2 Hz). The doublet of doublet of doublets in the aromatic region at δ 7.63 ppm (**H-2**) appears as a result of the short-range protons **H-1** (J = 8.1 Hz), **H-3** (J = 7.1 Hz) and the long-range **H-4** (J = 1.1 Hz) proton.

2.5.4 Aminated compound IV

The ^{1}H NMR and ^{13}C NMR spectra of intermediate **IV** (**Scheme 1**) are shown in **Figure 34** and **Figure 35** respectively.

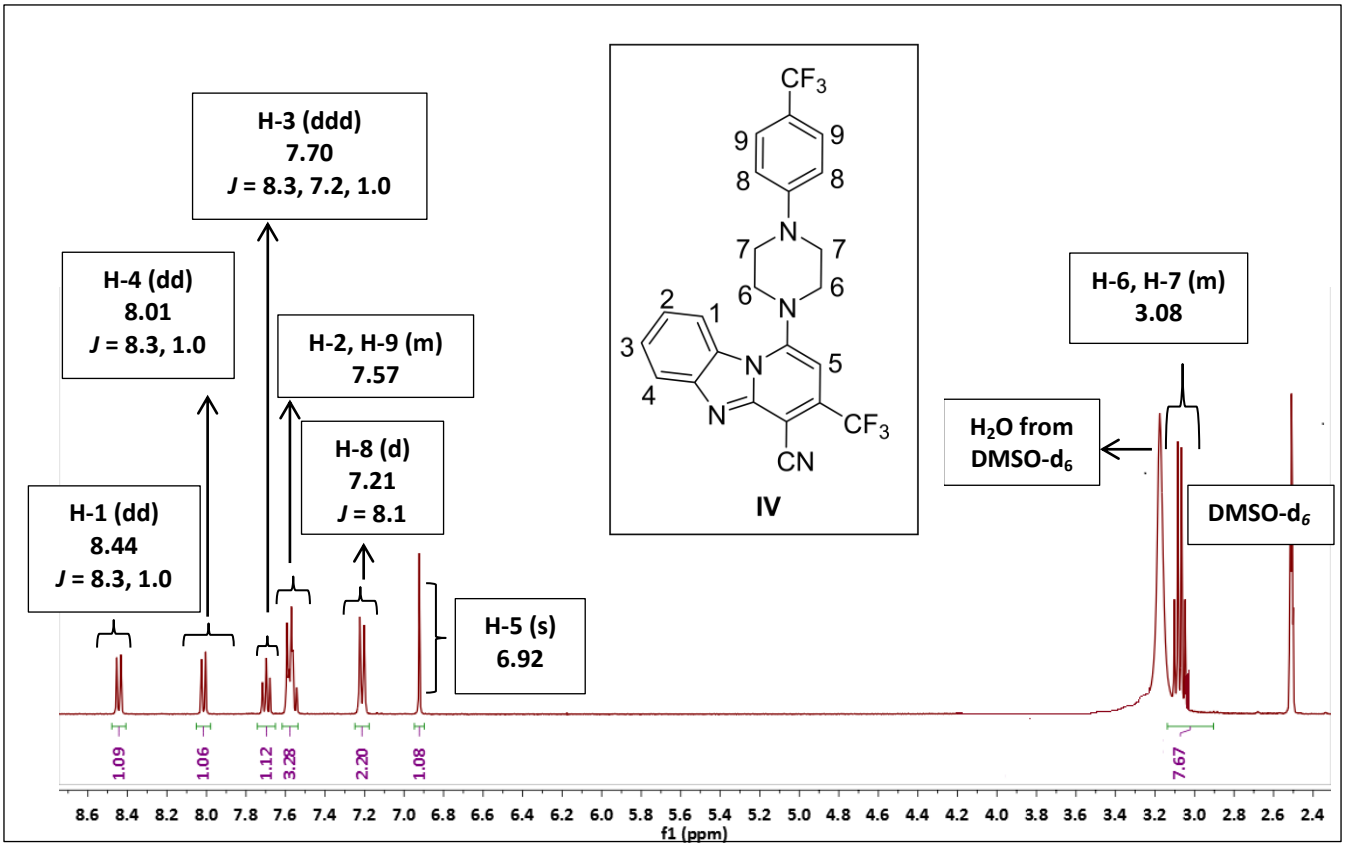

Figure 34: ^{1}H NMR spectrum of intermediate **IV** in DMSO-d_6 at 400 MHz.

The two doublets of doublets, arising from two hydrogens at δ 8.44 ppm and 8.01 ppm are attributed to the aromatic hydrogens, **H-1** and **H-4**. Another characteristic peak of target compound **IV** is the doublet of doublet of doublets (**H-3**), at δ 7.70 ppm, sandwiched between two neighbouring protons **H-4** (*J* = 8.3 Hz), **H-2** (*J* = 7.2 Hz), and the long-range proton **H-1** (*J* = 1.0 Hz). The doublet integrating for two protons (**H-8**; *J* = 8.1 Hz) at δ 7.21 ppm is owing to the adjacent **H-9** hydrogens. The sharp singlet that appears on the spectra is as a result of proton **H-5**, and is a common signal in all intermediates, appearing at δ 6.92 ppm attributable to the absence of neighbouring hydrogens. The multiplets correspond to the aromatic protons (**H-2**, **H-9**; δ 7.6 - 7.5 ppm) and piperazinyl hydrogens (**H-6**, **H-7**; δ 3.1-3.0 ppm), integrating for three protons and eight hydrogens respectively.

^{13}C NMR spectroscopy contributed to the confirmation of the chemical structures of the synthesized intermediates and final target compounds.

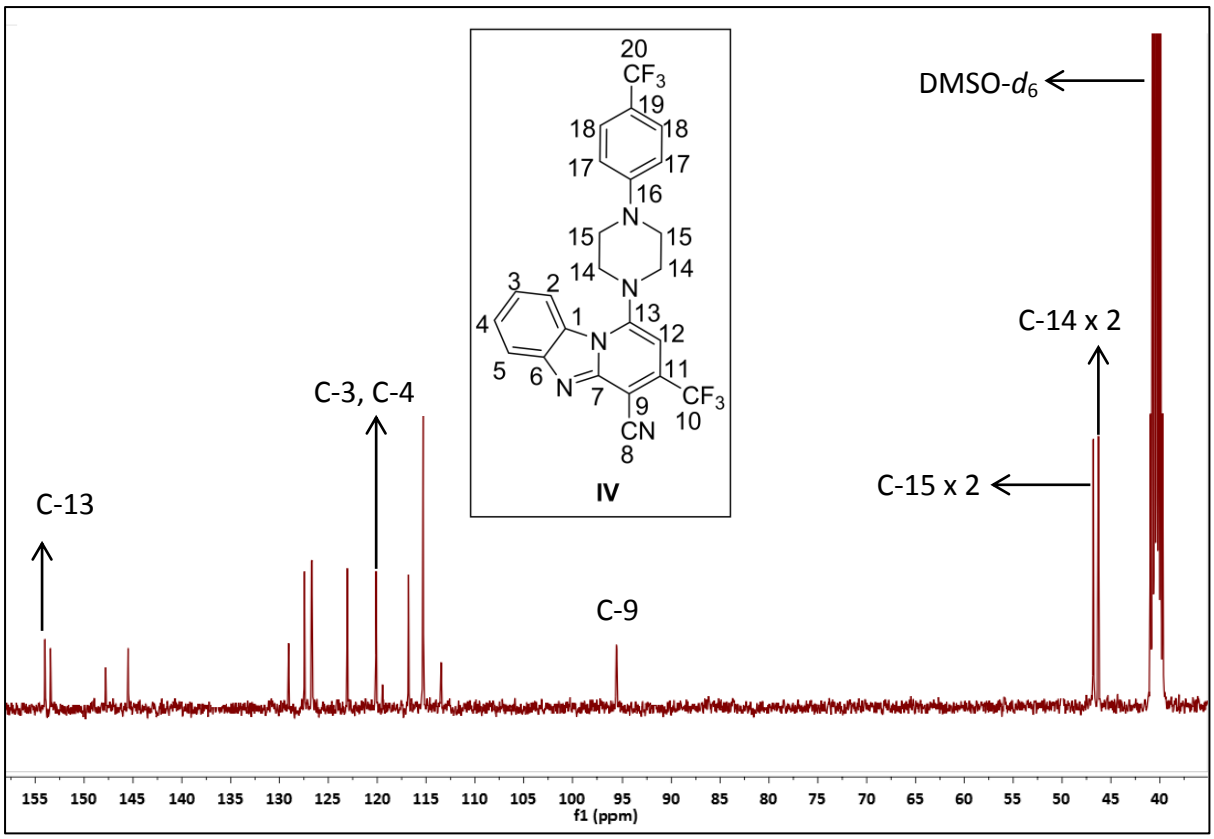

Figure 35: ^{13}C NMR spectrum of target compound **IV** in DMSO-d_6 at 101 MHz

The carbons labelled in **Figure 35** are some of the common signals that were found in target compounds. **C-13** is the most downfield-resonating carbon (δ 154.0) because of the neighbouring nitrogen atoms that cause considerable deshielding, giving rise to a high chemical shift value. In contrast, signals due to the piperazinyl carbons, appeared upfield on the spectrum with relatively high intensities due to each signal occupying two chemical shift-equivalent carbons **C-15** (δ 46.8) and **C-14** (δ 46.2). In addition, the similar electronic environments of aromatic carbons **C-3** and **C-4** resulted in a downfield signal, appearing at the same chemical shift (δ 120.1). The carbon on the pyridine ring of the pyrido[1,2-*a*]benzimidazole scaffold with a cyano group attached to it is another common signal in the targets and was assigned to carbon **C-9** (δ 96.8).

The isolated yields obtained at the different synthetic steps are indicated in **schemes 1 & 5** above. The procedures at the different reaction steps were optimized to yield target compounds with moderate to good yields (**Table 5**).

Table 5: Isolated percentage yields for PBI target compounds.

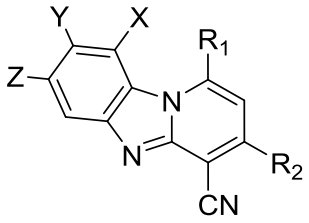

Compound	X	Y	Z	R_1	R_2	Yield (%)
1 (CN1-034)	H	H	H	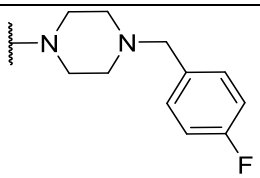	CF_3	86
2 (CN1-035)	H	H	H	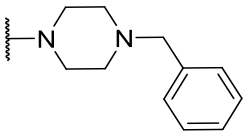	CF_3	81
3 (CN1-036)	H	H	H	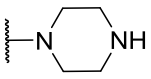	CF_3	83
4 (CN1-037)	H	H	H	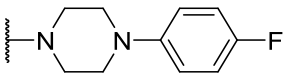	CF_3	83
5 (CN1-038)	H	H	H	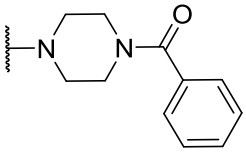	CF_3	83
6 (CN1-040)	H	H	H	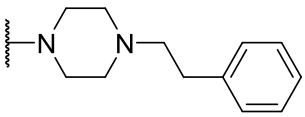	CF_3	90
7 (CN1-041)	H	H	H	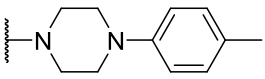	CF_3	67

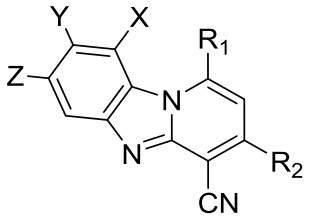

Compound	X	Y	Z	R_1	R_2	Yield (%)
8 (CN1-042)	H	H	H	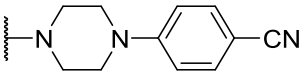	CF_3	86
9 (CN1-043)	H	H	H	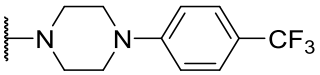	CF_3	75
10 (CN1-044)	H	H	H	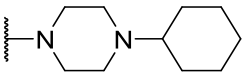	CF_3	67
11 (CN1-045)	H	H	H	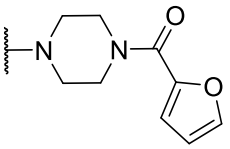	CF_3	91
12 (CN1-048)	H	H	H	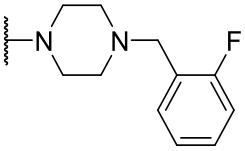	CF_3	93
13 (CN1-049)	H	H	H	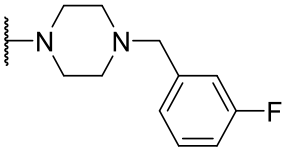	CF_3	90
14 (CN1-050)	H	H	H	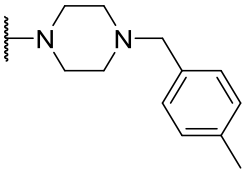	CF_3	87
15 (CN1-051)[a]	H	H	H	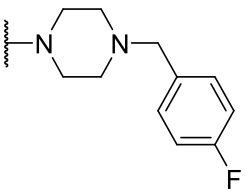		88

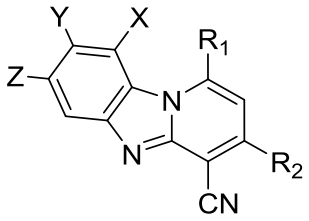

Compound	X	Y	Z	R_1	R_2	Yield (%)
16 (CN1-052)	H	H	H	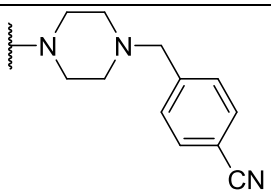	CF_3	80
17 (CN1-059)	H	Cl	Cl	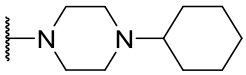	CF_3	66
18 (CN1-060)	H	Cl	Cl	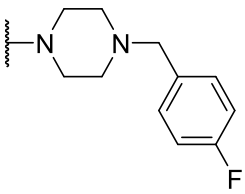	CF_3	82
19 (CN1-061)	H	Cl	Cl	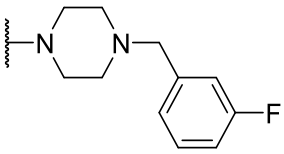	CF_3	72
20 (CN1-062)	H	Cl	Cl	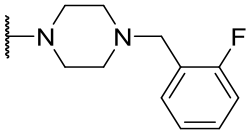	CF_3	89
21 (CN1-063)	H	H	H	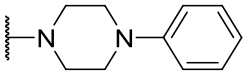	CF_3	70
22 (CN1-064)	H	H	H	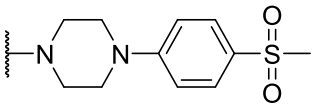	CF_3	88
23 (CN1-065)	H	H	H	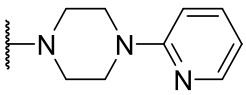	CF_3	91

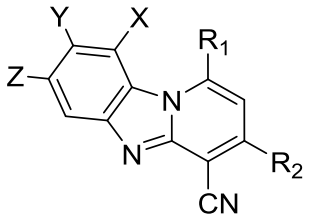

Compound	X	Y	Z	R_1	R_2	Yield (%)
24 (CN1-066)	H	H	H	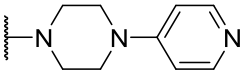	CF_3	90
25 (CN1-067)	H	H	H	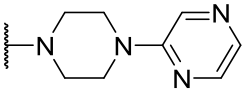	CF_3	63
26 (CN1-068)	H	H	H	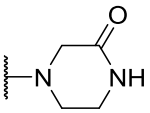	CF_3	63
27 (CN1-069)	H	H	H	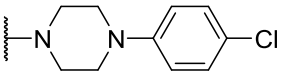	CF_3	77
28 (CN1-070)	H	H	H	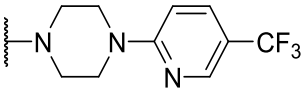	CF_3	65
29 (CN1-071)	H	H	H	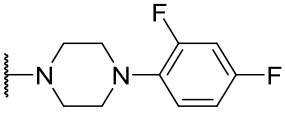	CF_3	84
30 (CN1-072)	H	H	H	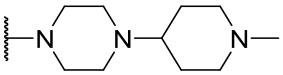	CF_3	67
31 (CN1-077)	Cl	H	Cl	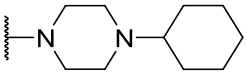	CF_3	91

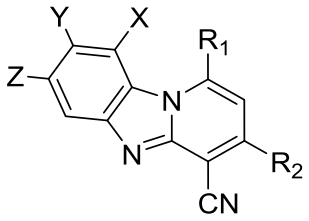

Compound	X	Y	Z	R_1	R_2	Yield (%)
32 (CN1-078)	Cl	H	Cl	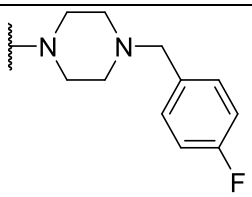	CF_3	76
33 (CN1-079)	H	F	F	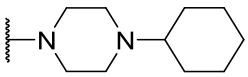	CF_3	74
34 (CN1-080)	H	F	F	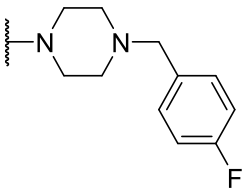	CF_3	73
35 (CN1-082)	H	H	H	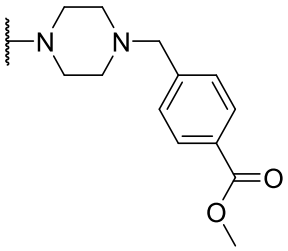	CF_3	90
36 (CN1-083)	H	H	H	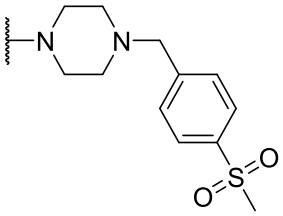	CF_3	73

a, lead compound (**TDR44047**)

2.6 References

1. Ndakala, A. J.; Gessner, R. K.; Gitari, P. W.; October, N.; White, K. L.; Hudson, A.; Fakorede, F.; Shackleford, D. M.; Kaiser, M.; Yeates, C.; Charman, S. A.; Chibale, K. Antimalarial Pyrido[1,2-*a*]benzimidazoles. *J. Med. Chem.* **2011**, *54* (13), 4581–4589.
2. Barot, K.; Nikolova, S.; Ivanov, I.; Ghate, M. Novel Research Strategies of Benzimidazole Derivatives: A Review. *Mini-Reviews Med. Chem.* **2013**, *13* (10), 1421-1447.
3. Bansal, Y.; Silakari, O. The Therapeutic Journey of Benzimidazoles: A Review. *Bioorganic and Medicinal Chemistry* **2012**, *20* (21), 6208-36.
4. Shaharyar, M.; Mazumder, A.; Salahuddin; Garg, R.; Pandey, R. D. Synthesis, Characterization and Pharmacological Screening of Novel Benzimidazole Derivatives. *Arab. J. Chem.* **2016**, *9* (1), 342–347.
5. Chandrika, N. T.; Shrestha, S. K.; Ngo, H. X.; Garneau-Tsodikova, S. Synthesis and Investigation of Novel Benzimidazole Derivatives as Antifungal Agents. *Bioorganic Med. Chem.* **2016**, *24* (16), 3680-3686.
6. Ateş-Alagöz, Z.; Kuş, C.; Çoban, T. Synthesis and Antioxidant Properties of Novel Benzimidazoles Containing Substituted Indole or 1,1,4,4-Tetramethyl-1,2,3,4-Tetrahydro-Naphthalene Fragments. *J. Enzyme Inhib. Med. Chem.* **2005**, *20* (4), 325-331.
7. Błaszczak-Świątkiewicz, K.; Olszewska, P.; Mikiciuk-Olasik, E. Antiproliferative Activity of New Benzimidazole Derivatives. *Acta Biochim. Pol.* **2013**, *60* (3), 427-433.
8. Velík, J.; Baliharová, V.; Fink-Gremmels, J.; Bull, S.; Lamka, J.; Skálová, L. Benzimidazole Drugs and Modulation of Biotransformation Enzymes. *Research in Veterinary Science* **2004**, *76* (2), 95-108.
9. Yoshikawa, T. T. Antiparasitic Drugs. *Am. Fam. Physician* **1980**, *21* (3), 132-138.
10. Salahuddin; Shaharyar, M.; Mazumder, A. Benzimidazoles: A Biologically Active Compounds. *Arabian Journal of Chemistry* **2017**, *10* (1), 157-173.
11. Refaat, H. M. Synthesis and Anticancer Activity of Some Novel 2-Substituted Benzimidazole Derivatives. *Eur. J. Med. Chem.* **2010**, *45* (7), 2949-2956.
12. Rida, S. M.; Soliman, F. S. G.; Badawey, E.-S. A. M.; El-Ghazzawi, E.; Kader, O.; Kappe, T. Benzimidazole Condensed Ring Systems. 1. Syntheses and Biological Investigations

of Some Substituted Pyrido[1,2-*a*]benzimidazoles. *J. Heterocycl. Chem.* **1988**, *25* (4), 1087–1093.

13. Refaat, H. M. Synthesis of Potential Anticancer Derivatives of Pyrido[1,2-*a*]benzimidazoles. *Med. Chem. Res.* **2012**, *21* (7), 1253-1260.
14. Singh, K.; Okombo, J.; Brunschwig, C.; Ndubi, F.; Barnard, L.; Wilkinson, C.; Njogu, P. M.; Njoroge, M.; Laing, L.; Machado, M.; Prudêncio, M.; Reader, J.; Botha, M.; Nondaba, S.; Birkholtz, L.M.; Lauterbach, S.; Churchyard, A.; Coetzer, T.L.; Burrows, J.N.; Yeates C.; Denti, P.; Wiesner L.; Egan, T. J.; Wittlin S.; Chibale, K. Antimalarial Pyrido[1,2-*a*]benzimidazoles: Lead Optimization, Parasite Life Cycle Stage Profile, Mechanistic Evaluation, Killing Kinetics, and in Vivo Oral Efficacy in a Mouse Model. *J. Med. Chem.* **2017**, *60* (4), 1432-1448.
15. Okombo, J.; Singh, K.; Mayoka, G.; Ndubi, F.; Barnard, L.; Njogu, P. M.; Njoroge, M.; Gibhard, L.; Brunschwig, C.; Vargas, M.; Keiser, J.; Egan, T. J., Chibale, K. Antischistosomal Activity of Pyrido[1,2‑*a*]benzimidazole Derivatives and Correlation with Inhibition of β‑Hematin Formation. *ACS Infect. Dis.* **2017**, *3* (6), 411-420.
16. Meister, I.; Ingram-Sieber, K.; Cowan, N.; Todd, M.; Robertson, M. N.; Meli, C.; Patra, M.; Gasser, G.; Keiser, J. Activity of Praziquantel Enantiomers and Main Metabolites against Schistosoma Mansoni. *Antimicrob. Agents Chemother.* **2014**, *58* (9), 5466-5472.
17. Cowan, N.; Keiser, J. Repurposing of Anticancer Drugs: In Vitro and in Vivo Activities against Schistosoma Mansoni. *Parasit. Vectors* **2015**, *8*, 417.
18. Ingram-Sieber, K.; Cowan, N.; Panic, G.; Vargas, M.; Mansour, N. R.; Bickle, Q. D.; Wells, T. N. C.; Spangenberg, T.; Keiser, J. Orally Active Antischistosomal Early Leads Identified from the Open Access Malaria Box. *PLoS Negl. Trop. Dis.* **2014**, *8* (1), e2610.
19. Yang, J. J.; Boissier, J.; Chen, J. L.; Yao, H.; Yang, S.; Rognon, A.; Qiao, C. Design, Synthesis and Biological Evaluation of Praziquantel and Endoperoxide Conjugates as Antischistosomal Agents. *Future Med. Chem.* **2015**, *7* (6), 713-725.
20. Keiser, J.; Vargas, M.; Rubbiani, R.; Gasser, G.; Biot, C. In Vitro and in Vivo Antischistosomal Activity of Ferroquine Derivatives. *Parasites and Vectors* **2014**, *7*, 424.

CHAPTER 3: PHARMACOLOGICAL EVALUATION

3.1 Introduction

The *in vitro* antiplasmodium activities of the final synthesized target compounds were evaluated against the blood-stage parasites of the chloroquine-sensitive *P. falciparum* NF54 strain (**Table 6**). Concurrently, antischistosomal activities against Newly Transformed Schistosomula (NTS) and adult *S. mansoni* were evaluated (**Table 8**). Pyrido[1,2-*a*]benzimidazole (PBI) derivatives were also screened for *in vitro* gametocytocidal activity using the luciferase-reporter NF54 line of *P. falciparum* and tested at a concentration of 1 and 5 µM (**Table 7**).

This research project also included a mechanistic study that explored the potential of piperazinyl PBIs to inhibit the formation of hemozoin (Hz) based on the hypothesis that the PBI scaffold can potentially adopt flat conformations that would encourage π–π stacking interactions with ferriprotoporphyrin IX (Fe(III)PPIX), the toxic by-product of host hemoglobin degradation. This interaction would inhibit Hz formation, leading to the death of the parasite via heme toxicity.

3.2 *In vitro* antiplasmodium (*Pf* NF54) and β-hematin inhibitory activities

One of the most active compounds in this PBI series was compound **10** (IC_{50} = 0.09 µM), which contains a piperazine ring and a cyclohexane saturated substituent. The saturated R_1 group confers approximately 39 times more potency than the unsaturated R_1 amine group in compound **21** (IC_{50} = 3.52 µM). However, the addition of the NMe group to the saturated cyclohexane part of the R_1 group in analogue **30** (IC_{50} > 6.00 µM) presumably interfered with the essential interactions required for potency.

The presence of either a methylene linker, in compound **2** (IC_{50} = 0.31 µM), or an ethylene linker, in compound **6** (IC_{50} = 0.33 µM), at the R_1 position resulted in significant activity, indicating the importance of these linkers for potency. The analogue containing a methylene

linker, PBI benzyl derivative **1** (IC_{50} = 0.17 μM), showed approximately a 3-fold increase in activity compared to the linker-free fluorobenzyl piperazine analogue **4** (IC_{50} = 0.43 μM). Although the directly linked phenyl piperazine compound **21** (IC_{50} = 3.52 μM) showed poor antiparasitic activity, the introduction of fluoro (compound **4**, IC_{50} = 0.43 μM), chloro (compound **27,** IC_{50} = 0.68 μM), and trifluoromethyl (compound **9**, IC_{50} = 0.91 μM) Craig plot substituents at the para position of the benzyl group enhanced antiplasmodium activity.

Introduction of a carbonyl group to the methylene linker resulted in the loss of antiplasmodium activity (compound **5**, IC_{50} = 6.00 μM).

Addition of the hydrophobic electron-withdrawing fluoro, chloro, and trifluoromethyl substituents favored antiplasmodium activity (compound **4**, IC_{50} = 0.43 μM; compound **9**, IC_{50} = 0.91 μM; and compound **27**, IC_{50} = 0.68 μM), compared to the hydrophobic electron-releasing methyl group (compound **7**, IC_{50} = 1.29 μM) and the hydrophilic electron-withdrawing cyano group (compound **8**, IC_{50} = 4.20 μM).

In the LHS-unsubstituted series of compounds, regio-isomerism on the benzyl moiety attached to the piperazine at R_1 showed no influence on activity: compounds **1** (IC_{50} = 0.17 μM), **12** (IC_{50} = 0.14 μM), and **13** (IC_{50} = 0.10 μM) displayed equipotent antiplasmodium activity. This observation was consistent with that seen in LHS-substituted compounds **18** (IC_{50} = 1.77 μM), **19** (IC_{50} = 1.58 μM), and **20** (IC_{50} = 1.96 μM), in which positional isomers demonstrated comparable antiplasmodium activity.

LHS-substituted analogues were synthesized to investigate the effect of di-substitution on *in vitro* antiplasmodium activity and BHIA. Dichloro- and difluoro-substituted analogues of the potent parent unsubstituted compounds were accordingly synthesized. The di-substituted compounds were synthesized with either the 1-(4-fluorobenzyl)piperazine, employed in analogue **1**, or the 1-cyclohexylpiperazine amine used to synthesize compound **10**. These amino side-chains were prioritized based on the high antiplasmodium activity they conferred to the LHS-unsubstituted analogues compounds **1** (IC_{50} = 0.17 μM) and **10** (IC_{50} = 0.09 μM).

The LHS-substituted 3,5 di-chlorinated analogues **31** (IC_{50} = 0.18 µM) and **32** (IC_{50} = 1.71 µM), and the 4,5 di-chlorinated analogues **17** (IC_{50} = 0.11 µM) and **18** (IC_{50} = 1.77 µM) displayed comparable activity but reduced antiplasmodium potency compared to that of their parent unsubstituted analogues (compounds **10**, IC_{50} = 0.09 µM, and **1**, IC_{50} = 0.17 µM). The LHS-substituted di-fluorinated analogues, however, displayed markedly enhanced antiplasmodium activity (compounds **33**, IC_{50} = 0.012 µM, and **34**, IC_{50} = 0.10 µM).

Table 6: *In vitro* activity against the chloroquine-sensitive *Plasmodium falciparum* (*Pf*) NF54 strain and inhibition of β-hematin formation by pyrido[1,2-*a*]benzimidazoles

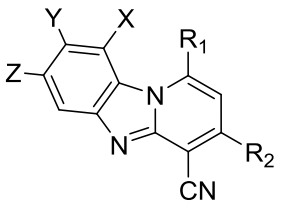

Compound	X	Y	Z	R_1	R_2	Antiplasmodium activity IC_{50} (µM) *Pf* NF54	IC_{50} BHIA (µM)
1 (CN1-034)	H	H	H	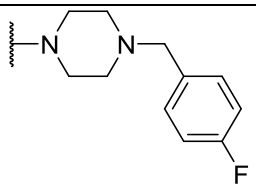	CF_3	0.17	580
2 (CN1-035)	H	H	H	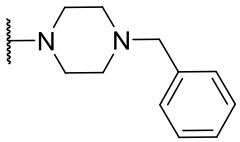	CF_3	0.31	689
3 (CN1-036)	H	H	H	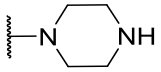	CF_3	4.60	85000
4 (CN1-037)	H	H	H	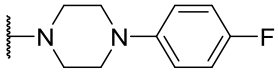	CF_3	0.43	606985
5 (CN1-038)	H	H	H	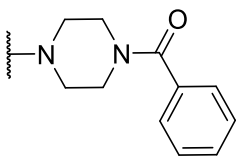	CF_3	6.00	n.a.

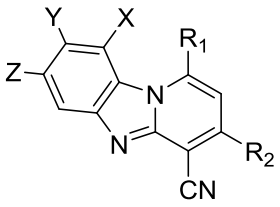

Compound	X	Y	Z	R_1	R_2	Antiplasmodium activity IC_{50} (µM) *Pf* NF54	IC_{50} BHIA (µM)
6 (CN1-040)	H	H	H	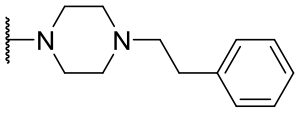	CF_3	0.33	1011
7 (CN1-041)	H	H	H	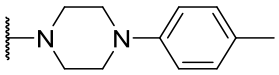	CF_3	1.29	n.a.
8 (CN1-042)	H	H	H	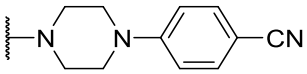	CF_3	4.20	1380
9 (CN1-043)	H	H	H	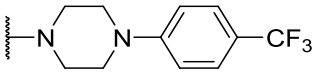	CF_3	0.91	685
10 (CN1-044)	H	H	H	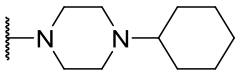	CF_3	0.09	20
11 (CN1-045)	H	H	H	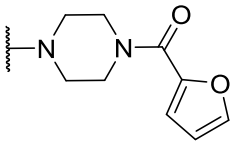	CF_3	5.46	n.a.
12 (CN1-048)	H	H	H	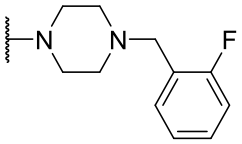	CF_3	0.14	17
13 (CN1-049)	H	H	H	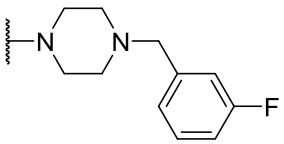	CF_3	0.10	239
14 (CN1-050)	H	H	H	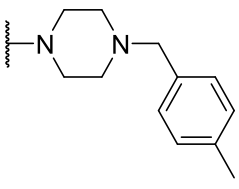	CF_3	1.11	3681

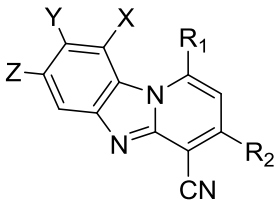

Compound	X	Y	Z	R_1	R_2	Antiplasmodium activity IC_{50} (µM) *Pf* NF54	IC_{50} BHIA (µM)
15 (CN1-051)[a]	H	H	H	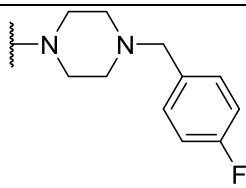		0.040	n.a.
16 (CN1-052)	H	H	H	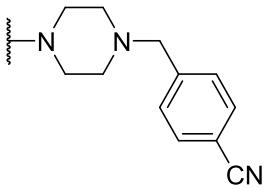	CF_3	2.62	n.a.
17 (CN1-059)	H	Cl	Cl	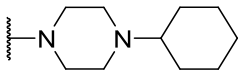	CF_3	0.11	288
18 (CN1-060)	H	Cl	Cl	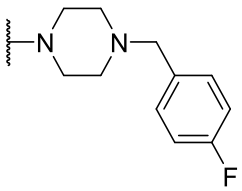	CF_3	1.77	379
19 (CN1-061)	H	Cl	Cl	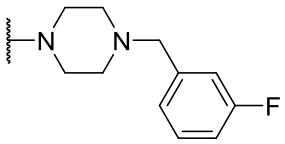	CF_3	1.58	513
20 (CN1-062)	H	Cl	Cl	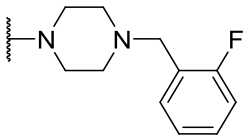	CF_3	1.96	122
21 (CN1-063)	H	H	H	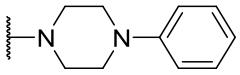	CF_3	3.52	n.a.
22 (CN1-064)	H	H	H	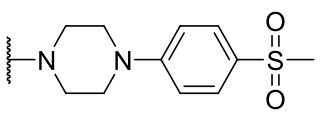	CF_3	3.58	1120

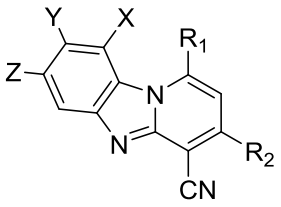

Compound	X	Y	Z	R_1	R_2	Antiplasmodium activity IC_{50} (µM) *Pf* NF54	IC_{50} BHIA (µM)
23 (CN1-065)	H	H	H	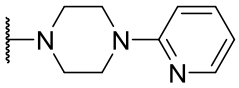	CF_3	1.83	30630
24 (CN1-066)	H	H	H	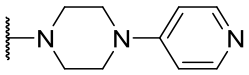	CF_3	3.84	n.a.
25 (CN1-067)	H	H	H	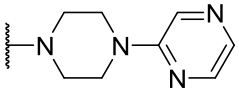	CF_3	2.36	340840
26 (CN1-068)	H	H	H	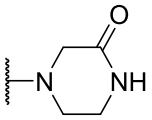	CF_3	> 6.00	n.a.
27 (CN1-069)	H	H	H	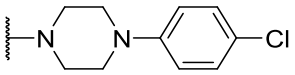	CF_3	0.68	895
28 (CN1-070)	H	H	H	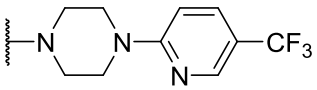	CF_3	0.62	48516
29 (CN1-071)	H	H	H	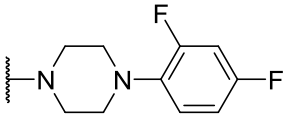	CF_3	1.45	6284
30 (CN1-072)	H	H	H	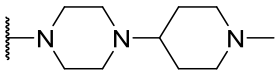	CF_3	> 6.00	29876
31 (CN1-077)	Cl	H	Cl	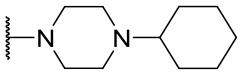	CF_3	0.18	420

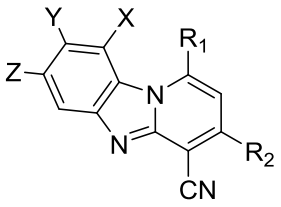

Compound	X	Y	Z	R_1	R_2	Antiplasmodium activity IC_{50} (μM) *Pf* NF54	IC_{50} BHIA (μM)
32 (CN1-078)	Cl	H	Cl	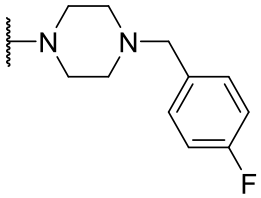	CF_3	1.71	255
33 (CN1-079)	H	F	F	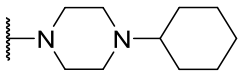	CF_3	0.012	138
34 (CN1-080)	H	F	F	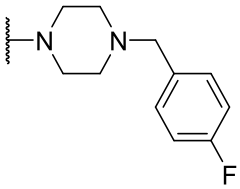	CF_3	0.10	689
35 (CN1-082)	H	H	H	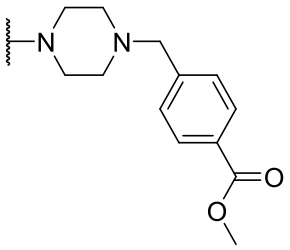	CF_3	1.78	2482
36 (CN1-083)	H	H	H	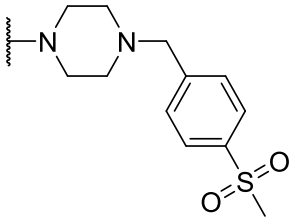	CF_3	2.54	19836
Chloroquine						0.014	17
Amodiaquine						0.009	15
Pyrimethamine						0.019	1018

a, lead compound (**TDR44047**)
BHIA, β-hematin inhibitory activity; n.a., not assessed

Generally, compounds that displayed potent BHIA also showed high antiplasmodium activity, as observed with compounds **10** (BHIA IC_{50} 20 µM, NF54 IC_{50} 0.09 µM), **12** (BHIA IC_{50} 17 µM, NF54 IC_{50} 0.14 µM), and **33** (BHIA IC_{50} 138 µM, NF54 IC_{50} 0.012 µM). Despite this observation, the linear correlation between the *Pf* NF54 whole-cell and the BHIA assays, although statistically significant, was weak. A graph plotting log IC_{50} and log BHIA for the 20 most potent compounds (NF54 IC_{50} < 2 µM) illustrates this trend (**Figure 37**). Although the plot shows a general trend, the relationship between the two properties cannot be concluded from the graph. The low R^2 value of the graph in **Figure 37** (R^2 = 0.1641) is an indication of the lack of correlation between these two properties, and suggests that β-hematin inhibition maybe potentially a contributing mode of action, rather than the sole mechanism of antiplasmodial activity for this class of compounds. However, it is important to note that the BHIA assay is a cell-free assay and therefore does not represent the true environment of the food vacuole. Furthermore, the BHIA assay is carried out in the absence of membranes, although *in vivo,* the drug would have to cross multiple membrane barriers to permeate the infected red blood cells and the parasite to reach its target in the digestive food vacuole. The compound's physicochemical properties are thus important to consider in predicting its ability to cross membranes. A cellular fractionation assay is therefore required to address the assay's shortcomings and further validate these results. In the cell fractionation assay, free heme and Hz are measured in ring-stage parasites treated with increasing doses of compound. A true β-hematin formation inhibitor displays a dose-dependent increase in toxic free heme and a decrease in Hz.

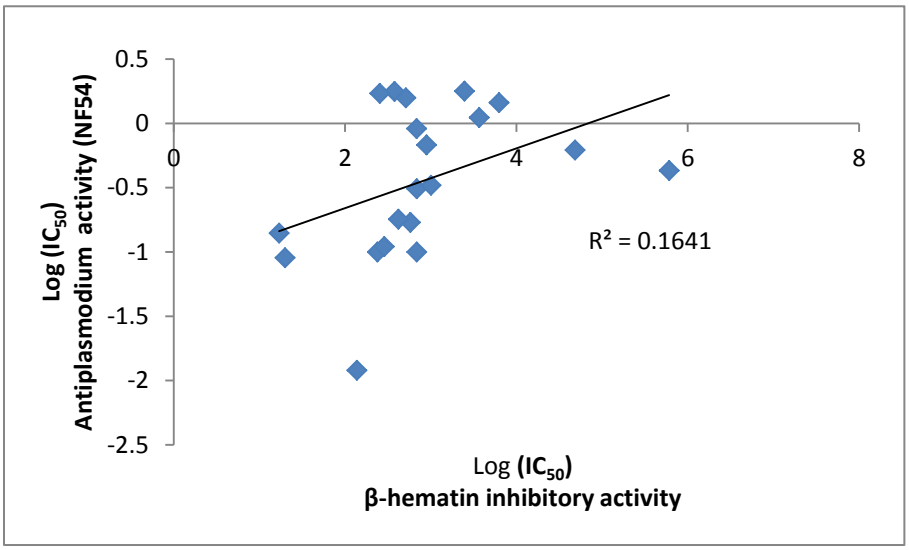

Figure 36: Correlation between antiplasmodium and β-hematin inhibitory activity of the PBI compounds

3.3 Gametocytocidal Activity

Compounds that display gametocytocidal activity are of interest with regard to malaria because of their transmission-blocking potential. The ability of this class of compounds to act as dual-action antimalarials was evaluated by screening compounds against luciferase reporter-expressing *P. falciparum* NF54 parasites. The percentage inhibition of each compound tested (1 µM and 5 µM) against early- and late-stage *P. falciparum* gametocytes (EGs and LGs, respectively) is shown in **Table 7**.

Table 7: *In vitro* gametocytocidal activity of compounds (1 µM and 5 µM) on early- and late-stage *Plasmodium falciparum* gametocytes

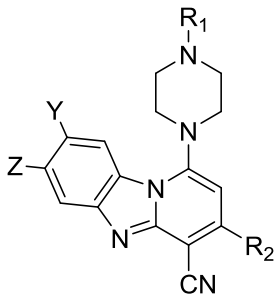

Compound	Y	Z	R_1	R_2	EG		LG	
					1 µM (%)	5 µM (%)	1 µM (%)	5 µM (%)
1 (CN1-034)	H	H	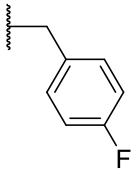	CF_3	19	15	3	5
2 (CN1-035)	H	H	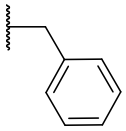	CF_3	17	15	2	14
4 (CN1-037)	H	H	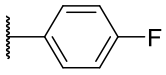	CF_3	15	7	11	4
6 (CN1-040)	H	H	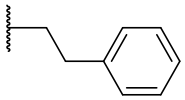	CF_3	22	20	20	28
7 (CN1-041)	H	H	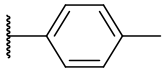	CF_3	1	9	4	2
9 (CN1-043)	H	H	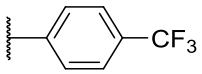	CF_3	4	1	28	15
10 (CN1-044)	H	H	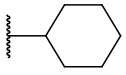	CF_3	32	28	26	0
12 (CN1-048)	H	H	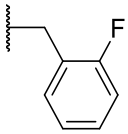	CF_3	23	23	12	15
13 (CN1-049)	H	H	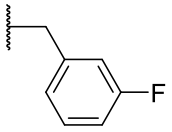	CF_3	8	37	24	24

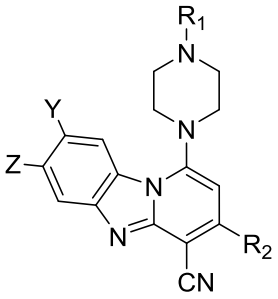

Compound	Y	Z	R_1	R_2	EG		LG	
					1 µM (%)	5 µM (%)	1 µM (%)	5 µM (%)
14 (CN1-050)	H	H	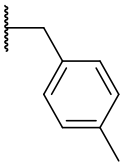	CF_3	0	0	8	9
15 (CN1-051)[a]	H	H	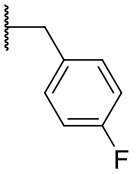		14	34	28	22
17 (CN1-059)	Cl	Cl	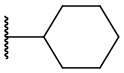	CF_3	3	29	0	19
23 (CN1-065)	H	H	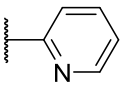	CF_3	2	3	1	3
25 (CN1-067)	H	H	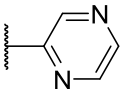	CF_3	1	2	1	8
27 (CN1-069)	H	H	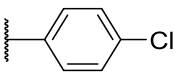	CF_3	2	2	27	34
28 (CN1-070)	H	H	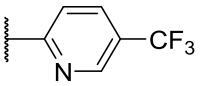	CF_3	13	18	32	36
29 (CN1-071)	H	H	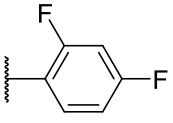	CF_3	0	0	4	7

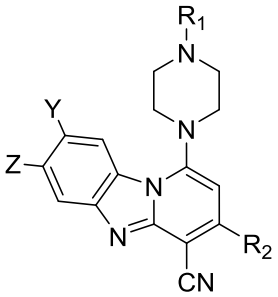

Compound	Y	Z	R_1	R_2	EG		LG	
					1 µM (%)	5 µM (%)	1 µM (%)	5 µM (%)
36 (CN1-083)	H	H	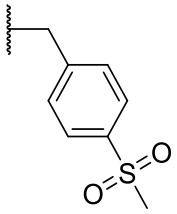	CF_3	1	7	2	7
Methylene blue					93		90	
Dihydro-artemisinin					75		70	
MMV390048					77		92	

a, lead compound (**TDR44047**)
EG, early-stage gametocytes; LG, late-stage gametocytes

Compounds that were tested for gametocytocidal activity showed minimal activity against both EGs and LGs (< 50% inhibition at both 5 µM and 1 µM).

3.4 *In vitro* antischistosomal activities

Twenty-three target compounds were screened against NTS and adult *S. mansoni* at an initial concentration of 10 µM (**Table 8**). In the case of NTS, compounds **4**, **9,** and **24** displayed potent activity against the juvenile parasite (>70% inhibition of worm viability). The compounds that met this threshold were selected for subsequent evaluation against adult *S. mansoni*.

Compounds **4** and **24** maintained their potency at the same drug concentration (10 µM), but compound **9** only caused 27% worm mortality (**Table 8**).

Table 8: *In vitro* efficacy of target pyrido[1,2-*a*]benzimidazoles against adult *Schistosoma mansoni* and newly transformed schistosomula

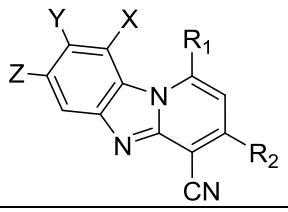

Compound	X	Y	Z	R_1	R_2	Antischistosomal activity Test conc. 10 µM (% inhibition)	
						NTS	Adult *S. mansoni*
1 (CN1-034)	H	H	H	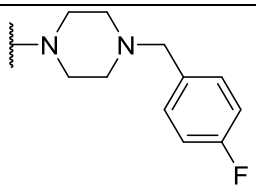	CF_3	46	n.a.
2 (CN1-035)	H	H	H	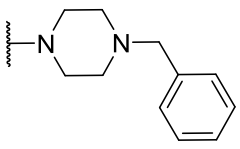	CF_3	4	n.a.
4 (CN1-037)	H	H	H	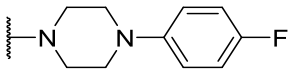	CF_3	100	100

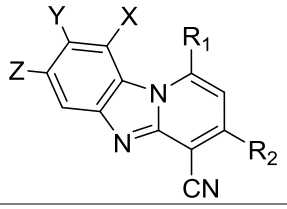

Compound	X	Y	Z	R_1	R_2	Antischistosomal activity Test conc. 10 µM (% inhibition)	
						NTS	Adult *S. mansoni*
5 (CN1-038)	H	H	H	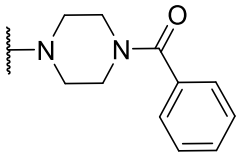	CF_3	64	n.a.
6 (CN1-040)	H	H	H	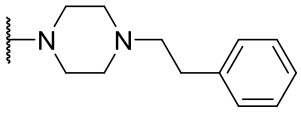	CF_3	64	n.a.
7 (CN1-041)	H	H	H	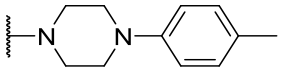	CF_3	26	n.a.
8 (CN1-042)	H	H	H	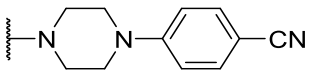	CF_3	45	n.a.
9 (CN1-043)	H	H	H	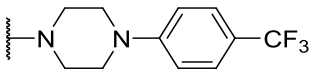	CF_3	71	27.3
10 (CN1-044)	H	H	H	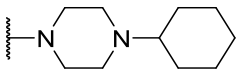	CF_3	12	n.a.
11 (CN1-045)	H	H	H	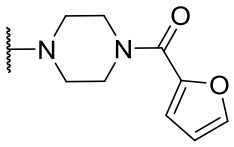	CF_3	29	n.a.
12 (CN1-048)	H	H	H	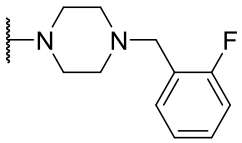	CF_3	20	n.a.

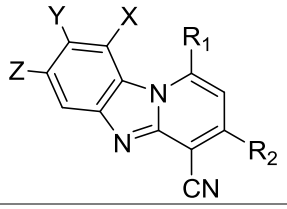

Compound	X	Y	Z	R_1	R_2	Antischistosomal activity Test conc. 10 µM (% inhibition)	
						NTS	Adult *S. mansoni*
13 (CN1-049)	H	H	H	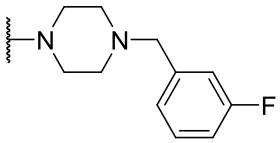	CF_3	19	n.a.
15 (CN1-051)[a]	H	H	H	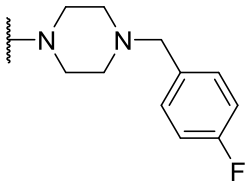		35	n.a.
21 (CN1-063)	H	H	H	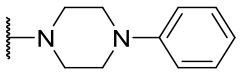	CF_3	63	n.a.
22 (CN1-064)	H	H	H	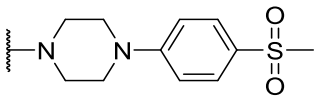	CF_3	48	n.a.
23 (CN1-065)	H	H	H	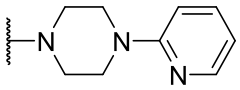	CF_3	60	n.a.
24 (CN1-066)	H	H	H	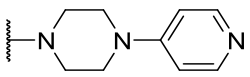	CF_3	100	100
25 (CN1-067)	H	H	H	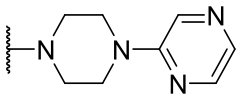	CF_3	22	n.a.
26 (CN1-068)	H	H	H	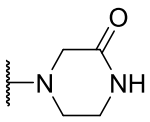	CF_3	33	n.a.
27 (CN1-069)	H	H	H	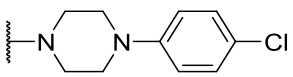	CF_3	67	n.a.

a, lead compound (**TDR44047**)

NTS, newly transformed schistosomula; n.a., not assessed

CHAPTER 4: PHYSICOCHEMICAL PROFILING

4.1 Introduction

A turbidimetric assay was carried out to evaluate the solubility of target PBI compounds. The melting points of the synthesized PBIs were determined to deduce and predict the various characteristics of the target compounds, including the strength of the intermolecular attractive forces, crystallinity, and solubility.

For the solubility assay, serial dilutions were prepared from 10 mM stock solutions in 96-well plates in triplicate, at concentrations ranging from 0.25 to 10 mM. A blank well containing no drug was included as a reference. From this plate, secondary dilutions of the samples were prepared in DMSO and 0.01 M phosphate-buffered saline (PBS, pH 7.4) in triplicate, in a second 96-well plate such that the final sample concentrations ranged from 0 to 200 µM. The plate was incubated at room temperature for 2 h and the absorbance was measured at 620 nm using a SpectraMax 340 PC384 microplate reader. This wavelength was deliberately selected because organic compounds do not commonly absorb ultraviolet (UV) radiation at this wavelength. Therefore, the absorbance of the insoluble particles that precipitate out of solution beyond the solubility threshold of the compound was measured.

The absorbance readings obtained were further analyzed by plotting a graph of the corrected absorbance against the concentration to determine the compound's solubility profile. The concentration at which the compound deviates from the baseline indicates the concentration at which the compound is insoluble, as the solution is turbid. In this kinetic turbidimetric assay, compounds with solubility < 1 µM are considered poorly soluble, those with solubility between 1 - 100 µM are moderately soluble, and those with solubility >100 µM are considered highly soluble. DMSO served as the internal standard to exclude compound absorption, and two other controls were included: hydrocortisone, which was soluble across all concentrations, and reserpine, which displayed moderate solubility (5-10 µM). These observations confirmed the validity of this solubility assay and the respective plots are illustrated in **Figures 38** and **39** below.

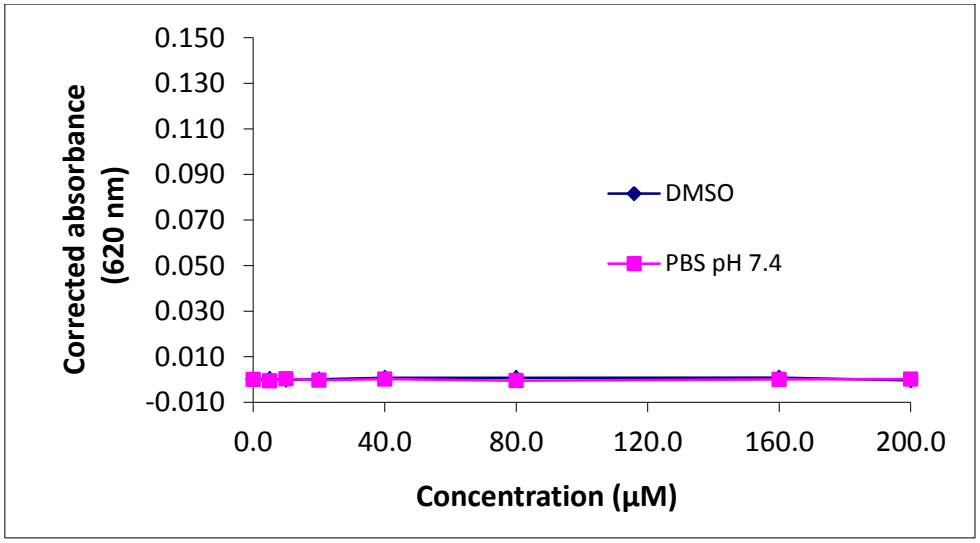

Figure 37: Plot of corrected absorbance versus concentration for hydrocortisone

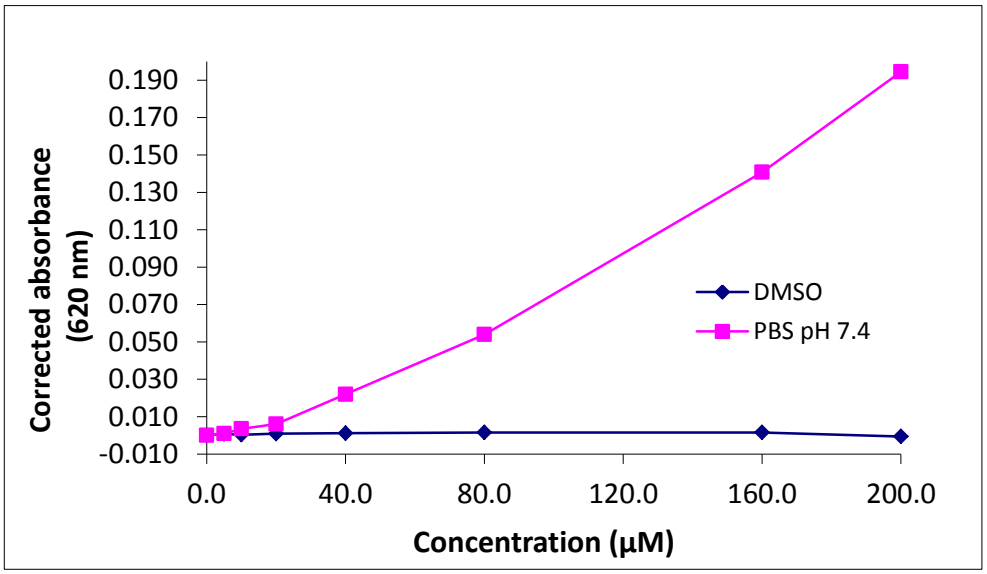

Figure 38: Plot of corrected absorbance versus concentration for reserpine

The predicted topological polar surface area (TPSA), a predictor of trans-membrane permeability and absorption, and calculated log P (cLogP), a measure of the compound's lipophilicity, were determined using ChemDraw version 16.0. The cLogP and TPSA of the synthesized compounds ranged from 2.92 to 7.18 and 45.87 to 80.11 $Å^2$, respectively. The polar surface area and cLogP properties ranged widely, and guided subsequent syntheses from lead compound **15** (TDR44047) to generate a diverse series of compounds whose physicochemical profiles are presented in **Table 9**.

Table 9: Calculated LogP, topological polar surface area, and solubility data for pyrido[1,2-*a*]benzimidazole target compounds

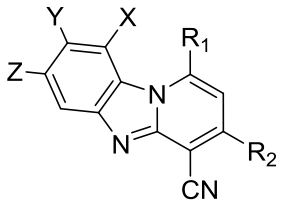

Compound	X	Y	Z	R_1	R_2	cLogP	TPSA ($Å^2$)	Melting point (°C)	Turbid-imetric solubility (µM)
1 (CN1-034)	H	H	H	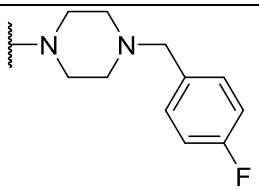	CF_3	5.76	45.87	254-256	5-10
2 (CN1-035)	H	H	H	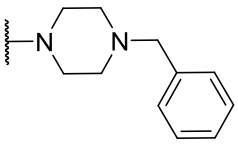	CF_3	5.61	45.87	267-269	5-10
3 (CN1-036)	H	H	H	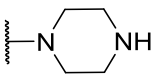	CF_3	3.32	54.66	264-266	20-40
4 (CN1-037)	H	H	H	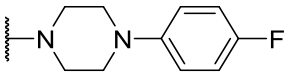	CF_3	5.64	45.87	244-246	5-10
5 (CN1-038)	H	H	H	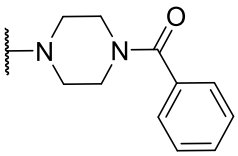	CF_3	4.50	62.94	255-257	10-20
6 (CN1-040)	H	H	H	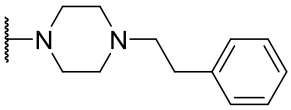	CF_3	5.87	45.87	248-250	5-10
7 (CN1-041)	H	H	H	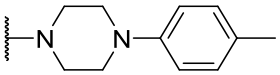	CF_3	5.82	45.87	269-271	5-10
8 (CN1-042)	H	H	H	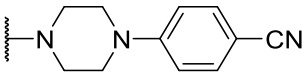	CF_3	5.15	69.66	259-261	10-20
9 (CN1-043)	H	H	H	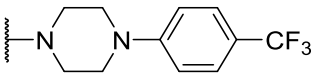	CF_3	6.50	45.87	254-256	5-10

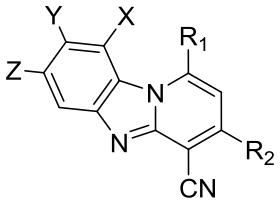

Compound	X	Y	Z	R_1	R_2	cLogP	TPSA (Å^2)	Melting point (°C)	Turbid-imetric solubility (µM)
10 (CN1-044)	H	H	H	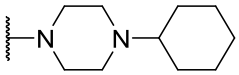	CF_3	5.71	45.87	256-258	5-10
11 (CN1-045)	H	H	H	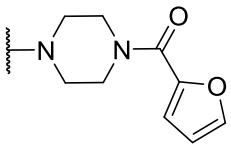	CF_3	3.67	72.17	278-280	20-40
12 (CN1-048)	H	H	H	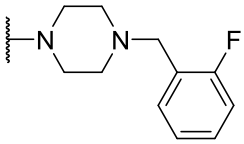	CF_3	5.76	45.87	269-271	5-10
13 (CN1-049)	H	H	H	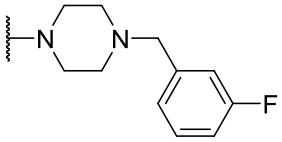	CF_3	5.76	45.87	259-261	5-10
14 (CN1-050)	H	H	H	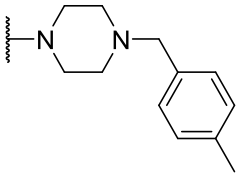	CF_3	6.11	45.87	254-256	5-10
15 (CN1-051)[a]	H	H	H	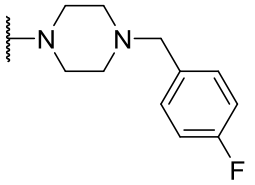		6.54	45.87	246-248	1-5
16 (CN1-052)	H	H	H	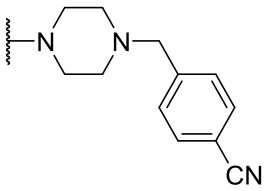	CF_3	5.05	69.66	272-273	5-10
17 (CN1-059)	H	Cl	Cl	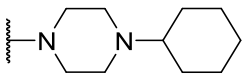	CF_3	7.02	45.87	264-266	1-5

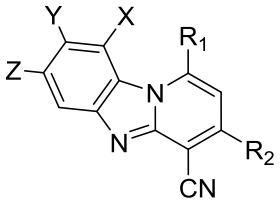

Compound	X	Y	Z	R_1	R_2	cLogP	TPSA (Å^2)	Melting point (°C)	Turbid-imetric solubility (µM)
18 (CN1-060)	H	Cl	Cl	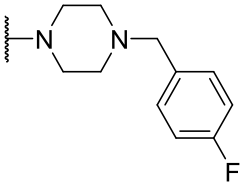	CF_3	7.06	45.87	258-260	1-5
19 (CN1-061)	H	Cl	Cl	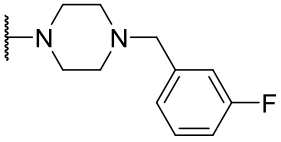	CF_3	7.06	45.87	277-279	1-5
20 (CN1-062)	H	Cl	Cl	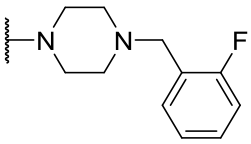	CF_3	7.06	45.87	256-258	1-5
21 (CN1-063)	H	H	H	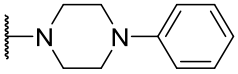	CF_3	5.32	45.87	271-273	5-10
22 (CN1-064)	H	H	H	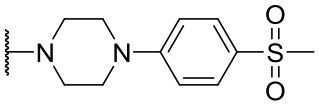	CF_3	4.11	80.11	260-262	10-20
23 (CN1-065)	H	H	H	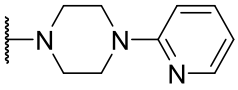	CF_3	4.37	58.23	275-277	10-20
24 (CN1-066)	H	H	H	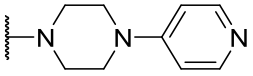	CF_3	4.37	58.23	274-276	10-20
25 (CN1-067)	H	H	H	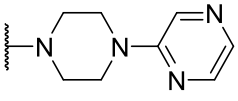	CF_3	3.61	70.59	256-258	20-40
26 (CN1-068)	H	H	H	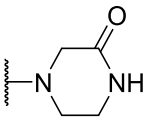	CF_3	2.92	71.73	263-265	40-80

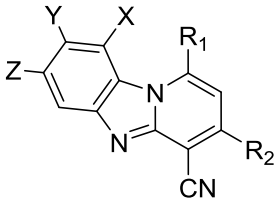

Compound	X	Y	Z	R_1	R_2	cLogP	TPSA (Å^2)	Melting point (°C)	Turbid-imetric solubility (µM)
27 (CN1-069)	H	H	H	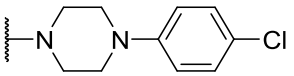	CF_3	6.21	45.87	265-267	1-5
28 (CN1-070)	H	H	H	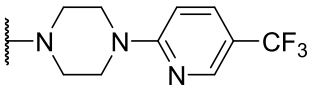	CF_3	5.40	58.23	266-268	5-10
29 (CN1-071)	H	H	H	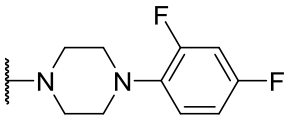	CF_3	5.84	45.87	270-272	5-10
30 (CN1-072)	H	H	H	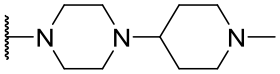	CF_3	3.86	49.11	265-267	10-20
31 (CN1-077)	Cl	H	Cl	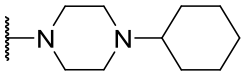	CF_3	7.14	45.87	269-271	1-5
32 (CN1-078)	Cl	H	Cl	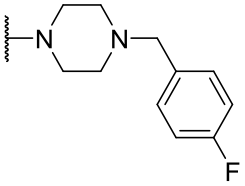	CF_3	7.18	45.87	273-275	< 5
33 (CN1-079)	H	F	F	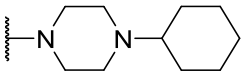	CF_3	5.93	45.87	254-256	5-10
34 (CN1-080)	H	F	F	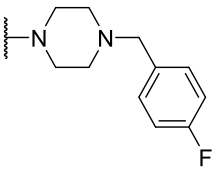	CF_3	5.97	45.87	274-276	1-5

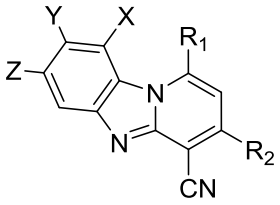

Compound	X	Y	Z	R_1	R_2	cLogP	TPSA ($Å^2$)	Melting point (°C)	Turbid-imetric solubility (µM)
35 (CN1-082)	H	H	H	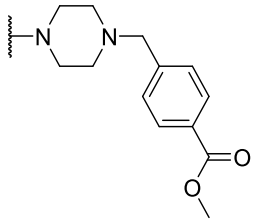	CF_3	5.58	72.17	265-267	1-5
36 (CN1-083)	H	H	H	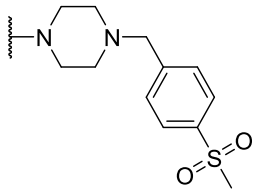	CF_3	3.97	80.01	260-262	20-40

a, lead compound
cLogP, calculated LogP; TPSA, topological polar surface area (determined using ChemDraw version 16.0)

4.2 Turbidimetric (kinetic) solubility

The turbidimetric solubility assay revealed that this series of compounds display low to moderate solubility (< 100 µM). This may be due to π-π stacking of the planar tricyclic core. The compounds that were soluble contained heteroatoms in their amino side-chains: for example, the solubility of compound **21** (5-10 µM) improved with the introduction of heteroatoms (compound **25**, 20-40 µM). Di-substituted PBI compounds displayed poor solubility compared to their unsubstituted parent compounds, because of their high lipophilicity resulting from the introduction of chloro and fluoro groups. Introducing a carbonyl group to the methylene linker on the piperazine ring, as in compounds **5** (10-20 µM) and **26** (40-80 µM), resulted in improved solubility. This improvement can be attributed to strong hydrogen bonding interactions between the compounds and water, which improve compound solubilization.

Compound **1** (5-10 µM) showed improved turbidimetric solubility compared to compound **15** (1-5 µM). Introducing a trifluoromethyl group in place of the propyl chain at R_2 thus improved the solubility of lead compound **15**. More than 85% of the LHS-unsubstituted compounds showed improved solubility compared to compound **15**, possibly because of the presence of the trifluoromethyl group at R_2, as well as that of amine substituents.

4.3 Melting points

Compounds in this series displayed relatively high melting points (> 244 °C), possibly because of their common structural planar tricyclic core, which promotes intermolecular interactions via π-π stacking.

4.4 Comparison of cLogP, TPSA, and antiplasmodium activity

LHS-unsubstituted compounds (cLogP 2.92 to 6.50) showed an average solubility range of 10-20 µM, while the average solubility range of LHS-substituted compounds (cLogP 5.93 - 7.18) was only 5-10 µM. As expected, introducing di-chlorination and di-fluorination to the LHS of the PBI core increased lipophilicity and therefore lowered the aqueous solubility.

In most cases, compounds with the same TPSA as the reference compound **15** (45.87 $Å^2$) displayed relatively high antiplasmodium activity, as shown in compounds **1** (IC_{50} = 0.17 µM)**, 10** (IC_{50} = 0.09 µM), and **33** (IC_{50} = 0.01 µM), among others. However, compounds that had a higher TPSA than compound **15** (45.87 $Å^2$) displayed lower antiplasmodium activity, with the exception of compound **28** (TPSA 58.23 $Å^2$, IC_{50} = 0.62 µM), which exhibited potent antiplasmodium activity. Thus, it is safe to conclude, on the basis of this data, that compounds with a similar TPSA to compound **15** favoured antiplasmodium activity of piperazinyl PBI analogues.

CHAPTER 5: SUMMARY AND FUTURE OUTLOOK

5.1 General summary and conclusion

In this dissertation, the design, synthesis, and characterization of piperazine-based PBI analogues with various amine side-chain substituents were undertaken. Diverse compounds with or without modifications on the benzyl portion of the PBI scaffold were synthesized, characterized via ^{1}H and ^{13}C NMR spectroscopy as well as LC-MS, and profiled for antiplasmodium and antischistosomal activities. Moreover, towards exploring a potential mechanism of action, the analogues were evaluated for β-hematin inhibitory activity. Physicochemical properties of target compounds were also determined including solubility and melting point.

Structure-activity and structure-property relationship trends emanating from this work may be summarised as follows:

- LHS di-fluoro substitution led to markedly improved antiplasmodium and β-hematin inhibition activity.
- Generally, there was a positive albeit weak correlation between BHI and antiplasmodium activities.
- Hydrophobic electron-withdrawing Craig plot substituents favoured antiplasmodium activity.
- Compounds bearing methylene- and ethylene-linked R_1 moieties (**Figure 40**) showed comparable activities.
- Introducing a carbonyl group to the methylene linker at R_1 or the piperazine ring (piperazin-2-one) resulted in enhanced solubility. However, this was accompanied by loss of antiplasmodium activity.
- Regio-isomerism showed no influence on antiplasmodium activity as *ortho*-, *meta*-, and *para*-substituted analogues were equipotent.
- 3,5- and 4,5- LHS-dichlorinated analogues displayed comparable activity but reduced activity relative to that of the parent unsubstituted analogues.
- Introducing a cyclohexane saturated substituent at R_1 (**Figure 40**) resulted in high antiplasmodium and β-hematin inhibition activities.

- LHS-substitution reduced turbidimetric solubility. Over 85% of the LHS-unsubstituted analogues showed significant improvement in solubility relative to that of lead compound **15**.
- Piperazinyl PBIs showed minimal gametocytocidal activity against both early and late gametocytes (< 50% inhibition at both 5 µM and 1 µM).
- Of the 23 compounds that were screened against NTS at a test concentration of 10 µM, compounds **4**, **9**, and **24** (**Figure 39**) displayed > 70% worm mortality. These three compounds were further evaluated against adult *S. mansoni* at the same initial concentration, and compounds **4** and **24** resulted in > 70% inhibition of worm viability. These frontrunner compounds are prioritised for further IC_{50} determination.

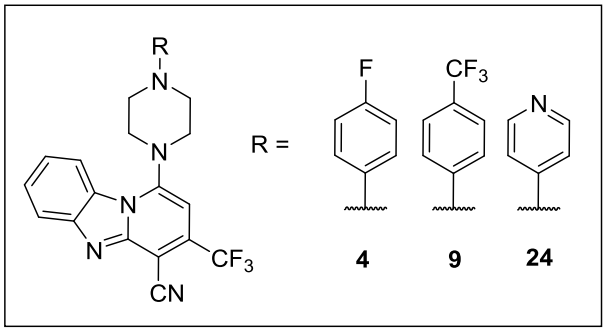

Figure 39: Chemical structures of compounds **4**, **9**, and **24** that displayed > 70% worm mortality against newly transformed schistosomula at a test concentration of 10 µM

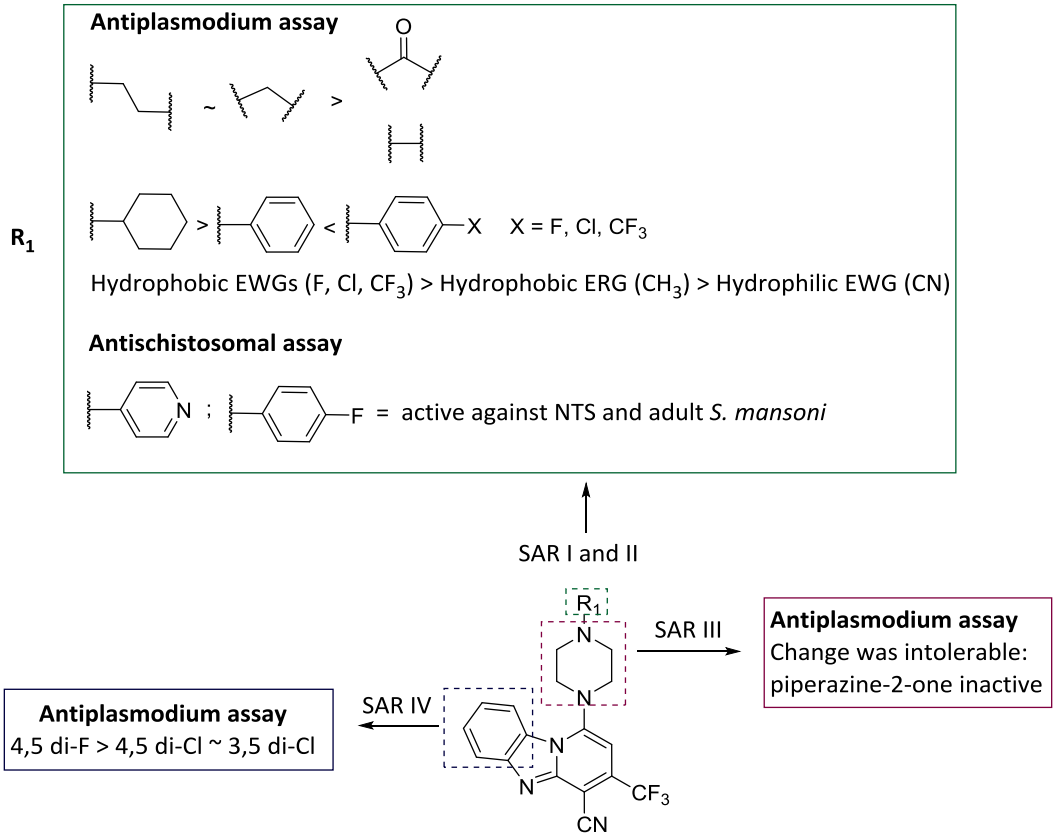

Figure 40: SAR Summary of the antiplasmodium and antischistosomal pyrido[1,2-*a*]benzimidazoles generated in this study (EWG, electron-withdrawing group; ERG, electron-releasing group; NTS, newly transformed schistosomula)

5.2 Future Work

Based on the identified SAR and SPR, future work suggested towards further profiling and optimization of frontrunner leads include:

- Further studies around the PBI core, to explore structure-activity and structure-property relationships to produce target compounds with improved drug-likeness (**Figure 41**).
- IC_{50} determination in adult *S. mansoni,* to draw conclusions about the antischistosomal activity of these PBI compounds.
- *P. falciparum* liver-stage screening, to evaluate stage-specificity and/or multi-stage activity.
- Cytotoxicity screens against the mammalian Chinese Hamster Ovarian (CHO) cell-line, to assess the compounds' cytotoxicity and to identify compounds with an

acceptable cytotoxicity profile for further evaluation of *in vitro* metabolic stability. Additionally, metabolically stable frontrunner compounds could be assessed *in vivo*.

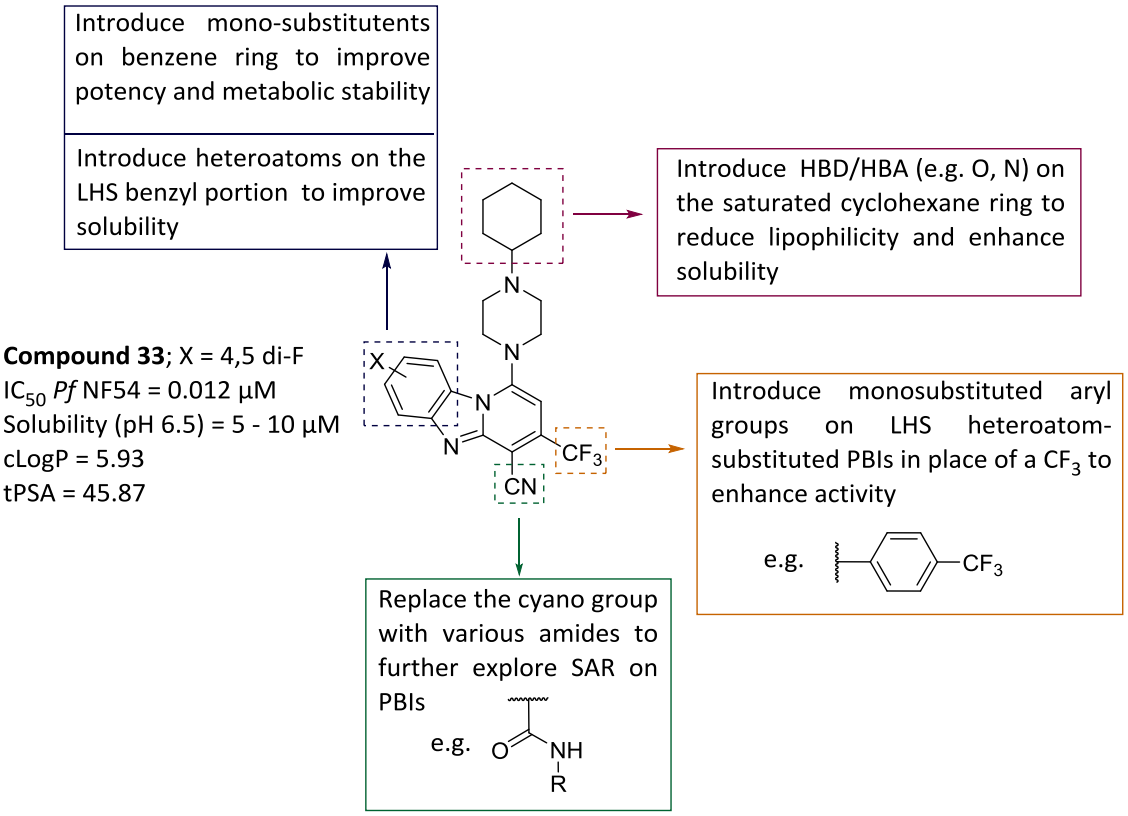

Examples of PBIs incorporating proposed changes to improve potency and solubility:

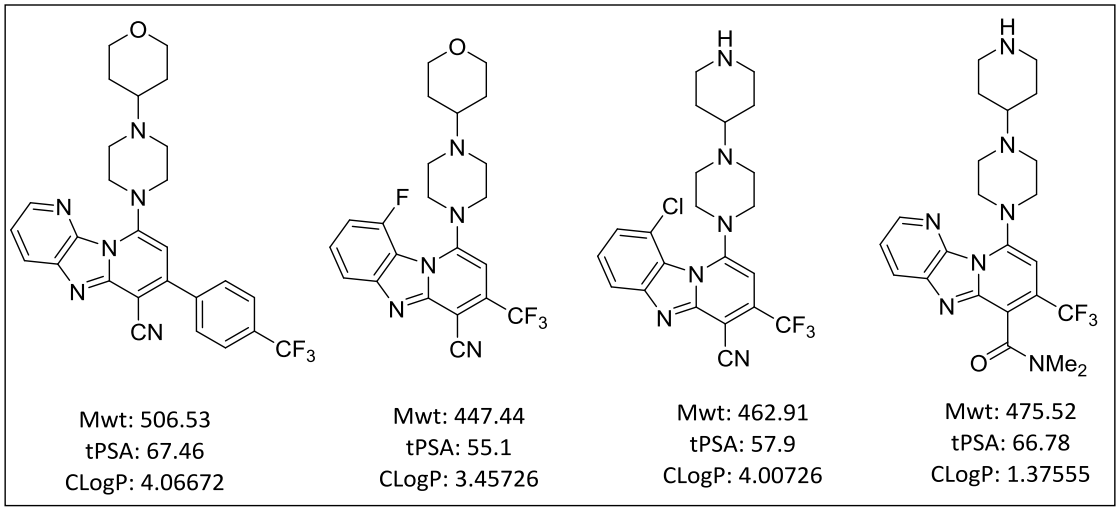

Figure 41: Proposed additional SAR strategy to piperazinyl pyrido[1,2-*a*]benzimidazole derivative **33** with potential to improve solubility (HBD, hydrogen-bond donor; HBA, hydrogen-bond acceptor; SAR, structure-activity relationship; PBI, pyrido[1,2-*a*]benzimidazole; Mwt, molecular weight)

CHAPTER 6: EXPERIMENTAL

6.1 Reagents, Solvents, Materials and Equipment

The commercially available analytical grade reagents and chemicals were purchased from either Sigma-Aldrich or Combi-Blocks and were used without purification. Reactions were monitored using Fluka or Merck F254 aluminium-backed pre-coated silica gel thin-layer chromatography (TLC) plates, and employing appropriately constituted mobile phases that comprised of ethyl acetate (EtOAc) and hexane or methanol (MeOH) and dichloromethane (DCM). TLC plates were visualized under ultraviolet light at wavelengths of 254 nm and 365 nm.

The Agilent LC-MS (liquid chromatography–mass spectrometry) instrument was used to determine the compound purity by comparing peak areas, the compound's molecular ion, and the retention time of the synthesized analogues. The LC-MS equipment comprised of Agilent 1260® Infinity Binary Pump, Agilent 1260® Infinity Diode Array Detector, Agilent 1290® Infinity Column Compartment, Agilent 1260® Infinity Autosampler, Agilent 6120® Quadrupole LC/MS and Peak Scientific® Genius 1050 Nitrogen Generator. The instrument was fitted with a Kinetex Core C18, 2.6 µm, 3 x 50 mm, 100 Å column which was maintained at 40 °C. The diode array detector was set to scan eluents at wavelengths in the range of 210-640 nm with mass spectra acquired using Electron Spray ionization (ESI) and Atmospheric Pressure Chemical Ionization (APCI) in the positive or negative mode. An injection volume of 2 µL and flow rate of 0.9 mL/min was used with the HPLC (high Performance Liquid Chromatography) composition and gradient conditions of the mobile phase as indicated in **Table 10** below.

Table 10: The HPLC mobile phase composition and gradient conditions

Time (min)	% A	% B	Composition	
			A	B
0.00-1.00	90	10	10 mM NH_4OAc in buffer (0.4% acetic acid)	10 mM NH_4OAc (0.4% acetic acid) in 90% HPLC grade MeOH in H_2O
1.00-3.00	5	95		
3.00-5.00	5	95		
5.00-6.50	90	10		
6.50-7.00	90	10		

^{1}H NMR spectra were recorded on a Varian Mercury (300 MHz), a Bruker Ultrashield-Plus (400 MHz) spectrometer or a Bruker (600 MHz). ^{13}C NMR spectra were recorded on the same instruments at 101 MHz or 151 MHz. NMR samples were prepared using deuterated dimethyl sulfoxide (DMSO-d_6). The *J* values represent the coupling constants and are given in Hertz (Hz). The multiplicities are abbreviated as s, d, t, m, dd, and ddd which represent the presence of a singlet, doublet, triplet, multiplet, doublet of doublets, and doublet of doublet of doublets on the ^{1}H NMR spectra, respectively. Melting points were determined using the STUART® automatic melting point machine in accordance with manufacturer's instructions.

6.2 Synthesis and Characterization

6.2.1 General Procedures and characterization of intermediates

6.2.1.1 Synthesis of intermediate I

To a suspension of the appropriately substituted diaminobenzene (1.0 equivalent) in DMF (0.7 mL), ethyl 2-cyanoacetate (3.0 equivalents) was added. The resulting reaction mixture was heated at 160 °C with stirring and monitored hourly using TLC. When the reaction was complete (9 - 12 h), the mixture was cooled to room temperature and the solvent evaporated with toluene (3 x 20 mL). The residue was then triturated by stirring in diethyl ether (20 mL), filtered and dried *in vacuo* to furnish the desired 2-benzimidazole acetonitrile-based intermediates **I** (**a-c**).

2-(5,7-dichloro-1H-benzo[*d*]imidazol-2-yl)acetonitrile (I-a)

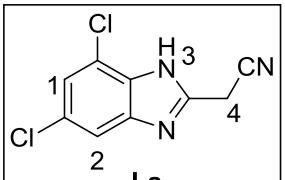

I-a

$C_9H_5Cl_2N_3$

Exact Mass: 224.99

Mwt: 226.06

Obtained from 3,5-dichlorobenzene-1,2-diamine as a light brown solid (0.50 g, 74%); R_f (EtOAc:Hex, 1:1) 0.32; ^{1}H NMR (300 MHz, DMSO-d_6) δ 13.17 (s, 1H, H^3), 7.63 (d, *J* = 1.8 Hz, 1H, H^2), 7.39 (d, *J* = 1.8 Hz, 1H, H^1), 4.43 (s, 2H, H^4); ^{13}C NMR (101 MHz, DMSO-d_6) 149.2, 147.9, 143.4, 127.1 (2C), 116.1, 113.5, 110.2, 20.6; HPLC-MS (APCI/ESI): Purity = 97%, t_R = 2.571 min, *m/z* $[M+H]^+$ = 226.0.

2-(5,6-dichloro-1H-benzo[*d*]imidazol-2-yl)acetonitrile (I-b)

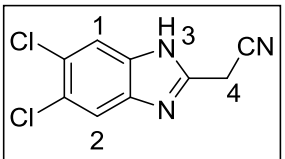

I-b

$C_9H_5Cl_2N_3$

Exact Mass: 224.99

Mwt: 226.06

Obtained from 4,5-dichlorobenzene-1,2-diamine as a light brown solid (0.50 g, 85%); R_f (EtOAc:Hex, 1:1) 0.36; ^{1}H NMR (300 MHz, DMSO-d_6) δ 12.82 (s, 1H, H^3), 7.83 (s, 2H, $H^{1,2}$), 4.41 (s, 2H, H^4); ^{13}C NMR (101 MHz, DMSO-d_6) δ 148.6, 145.1, 143.5, 123.6 (2C), 116.2, 113.3, 110.2, 19.9; HPLC-MS (APCI/ESI): Purity = 98%, t_R = 2.681 min, *m/z* $[M+H]^+$ = 226.0.

2-(5,6-difluoro-1H-benzo[*d*]imidazol-2-yl)acetonitrile (I-c)

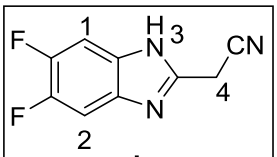

I-c

$C_9H_5F_2N_3$

Exact Mass: 193.05

Mwt: 193.16

Obtained from 4,5-difluorobenzene-1,2-diamine as a dark brown solid (0.50 g, 64%); R_f (EtOAc:Hex, 3:2) 0.26; ^{1}H NMR (400 MHz, DMSO-d_6) δ 12.80 (s, 1H, H^3), 7.62 – 7.45 (m, 2H, $H^{1,2}$), 4.39 (s, 2H, H^4); ^{13}C NMR (101 MHz, DMSO-d_6) δ 148.5, 148.2, 147.4, 146.1 (2C), 116.8, 106.1, 101.6, 18.93; HPLC-MS (APCI/ESI): Purity = 97%, t_R = 2.465 min, *m/z* $[M+H]^+$ = 194.1.

6.2.1.2 Synthesis of intermediate II

A mixture of the appropriately substituted benzimidazole acetonitrile (1.0 equivalent), ammonium acetate (2.0 equivalents), and ethyl 4,4,4-trifluoro-3-oxobutanoate (1.2 equivalents) were stirred at 150 °C for 10 h. Reaction mixture was cooled to 70 °C, a minimum amount of acetonitrile (15 - 20 mL) added, and the mixture stirred for a further 15 minutes followed by cooling to room temperature and then on ice. The cooled mixture was

filtered and dried to furnish the desired intermediates **II** (**a**–**d**), which were used in subsequent steps without further purification.

1-hydroxy-3-(trifluoromethyl)benzo[4,5]imidazo[1,2-*a*]pyridine-4-carbonitrile (II-a)

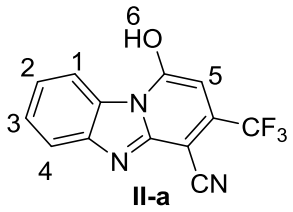

II-a

$C_{13}H_6F_3N_3O$
Exact Mass: 277.05
Mwt: 277.21

Obtained from 2-(1H-benzo[*d*]imidazol-2-yl)acetonitrile as a light brown solid (0.80 g, 85%), R_f (EtOAc:Hex, 1:1) 0.36; ^{1}H NMR (400 MHz, DMSO-d_6) δ 8.59 (dd, *J* = 8.2, 1.1 Hz, 1H, H^1), 7.63 (dd, *J* = 8.3, 1.0 Hz, 1H, H^4), 7.61 (ddd, *J* = 8.2, 7.2, 1.1 Hz, 1H, H^3), 7.45 (ddd, *J* = 8.3, 7.1, 1.2 Hz, 1H, H^2), 6.41 (s, 1H, H^5); ^{13}C NMR (101 MHz, DMSO-d_6) δ 168.0, 148.1, 138.5, 132.2, 127.4, 123.9 (2C), 121.3, 116.7, 114.6, 112.2, 103.2, 98.5; HPLC-MS (APCI/ESI): Purity = 98%, t_R = 2.628 min, *m/z* $[M-H]^-$ = 276.1.

7,9-dichloro-1-hydroxy-3-(trifluoromethyl)benzo[4,5]imidazo[1,2-*a*]pyridine-4-carbonitrile (II-b)

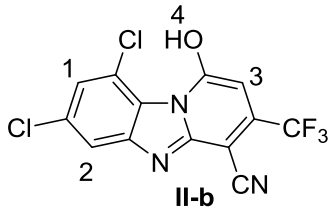

II-b

$C_{13}H_4Cl_2F_3N_3O$
Exact Mass: 344.97
Mwt: 346.09

Obtained from **I-a** as a light brown solid (0.30 g, 66%), R_f (EtOAc:Hex, 3:2) 0.35; ^{1}H NMR (400 MHz, DMSO-d_6) δ 8.45 (d, *J* = 2.0 Hz, 1H, H^2), 7.64 (d, *J* = 2.0 Hz, 1H, H^1), 6.02 (s, 1H, H^3); ^{13}C NMR (101 MHz, DMSO-d_6) δ 169.7, 153.2 (2C), 139.4, 131.4, 123.9 (2C), 121.4, 120.6, 116.9, 114.4 (2C), 97.5; HPLC-MS (APCI/ESI): Purity = 98%, t_R = 2.784 min, *m/z* $[M-H]^-$ = 343.9.

7,8-dichloro-1-hydroxy-3-(trifluoromethyl)benzo[4,5]imidazo[1,2-*a*]pyridine-4-carbonitrile (II-c)

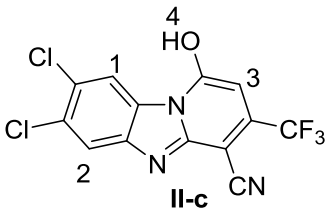

II-c

$C_{13}H_4Cl_2F_3N_3O$
Exact Mass: 344.97
Mwt: 346.09

Obtained from **I-b** as a light brown solid (0.30 g, 78%), R_f (EtOAc:Hex, 3:2) 0.34; ^{1}H NMR (400 MHz, DMSO-d_6) δ 8.61 (s, 1H, H^1), 7.79 (s, 1H, H^2), 6.10 (s, 1H, H^3); ^{13}C NMR (101 MHz, DMSO-d_6) δ 169.4, 153.8, 149.1, 143.9, 129.7, 127.4, 124.2, 120.9, 117.7, 117.2, 116.5 (2C), 96.5; HPLC-MS (APCI/ESI): Purity = 98%, t_R = 2.750 min, *m/z* $[M-H]^-$ = 343.9.

7,8-difluoro-1-hydroxy-3-(trifluoromethyl)benzo[4,5]imidazo[1,2-*a*]pyridine-4-carbonitrile (II-d)

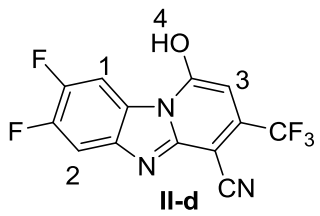

II-d

$C_{13}H_4F_5N_3O$
Exact Mass: 313.03
Mwt:313.19

Obtained from **I-c** as a brown solid (0.30 g, 80%), R_f (EtOAc:Hex, 3:2) 0.40; ^{1}H NMR (400 MHz, DMSO-d_6) δ 8.39 (dd, J = 11.0, 7.4 Hz, 1H, H^1), 7.72 (dd, J = 10.8, 7.3 Hz, 1H, H^2), 6.31 (s, 1H, H^3); ^{13}C NMR (101 MHz, DMSO-d_6) δ 168.4, 153.2 (2C), 144.9, 130.0, 127.4, 124.9, 120.7, 117.6, 117.0, 116.5 (2C), 98.2; HPLC-MS (APCI/ESI): Purity = 98%, t_R = 2.650 min, *m/z* $[M-H]^-$ = 312.1.

6.2.1.3 Synthesis of intermediate III

A mixture of the hydroxyl intermediate **II** (1 equivalent) and $POCl_3$ (20 equivalents) was stirred and heated at 130 °C. The reaction was monitored hourly using TLC and completed after 8 h. Excess $POCl_3$ was removed under reduced pressure and ice-cold water (20 mL) was slowly added to the mixture while stirring, yielding a yellow precipitate. The reaction mixture was neutralized with saturated $NaHCO_3$, filtered, and the resulting residue washed with ice-cold water (4 x 20 mL), dried *in vacuo* and used without further purification.

1-chloro-3-(trifluoromethyl)benzo[4,5]imidazo[1,2-*a*]pyridine-4-carbonitrile (III-a)

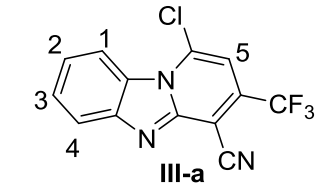

III-a

$C_{13}H_5ClF_3N_3$
Exact Mass: 295.01
Mwt: 295.65

Obtained from **II-a** as a yellow solid (0.60 g, 77%), R_f (EtOAc:Hex, 1:1) 0.40; ^{1}H NMR (600 MHz, DMSO-d_6) δ 8.78 (dd, J = 8.2, 1.0 Hz, 1H, H^1), 8.11 (dd, J = 8.2, 1.1 Hz, 1H, H^4), 7.81 (ddd, J = 8.2, 7.2, 1.0 Hz, 1H, H^3), 7.79 (s, 1H, H^5), 7.63 (ddd, J = 8.1, 7.1, 1.1 Hz, 1H, H^2); ^{13}C NMR (101 MHz, DMSO-d_6) δ 158.1, 147.9, 138.6, 132.3, 127.8, 123.9, 123.5, 121.0 (2C), 116.7, 114.6, 112.1, 100.3; HPLC-MS (APCI/ESI): Purity = 99%, t_R = 2.829 min, *m/z* $[M+H]^+$ = 296.1.

1,7,9-trichloro-3-(trifluoromethyl)benzo[4,5]imidazo[1,2-*a*]pyridine-4-carbonitrile (III-b)

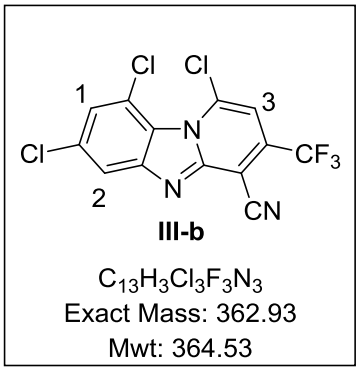

III-b

$C_{13}H_3Cl_3F_3N_3$
Exact Mass: 362.93
Mwt: 364.53

Obtained from **II-b** as a yellow solid (0.15 g, 80%), R_f (EtOAc:Hex, 1:1) 0.20; ^{1}H NMR (400 MHz, DMSO-d_6) δ 8.78 (d, J = 2.0 Hz, 1H, H^2), 8.09 (d, J = 2.0 Hz, 1H, H^1), 7.84 (s, 1H, H^3); ^{13}C NMR (101 MHz, DMSO-d_6) δ 163.7, 157.6, 149.9, 143.1, 139.8, 133.6, 130.5, 126.6 (2C), 121.9, 115.4 (2C), 100.6; HPLC-MS (APCI/ESI): Purity = 98%, t_R = 2.677 min, *m/z* [M+H]$^+$ = 363.9.

1,7,8-trichloro-3-(trifluoromethyl)benzo[4,5]imidazo[1,2-*a*]pyridine-4-carbonitrile (III-c)

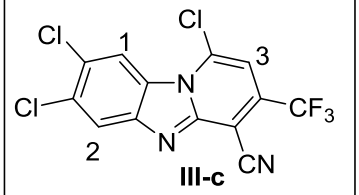

III-c

$C_{13}H_3Cl_3F_3N_3$
Exact Mass: 362.93
Mwt: 364.53

Obtained from **II-c** as a yellow solid (0.15 g, 84%), R_f (EtOAc:Hex, 3:2) 0.42; ^{1}H NMR (400 MHz, DMSO-d_6) δ 8.76 (s, 1H, H^1), 8.45 (s, 1H, H^2), 7.76 (s, 1H, H^3); ^{13}C NMR (101 MHz, DMSO-d_6) δ 158.7, 150.6, 139.1, 132.9, 130.4, 127.1, 124.8, 120.6, 117.6 (2C), 114.5, 112.7, 98.0; HPLC-MS (APCI/ESI): Purity = 98%, t_R = 2.870 min, *m/z* [M+H]$^+$ = 363.9.

1-chloro-7,8-difluoro-3-(trifluoromethyl)benzo[4,5]imidazo[1,2-*a*]pyridine-4-carbonitrile (III-d)

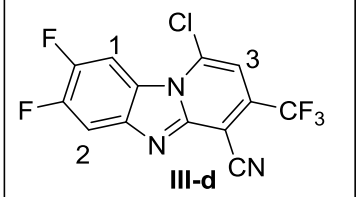

III-d

$C_{13}H_3ClF_5N_3$
Exact Mass: 330.99
Mwt:331.63

Obtained from **II-d** as a yellow solid (0.15 g, 71%), R_f (EtOAc:Hex, 2:3) 0.46; ^{1}H NMR (400 MHz, DMSO-d_6) δ 8.50 (dd, J = 11.0, 7.4 Hz, 1H, H^1), 7.74 (dd, J = 10.9, 7.3 Hz, 1H, H^2), 6.43 (s, 1H, H^3); ^{13}C NMR (101 MHz, DMSO-d_6) δ 158.4, 152.2, 150.1, 143.7, 130.2, 127.6, 124.1, 121.7, 117.9, 117.1, 116.4 (2C), 100.0; HPLC-MS (APCI/ESI): Purity = 97%, t_R = 2.693 min, *m/z* [M+H]$^+$ = 331.9.

6.2.2 General Procedures and characterization of final target compounds

6.2.2.1 Synthesis of target compounds IV

The stirred mixture of the chlorinated intermediate **III** (1 equivalent), triethylamine (2 equivalents), THF (5 mL) and the appropriate amine (1.2 equivalents) were irradiated in a microwave at 150 W (55 - 80 °C) for 20 - 60 minutes. The reaction was monitored every 10 minutes using TLC and LC-MS. THF was removed *in vacuo* and the residue was purified by column chromatography (SiO_2, 10% MeOH: DCM) to furnish target compounds **IV** (**1-36**).

1-(4-(4-fluorobenzyl)piperazin-1-yl)-3-(trifluoromethyl)benzo[4,5]imidazo[1,2-*a*]pyridine-4-carbonitrile (1)

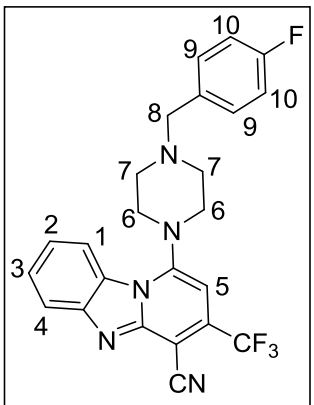

1

$C_{24}H_{19}F_4N_5$

Exact Mass: 453.16

Mwt: 453.44

Obtained from **III-a** as a yellow solid (0.86 g, 86%); m.p. 254 – 256 °C; R_f (EtOAc:Hex, 3:7) 0.40; ^{1}H NMR (400 MHz, DMSO-d_6) δ 8.31 (dd, *J* = 8.3, 1.0 Hz, 1H, H^1), 7.98 (dd, *J* = 8.3, 1.1 Hz, 1H, H^4), 7.67 (ddd, *J* = 8.2, 7.1, 1.0 Hz, 1H, H^3), 7.54 (dd, *J* = 8.6, 5.6 Hz, 2H, H^9), 7.22 (ddd, *J* = 8.2, 7.2, 1.2 Hz, 1H, H^2), 7.11 (dd, *J* = 9.8, 8.5 Hz, 2H, H^{10}), 6.85 (s, 1H, H^5), 3.64 (s, 2H, H^8), 3.52 - 3.44 (m, 4H, H^6), 2.98 - 2.77 (m, 4H, H^7); ^{13}C NMR (101 MHz, DMSO-d_6) δ 159.8, 154.2, 147.8, 145.3, 141.8, 134.5, 131.2, 128.9, 127.4 (2C), 122.9 (2C), 120.0, 116.6, 115.5 (2C), 115.3, 113.6, 95.3, 61.2, 51.7 (2C), 46.1 (2C); HPLC-MS (APCI/ESI): Purity = 97%, t_R = 3.209 min, *m/z* $[M+H]^+$ = 454.2.

1-(4-benzylpiperazin-1-yl)-3-(trifluoromethyl)benzo[4,5]imidazo[1,2-*a*]pyridine-4-carbonitrile (2)

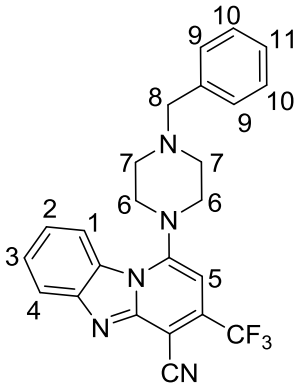

2

$C_{24}H_{20}F_3N_5$

Exact Mass: 435.17

Mwt: 435.45

Obtained from **III-a** as a yellow solid (0.81 g, 81%); m.p. 267 – 269 °C; R_f (EtOAc:Hex, 3:7) 0.30; ^{1}H NMR (400 MHz, DMSO-d_6) δ 8.31 (dd, *J* = 8.4, 1.0 Hz, 1H, H^1), 7.98 (dd, *J* = 8.3, 1.1 Hz, 1H, H^4), 7.67 (ddd, *J* = 8.2, 7.2, 1.0 Hz, 1H, H^3), 7.54 (ddd, *J* = 8.1, 7.3, 1.0 Hz, 1H, H^2), 7.42 - 7.35 (m, 2H, H^9), 7.29 - 7.23 (m, 3H, $H^{10,11}$), 6.85 (s, 1H, H^5), 3.65 (s, 1H, 2H, H^8), 3.09 - 3.02 (m, 4H, H^6), 2.67 - 2.52 (m, 4H, H^7); ^{13}C NMR (101 MHz, DMSO-d_6) δ 154.2, 147.8, 145.3, 138.3, 137.5 (2C), 133.9, 129.4, 128.9 (2C), 127.9, 123.6 (2C), 120.2, 119.6, 116.6, 113.6, 112.6, 95.3, 62.2, 50.3 (2C), 49.4 (2C); HPLC-MS (APCI/ESI): Purity = 98%, t_R = 3.038 min, *m/z* $[M+H]^+$ = 436.1.

1-(piperazin-1-yl)-3-(trifluoromethyl)benzo[4,5]imidazo[1,2-*a*]pyridine-4-carbonitrile (3)

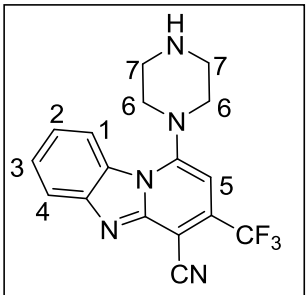

3

$C_{17}H_{14}F_3N_5$

Exact Mass: 345.12

Mwt: 345.33

Obtained from **III-a** as a yellow solid (0.83 g, 83%); m.p. 264 – 266 °C; R_f (EtOAc:Hex, 2:3) 0.30; ^{1}H NMR (400 MHz, DMSO-d_6) δ 8.34 (dd, *J* = 8.3, 1.1 Hz, 1H, H^1), 7.99 (dd, *J* = 8.2, 1.1 Hz, 1H, H^4), 7.68 (ddd, *J* = 8.1, 7.1, 1.1 Hz, 1H, H^3), 7.56 (ddd, *J* = 8.4, 7.1, 1.2 Hz, 1H, H^2), 6.83 (s, 1H, H^5), 3.48 - 3.43 (m, 4H, H^6), 3.10 - 3.06 (m, 4H, H^7); ^{13}C NMR (101 MHz, DMSO-d_6) δ 156.4, 147.8, 145.3, 128.9, 127.3, 122.8 (2C), 121.2, 119.9, 116.6, 113.6, 112.1, 95.0, 51.2 (2C), 47.6 (2C); HPLC-MS (APCI/ESI): Purity = 98%, t_R = 2.441 min, *m/z* $[M+H]^+$ = 346.1.

1-(4-(4-fluorophenyl)piperazin-1-yl)-3-(trifluoromethyl)benzo[4,5]imidazo[1,2-*a*]pyridine-4-carbonitrile (4)

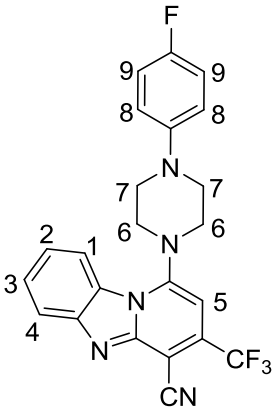

4

$C_{23}H_{17}F_4N_5$
Exact Mass: 439.14
Mwt: 439.42

Obtained from **III-a** as a yellow solid (0.83 g, 83%); m.p. 244 – 246 °C; R_f (EtOAc:Hex, 3:7) 0.33; ^{1}H NMR (400 MHz, DMSO-d_6) δ 8.40 (dd, *J* = 8.3, 1.1 Hz, 1H, H^1), 8.00 (dd, *J* = 8.3, 1.0 Hz, 1H, H^4), 7.68 (ddd, *J* = 8.2, 7.1, 1.1 Hz, 1H, H^3), 7.55 (ddd, *J* = 8.2, 7.2, 1.2 Hz, 1H, H^2), 7.14 (dd, *J* = 9.8, 8.5 Hz, 2H, H^9), 7.09 (dd, *J* = 8.6, 5.5 Hz, 2H, H^8), 6.92 (s, 1H, H^5), 3.67 - 3.50 (m, 4H, H^7), 3.18 - 3.07 (m, 4H, H^6); ^{13}C NMR (101 MHz, DMSO-d_6) δ 158.0, 155.7, 154.1, 147.9, 147.7, 145.3, 136.3, 127.4 (2C), 123.0, 120.0, 118.3, 116.8 (2C), 115.9 (2C), 113.6, 112.1, 95.4, 48.6 (2C), 46.1 (2C); HPLC-MS (APCI/ESI): Purity = 98%, t_R = 3.034 min, *m/z* $[M+H]^+$ = 440.1.

1-(4-benzoylpiperazin-1-yl)-3-(trifluoromethyl)benzo[4,5]imidazo[1,2-*a*]pyridine-4-carbonitrile (5)

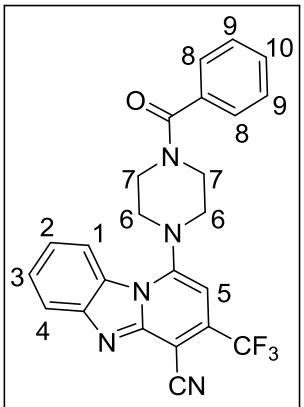

5

$C_{24}H_{18}F_3N_5O$
Exact Mass: 449.15
Mwt: 449.44

Obtained from **III-a** as a yellow solid (0.83 g, 83%); m.p. 255 – 257 °C; R_f (EtOAc:Hex, 2:3) 0.30; ^{1}H NMR (400 MHz, DMSO-d_6) δ 8.42 (dd, *J* = 8.4, 1.0 Hz, 1H, H^1), 8.03 - 7.96 (m, 2H, H^8), 7.69 (ddd, *J* = 8.2, 7.1, 1.1 Hz, 1H, H^4), 7.56 (ddd, *J* = 8.3, 7.1, 1.2 Hz, 1H, H^3), 7.51 - 7.46 (m, 3H, $H^{9,10}$), 7.44 (ddd, *J* = 8.2, 7.1, 1.2 Hz, 1H, H^2), 6.94 (s, 1H, H^5), 3.64 -3.57 (m, 4H, H^7), 3.16 - 3.08 (m, 4H, H^6); ^{13}C NMR (101 MHz, DMSO-d_6) δ 169.8, 153.8, 147.7, 145.3, 136.5, 135.9, 135.2, 130.3, 130.0 (2C), 128.9 (2C), 123.1 (2C), 120.0, 119.8, 116.7, 113.5, 112.4, 96.0, 50.2 (2C), 46.0 (2C); HPLC-MS (APCI/ESI): Purity = 98%, t_R = 2.832 min, *m/z* $[M+H]^+$ = 450.2.

1-(4-phenethylpiperazin-1-yl)-3-(trifluoromethyl)benzo[4,5]imidazo[1,2-*a*]pyridine-4-carbonitrile (6)

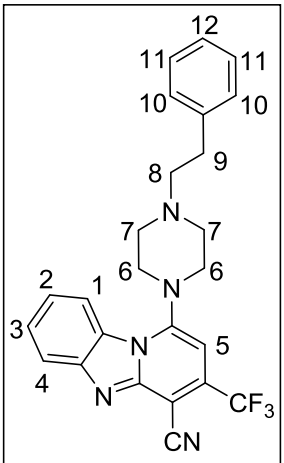

6

$C_{25}H_{22}F_3N_5$

Exact Mass: 449.18

Mwt: 449.48

Obtained from **III-a** as a yellow solid (0.90 g, 90%); m.p. 248 – 250 °C; R_f (EtOAc: Hex, 1:1) 0.48; ^{1}H NMR (400 MHz, DMSO-d_6) δ 8.34 (dd, *J* = 8.4, 1.0 Hz, 1H, H^1), 8.00 (dd, *J* = 8.2, 1.2 Hz, 1H, H^4), 7.69 (ddd, *J* = 8.3, 7.1, 1.1 Hz, 1H, H^3), 7.56 (ddd, *J* = 8.5, 7.1, 1.2 Hz, 1H, H^2), 7.44 - 7.38 (m, 2H, H^{10}), 7.34 - 7.27 (m, 3H, $H^{11,12}$), 6.87 (s, 1H, H^5), 3.62 - 3.55 (m, 4H, H^7), 3.11 - 3.05 (m, 4H, H^6), 2.84 (t, *J* = 7.4 Hz, 2H, H^8), 2.59 (t, *J* = 7.2 Hz, 2H, H^9); ^{13}C NMR (101 MHz, DMSO-d_6) δ 154.2, 147.8, 145.3, 141.7, 139.1, 135.1, 128.9 (2C), 127.4 (2C), 126.3, 123.8 (2C), 120.0, 119.3, 116.6, 113.6, 112.1, 95.2, 59.6, 51.8 (2C), 49.6 (2C), 33.1; HPLC-MS (APCI/ESI): Purity = 98%, t_R = 3.081 min, *m/z* $[M+H]^+$ = 450.2.

1-(4-(p-tolyl)piperazin-1-yl)-3-(trifluoromethyl)benzo[4,5]imidazo[1,2-*a*]pyridine-4-carbonitrile (7)

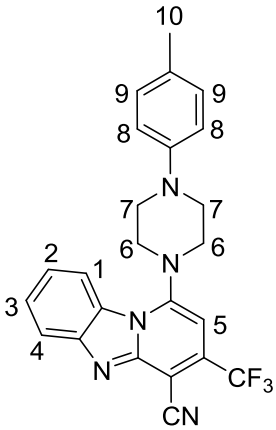

7

$C_{24}H_{20}F_3N_5$

Exact Mass: 435.17

Mwt: 435.45

Obtained from **III-a** as a yellow solid (0.67 g, 67%); m.p. 269 – 271 °C; R_f (EtOAc: Hex, 2:3) 0.34; ^{1}H NMR (400 MHz, DMSO-d_6) δ 8.42 (dd, *J* = 8.4, 1.0 Hz, 1H, $H^{1)}$, 8.01 (dd, *J* = 8.2, 1.1 Hz, 1H, H^4), 7.69 (ddd, *J* = 8.3, 7.1, 1.1 Hz, 1H, H^3), 7.56 (ddd, *J* = 8.3, 7.1, 1.4 Hz, 1H, H^2), 7.10 (d, *J* = 7.9 Hz, 2H, H^9), 6.98 (d, *J* = 8.1 Hz, 2H, H^8), 6.90 (s, 1H, H^5), 3.19 - 3.12 (m, 4H, H^7), 3.07 - 3.00 (m, 4H, H^6), 2.26 (s, 3H, H^{10}); ^{13}C NMR (101 MHz, DMSO-d_6) δ 154.1, 149.0, 147.8, 145.4, 136.6, 129.4, 129.0, 127.4 (2C), 123.0 (2C), 120.0, 119.8, 117.7, 113.4, 112.3 (2C), 111.9, 95.4, 50.4 (2C), 48.5 (2C), 20.4; HPLC-MS (APCI/ESI): Purity = 97%, t_R = 3.115 min, *m/z* $[M+H]^+$ = 436.2.

1-(4-(4-cyanophenyl)piperazin-1-yl)-3-(trifluoromethyl)benzo[4,5]imidazo[1,2-*a*]pyridine-4-carbonitrile (8)

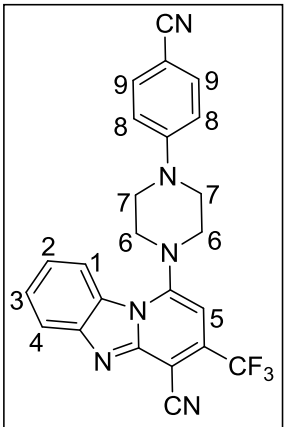

8

$C_{24}H_{17}F_3N_6$
Exact Mass: 446.15
Mwt: 446.44

Obtained from **III-a** as a yellow solid (0.86 g, 86%); m.p. 259 – 261 °C; R_f (EtOAc: Hex, 2:3) 0.27; ^{1}H NMR (400 MHz, DMSO-d_6) δ 8.45 (dd, *J* = 8.2, 1.0 Hz, 1H, H^1), 8.03 (dd, *J* = 8.2, 1.0 Hz, 1H, H^4), 7.75 (ddd, *J* = 8.3, 7.1, 1.4 Hz, 1H, H^3), 7.70 (ddd, *J* = 8.3, 7.2, 1.4 Hz, 1H, H^2), 7.59 (d, *J* = 7.8 Hz, 1H, H^9), 7.24 (d, *J* = 7.9 Hz, 2H, H^8), 6.92 (s, 1H, H^5), 3.16 - 3.11 (m, 4H, H^7), 3.09 - 3.01 (m, 4H, H^6); ^{13}C NMR (101 MHz, DMSO-d_6) δ 154.0, 153.4, 145.4, 141.5, 139.0, 135.1, 133.8 (2C), 123.4 (2C), 120.1, 119.8, 118.0, 117.7,113.7, 112.1, 110.7 (2C), 102.1, 100.1, 49.9 (2C), 47.3 (2C); HPLC-MS (APCI/ESI): Purity = 97%, t_R = 2.810 min, *m/z* $[M+H]^+$ = 447.2.

3-(trifluoromethyl)-1-(4-(4-(trifluoromethyl)phenyl)piperazin-1-yl)benzo[4,5]imidazo[1,2-*a*]pyridine-4-carbonitrile (9)

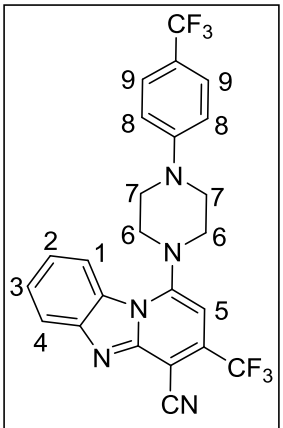

9

$C_{24}H_{17}F_6N_5$
Exact Mass: 489.14
Mwt: 489.43

Obtained from **III-a** as a yellow solid (0.75 g, 75%); m.p. 254 – 256 °C; R_f (EtOAc: Hex, 1:1) 0.49; ^{1}H NMR (400 MHz, DMSO-d_6) δ 8.44 (dd, *J* = 8.3, 1.0 Hz, 1H, H^1), 8.01 (dd, *J* = 8.3, 1.0 Hz, 1H, H^4), 7.70 (ddd, *J* = 8.3, 7.2, 1.0 Hz, 1H, H^3), 7.62 - 7.54 (m, 3H, $H^{2,9}$), 7.21 (d, *J* = 8.1 Hz, 2H, H^8), 6.92 (s, 1H, H^5), 3.15 - 2.98 (m, 8H, $H^{6,7}$); ^{13}C NMR (101 MHz, DMSO-d_6) δ 154.0, 153.4, 147.4, 144.5, 129.0, 127.1 (2C), 126.8 (2C), 123.4 (2C), 120.1 (2C), 119.9, 117.7, 115.7 (3C), 114.1, 96.8, 47.7 (2C), 46.2 (2C); HPLC-MS (APCI/ESI): Purity = 97%, t_R = 3.080 min, *m/z* $[M+H]^+$ = 490.1.

1-(4-cyclohexylpiperazin-1-yl)-3-(trifluoromethyl)benzo[4,5]imidazo[1,2-*a*]pyridine-4-carbonitrile (10)

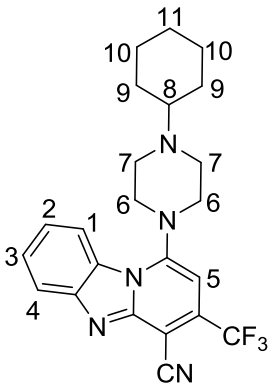

10

$C_{23}H_{24}F_3N_5$
Exact Mass: 427.20
Mwt: 427.48

Obtained from **III-a** as a yellow solid (0.67 g, 67%); m.p. 256 – 258 °C; Rf (EtOAc: Hex, 2:3) 0.40; ^{1}H NMR (400 MHz, DMSO-d_6) δ 8.34 (dd, *J* = 8.5, 1.0 Hz, 1H, H^1), 8.00 (dd, *J* = 8.2, 1.0 Hz, 1H, H^4), 7.73 (ddd, *J* = 8.3, 7.2, 1.1 Hz, 1H, H^3), 7.57 (ddd, *J* = 8.3, 7.1, 1.2 Hz, 1H, H^2), 6.83 (s, 1H, H^5), 3.16 - 3.11 (m, 4H, H^6), 3.07 - 3.01 (m, 5H, H^{7,8}), 1.85 - 1.79 (m, 4H, H^9), 1.69 - 1.63 (m, 2H, H^{11}), 1.31 - 1.23 (m, 4H, H^{10}); ^{13}C NMR (101 MHz, DMSO-d_6) δ 158.2, 147.8, 145.4, 136.6, 129.0, 123.9 (2C), 122.8, 121.2, 120.0, 116.6, 113.5, 100.1, 68.0, 51.9 (2C), 48.5 (2C), 28.9 (2C), 26.5, 25.1 (2C); HPLC-MS (APCI/ESI): Purity = 97%, t_R = 2.645 min, *m/z* $[M+H]^+$ = 428.2.

1-(4-(furan-2-carbonyl)piperazin-1-yl)-3-(trifluoromethyl)benzo[4,5]imidazo[1,2-*a*]pyridine-4-carbonitrile (11)

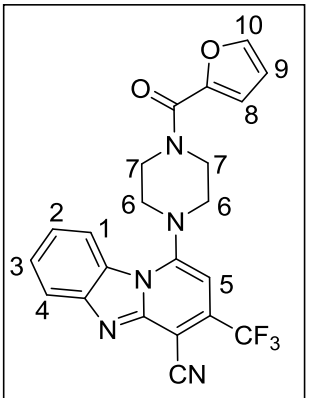

11

$C_{22}H_{16}F_3N_5O_2$
Exact Mass: 439.13
Mwt: 439.40

Obtained from **III-a** as a yellow solid (0.91 g, 91%); m.p. 278 – 280 °C; R_f (MeOH:DCM, 1:9) 0.53; ^{1}H NMR (400 MHz, DMSO-d_6) δ 8.44 (dd, *J* = 8.4, 1.1 Hz, 1H, H^1), 8.01 (dd, *J* = 8.2, 1.0 Hz, 1H, H^4), 7.83 (dd, *J* = 7.8, 1.7 Hz, 1H, H^{10}), 7.70 (ddd, *J* = 8.2, 7.1, 1.2 Hz, 1H, H^3), 7.57 (ddd, *J* = 8.3, 7.1, 1.2 Hz, 1H, H^2), 7.08 (dd, *J* = 7.7, 1.9 Hz, 1H, H^8), 6.72 - 6.64 (m, 1H, H^9), 3.92 (s, 1H, H^5), 3.23 - 3.16 (m, 4H, H^7), 3.11 - 3.07 (m, 4H, H^6); ^{13}C NMR (101 MHz, DMSO-d_6) δ 159.1, 153.7, 147.4, 145.4, 145.2, 136.6, 129.0, 127.4, 123.1 (2C), 120.0, 119.6, 117.7, 116.6, 116.3, 113.4, 111.8, 95.9, 50.4 (2C), 46.2 (2C); HPLC-MS (APCI/ESI): Purity = 97%, t_R = 2.767 min, *m/z* $[M+H]^+$ = 440.1.

1-(4-(2-fluorobenzyl)piperazin-1-yl)-3-(trifluoromethyl)benzo[4,5]imidazo[1,2-*a*]pyridine-4-carbonitrile (12)

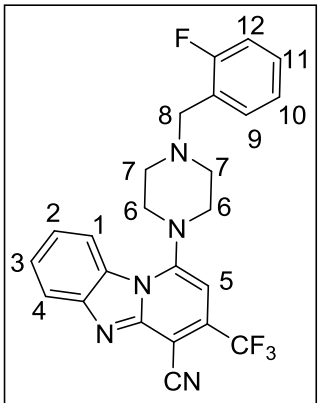

12

$C_{24}H_{19}F_4N_5$
Exact Mass: 453.16
Mwt: 453.44

Obtained from **III-a** as a yellow solid (0.93 g, 93%); m.p. 269 – 271 °C; R_f (EtOAc: Hex, 2:3) 0.50; ^{1}H NMR (600 MHz, DMSO-d_6) δ 8.33 (dd, *J* = 8.3, 1.0 Hz, 1H, H^1), 7.99 (dd, *J* = 8.2 , 1.1 Hz, 1H, H^4), 7.68 - 7.53 (m, 2H, $H^{11,12}$), 7.45 (ddd, *J* = 8.2, 7.1, 1.2 Hz, 1H, H^3), 7.29 (ddd, *J* = 8.2, 7.1, 1.0 Hz, 1H, H^2), 7.22 - 7.14 (m, 2H, $H^{9,10}$), 6.87 (s, 1H, H^5), 3.72 (s, 2H, H^8), 3.32 - 3.26 (m, 4H, H^6), 3.16 - 3.08 (m, 4H, H^7); ^{13}C NMR (101 MHz, DMSO-d_6) δ 160.4, 154.2, 147.7, 145.3, 132.2, 132.1 (2C), 129.9 (2C), 128.9, 127.4, 124.0, 123.9, 122.8, 120.0, 116.6, 115.7, 113.6, 95.3, 54.8, 51.7 (2C), 45.2 (2C); HPLC-MS (APCI/ESI): Purity = 99%, t_R = 3.325 min, *m/z* $[M+H]^+$ = 454.2.

1-(4-(3-fluorobenzyl)piperazin-1-yl)-3-(trifluoromethyl)benzo[4,5]imidazo[1,2-*a*]pyridine-4-carbonitrile (13)

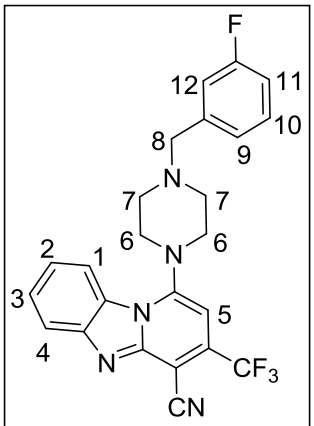

13

$C_{24}H_{19}F_4N_5$
Exact Mass: 453.16
Mwt: 453.44

Obtained from **III-a** as a yellow solid (0.90 g, 90%); m.p. 259 – 261 °C; R_f (EtOAc: Hex, 2:3) 0.44; ^{1}H NMR (400 MHz, DMSO-d_6) δ 8.35 (dd, *J* = 8.2, 1.0 Hz, 1H, H^1), 7.99 (dd, *J* = 8.1, 1.1 Hz, 1H, H^4), 7.68 - 7.55 (m, 2H, $H^{11,12}$), 7.44 (ddd, *J* = 8.2, 7.1, 1.2 Hz, 1H, H^3), 7.25 (ddd, *J* = 8.2, 7.1, 1.1 Hz, 1H, H^2), 7.19 - 7.13 (m, 2H, $H^{9,10}$), 6.85 (s, 1H, H^5), 3.72 (s, 2H, H^8), 3.27 - 3.21 (m, 4H, H^6), 3.19 - 3.08 (m, 4H, H^7); ^{13}C NMR (101 MHz, DMSO-d_6) δ 160.0, 154.1, 147.8, 145.4, 130.5, 130.5 (2C), 129.0 (2C), 128.6, 127.3, 125.1, 123.8, 122.8, 120.0, 116.6, 115.7, 113.4, 95.3, 54.8, 50.5 (2C), 49.4 (2C); HPLC-MS (APCI/ESI): Purity = 96%, t_R = 3.319 min, *m/z* $[M+H]^+$ = 454.1

1-(4-(4-methylbenzyl)piperazin-1-yl)-3-(trifluoromethyl)benzo[4,5]imidazo[1,2-*a*]pyridine-4-carbonitrile (14)

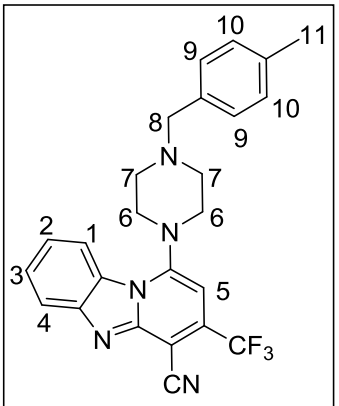

14

$C_{25}H_{22}F_3N_5$
Exact Mass: 449.18
Mwt: 449.48

Obtained from **III-a** as a yellow solid (0.78 g, 86%); m.p. 254 – 256 °C; R_f (EtOAc: Hex, 2:3) 0.50; ^{1}H NMR (400 MHz, DMSO-d_6) δ 8.35 (dd, *J* = 8.4, 1.0 Hz, 1H, H^1), 7.92 (dd, *J* = 8.3, 1.1 Hz, 1H, H^4), 7.68 (ddd, *J* = 8.2, 7.1, 1.1 Hz, 1H, H^3), 7.28 (ddd, *J* = 8.2, 7.1, 1.1 Hz, 1H, H^2), 7.17 (d, *J* = 7.8 Hz, 2H, H^9), 7.12 (d, *J* = 7.9, 2H, H^{10}), 6.34 (s, 1H, H^5), 3.67 (s, 2H, H^8), 3.30 - 3.23 (m, 4H, H^6), 3.18 - 3.09 (m, 4H, H^7), 2.31 (s, 3H, H^{11}); ^{13}C NMR (101 MHz, DMSO-d_6) δ 160.0, 154.9, 147.2, 145.6, 141.8, 135.0, 131.4, 128.5, 127.6 (2C), 122.9 (2C), 120.5, 116.3, 115.3 (2C), 115.0, 113.7, 95.9, 61.5, 51.8 (2C), 47.1 (2C), 21.0; HPLC-MS (APCI/ESI): Purity = 98%, t_R = 3.370 min, *m/z* $[M+H]^+$ = 450.2.

1-(4-(4-fluorobenzyl)piperazin-1-yl)-3-propylbenzo[4,5]imidazo[1,2-*a*]pyridine-4-carbonitrile (15)

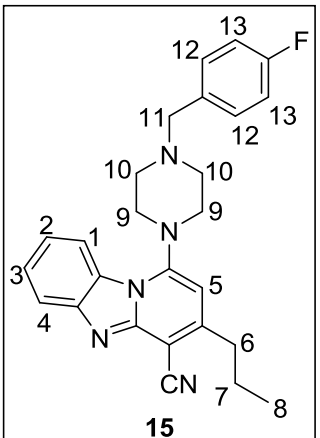

15

$C_{26}H_{26}FN_5$
Exact Mass: 427.22
Mwt: 427.53

Obtained from **III-a** as a yellow solid (0.88 g, 88%); m.p. 246 – 248 °C; R_f (EtOAc: Hex, 2:3) 0.50; ^{1}H NMR (400 MHz, DMSO-d_6) δ 8.29 (dd, *J* = 8.3, 1.1 Hz, 1H, H^1), 7.87 (dd, *J* = 8.1, 1.1 Hz, 1H, H^4), 7.56 (ddd, *J* = 8.2, 7.2, 1.1 Hz, 1H, H^3), 7.47 (dd, *J* = 8.5, 5.1 Hz, 2H, H^{12}), 7.43 (ddd, *J* = 8.2, 7.2, 1.2 Hz, 1H, H^2), 7.15 (dd, *J* = 9.8, 8.6 Hz, 2H, H^{13}), 6.64 (s, 1H, H^5), 3.64 (s, 2H, H^{11}), 3.52 - 3.44 (m, 4H, H^9), 3.10 (t, *J* = 7.0 Hz, 2H, H^6), 3.01 - 2.87 (m, 4H, H^{10}), 1.86 - 1.79 (m, 2H, H^7), 1.23 (t, *J* = 7.3 Hz, 3H, H^8); ^{13}C NMR (101 MHz, DMSO-d_6) δ 159.8, 154.2, 147.8, 145.3, 141.8, 134.5, 131.2, 128.9, 127.4 (2C), 122.9 (2C), 120.0, 116.6, 115.5 (2C), 113.6, 100.8, 64.4, 54.9 (2C), 48.7 (2C), 34.9, 23.6, 15.9; HPLC-MS (APCI/ESI): Purity = 98%, t_R = 3.150 min, *m/z* $[M+H]^+$ = 428.2.

1-(4-(4-cyanobenzyl)piperazin-1-yl)-3-(trifluoromethyl)benzo[4,5]imidazo[1,2-*a*]pyridine-4-carbonitrile (16)

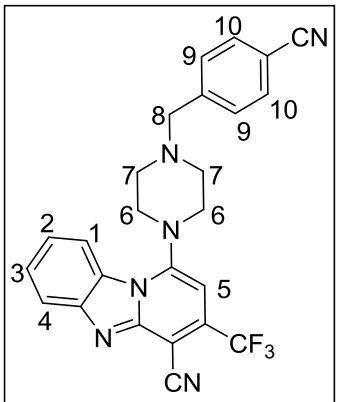

16

$C_{25}H_{19}F_3N_6$
Exact Mass: 460.16
Mwt: 460.46

Obtained from **III-a** as a yellow solid (0.80 g, 80 %); m.p. 272 – 274 °C; R_f (EtOAc: Hex, 2:3) 0.48; ^{1}H NMR (400 MHz, DMSO-d_6) δ 8.35 (dd, *J* = 8.4, 1.0 Hz, 1H, H^1), 8.00 (dd, *J* = 8.3, 1.1 Hz, 1H, H^4), 7.82 (d, *J* = 8.1 Hz, 2H, H^{10}), 7.71 (ddd, *J* = 8.3, 7.1, 1.0 Hz, 1H, H^3), 7.63 (d, *J* = 8.1 Hz, 2H, H^9), 7.55 (ddd, *J* = 8.3, 7.2, 1.2 Hz, 1H, H^2), 6.83 (s, 1H, H^5), 3.51 (s, 2H, H^8), 3.44 - 3.38 (m, 4H, H^6), 2.89 - 2.74 (m, 4H, H^7); ^{13}C NMR (101 MHz, DMSO-d_6) δ 158.0, 154.6, 147.8, 145.4, 130.7 (2C), 129.3 (2C), 128.5, 127.5, 125.8, 123.4, 122.2, 120.1, 118.9 117.0, 115.5, 113.6, 112.9, 96.1, 54.6, 50.6 (2C), 49.2 (2C); HPLC-MS (APCI/ESI): Purity = 97%, t_R = 2.904 min, *m/z* $[M+H]^+$ = 461.2.

7,8-dichloro-1-(4-cyclohexylpiperazin-1-yl)-3-(trifluoromethyl)benzo[4,5]imidazo[1,2-*a*]pyridine-4-carbonitrile (17)

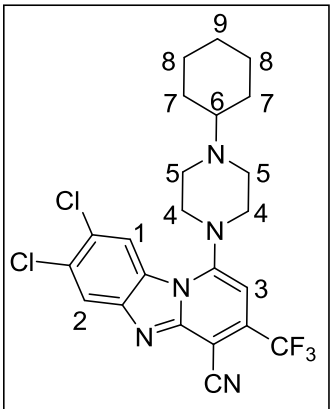

17

$C_{23}H_{22}Cl_2F_3N_5$
Exact Mass: 495.12
Mwt: 496.36

Obtained from **III-c** as a yellow solid (0.66 g, 66%); m.p. 264 – 266 °C; R_f (EtOAc: Hex, 2:3) 0.50; ^{1}H NMR (300 MHz, DMSO-d_6) δ 8.83 (s, 1H, H^1), 8.34 (s, 1H, H^2), 6.78 (s, 1H, H^3), 3.16 - 3.11 (m, 4H, H^4), 3.07 - 3.01 (m, 5H, $H^{5,6}$), 1.87 - 1.79 (m, 4H, H^7), 1.68 - 1.63 (m, 2H, H^9), 1.37 - 1.31 (m, 4H, H^8); ^{13}C NMR (101 MHz, DMSO-d_6) δ 158.2, 147.8, 145.4, 141.6, 133.0, 127.9 (2C), 120.8, 118.0 (2C), 117.6, 114.5, 100.0, 70.0, 50.9 (2C), 48.0 (2C), 29.0 (2C), 26.3, 25.6 (2C); HPLC-MS (APCI/ESI): Purity = 96%, t_R = 3.052 min, *m/z* $[M+H]^+$ = 496.1.

7,8-dichloro-1-(4-(4-fluorobenzyl)piperazin-1-yl)-3-propylbenzo[4,5]imidazo[1,2-*a*]pyridine-4-carbonitrile (18)

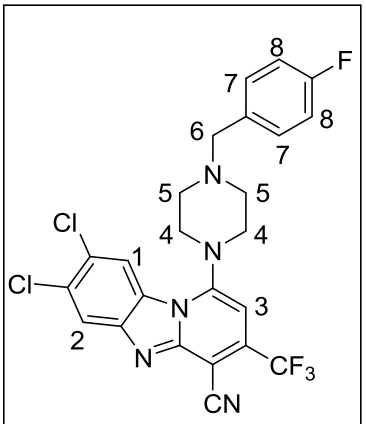

18

$C_{24}H_{17}Cl_2F_4N_5$

Exact Mass: 521.08

Mwt: 522.33

Obtained from **III-c** as a yellow solid (0.82 g, 82%); m.p. 258 – 260 °C; R_f (EtOAc: Hex, 1:1) 0.33; ^{1}H NMR (400 MHz, DMSO-d_6) δ 8.29 (s, 1H, H^1), 7.98 (s, 1H, H^2), 7.58 (dd, *J* = 8.3, 5.4 Hz, 2H, H^7), 7.26 (dd, *J* = 9.8, 8.4 Hz, 2H, H^8), 6.85 (s, 1H, H^3), 3.65 (s, 2H, H^6), 3.78 - 3.57 (m, 4H, H^4), 3.22 - 3.14 (m, 4H, H^5); ^{13}C NMR (101 MHz, DMSO-d_6) δ 159.8, 154.2, 148.8, 146.3, 143.8, 134.5, 131.2, 128.9 (2C), 127.3 (2C), 121.9, 120.3, 116.6, 115.6 (2C), 115.3, 113.6, 98.3, 70.2, 51.7 (2C), 46.1 (2C); HPLC-MS (APCI/ESI): Purity = 97%, t_R = 3.262 min, *m/z* $[M+H]^+$ = 522.1.

7,8-dichloro-1-(4-(3-fluorobenzyl)piperazin-1-yl)-3-(trifluoromethyl)benzo[4,5]imidazo [1,2-*a*]pyridine-4-carbonitrile (19)

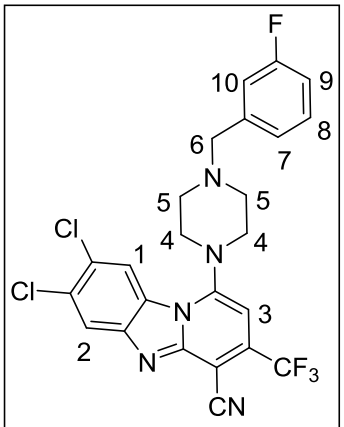

19

$C_{24}H_{17}Cl_2F_4N_5$

Exact Mass: 521.08

Mwt: 522.33

Obtained from **III-c** as a yellow solid (0.72 g, 72%); m.p. 277 – 279 °C; R_f (EtOAc: Hex, 2:3) 0.50; ^{1}H NMR (300 MHz, DMSO-d_6) δ 8.38 (s, 1H, H^1), 8.02 (s, 1H, H^2), 7.58 - 7.52 (m, 2H, $H^{9,10}$), 7.28 - 7.19 (m, 2H, $H^{7,8}$), 6.78 (s, 1H, H^3), 3.72 (s, 2H, H^6), 3.71 - 3.58 (m, 4H, H^4), 3.15 - 3.03 (m, 4H, H^5); ^{13}C NMR (101 MHz, DMSO-d_6) δ 159.5, 154.7, 148.5, 146.0, 143.9, 134.5, 131.2, 128.1, 127.7, 126.9, 122.0 (2C), 120.3, 119.6, 116.7 (2C), 115.1, 112.7, 98.3, 60.9, 52.7 (2C), 45.6 (2C); HPLC-MS (APCI/ESI): Purity = 97%, t_R = 3.415 min, *m/z* $[M+H]^+$ = 522.1.

7,8-dichloro-1-(4-(2-fluorobenzyl)piperazin-1-yl)-3-(trifluoromethyl)benzo[4,5]imidazo [1,2-*a*]pyridine-4-carbonitrile (20)

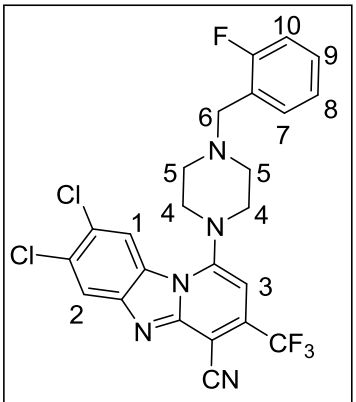

20
$C_{24}H_{17}Cl_2F_4N_5$
Exact Mass: 521.08
Mwt: 522.33

Obtained from **III-c** as a yellow solid (0.93 g, 93%); m.p. 256 – 258 °C; R_f (EtOAc: Hex, 2:3) 0.50; ^{1}H NMR (400 MHz, DMSO-d_6) δ 8.35 (s, 1H, H^1), 8.27 (s, 1H, H^2), 7.58 - 7.33 (m, 2H, $H^{9,10}$), 7.18 (m, 2H, $H^{7,8}$), 6.87 (s, 1H, H^3), 3.82 (s, 2H, H^6), 3.78 - 3.61 (m, 4H, H^4), 3.29 - 3.18 (m, 4H, H^5); ^{13}C NMR (101 MHz, DMSO-d_6) δ 159.6, 154.1, 149.0, 146.8, 142.9, 133.5, 130.9, 129.1, 126.9 (2C), 122.0 (2C), 120.3, 119.6, 116.7, 115.9, 115.1, 112.7, 98.3, 60.9, 52.7 (2C), 45.6 (2C); HPLC-MS (APCI/ESI): Purity = 97%, t_R = 3.347 min, *m/z* $[M+H]^+$ = 522.1.

1-(4-phenylpiperazin-1-yl)-3-(trifluoromethyl)benzo[4,5]imidazo[1,2-*a*]pyridine-4-carbonitrile (21)

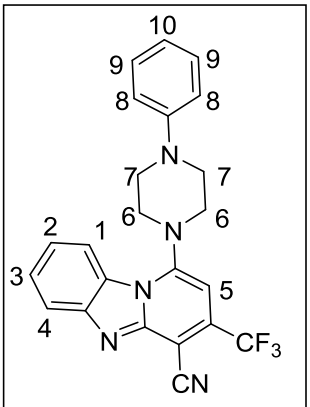

21
$C_{23}H_{18}F_3N_5$
Exact Mass: 421.15
Mwt: 421.43

Obtained from **III-a** as a yellow solid (0.93 g, 93%); m.p. 271 – 273 °C; R_f (EtOAc: Hex, 2:3) 0.47; ^{1}H NMR (400 MHz, DMSO-d_6) δ 8.29 (dd, *J* = 8.2 Hz, 1.0Hz, 1H, H^1), 7.97 (dd, *J* = 8.3, 1.1 Hz, 1H, H^4), 7.67 (ddd, *J* = 8.2, 7.2, 1.0 Hz, 1H, H^3), 7.54 (ddd, *J* = 8.1, 7.1, 1.0 Hz, 1H, H^2), 7.42 - 7.35 (m, 2H, H^8), 7.22 - 7.14 (m, 3H, $H^{9,10}$), 6.77 (s, 1H, H^5), 3.09 - 3.02 (m, 4H, H^6), 2.67 - 2.52 (m, 4H, H^7); ^{13}C NMR (101 MHz, DMSO-d_6) δ 157.2, 148.8, 145.6, 138.7, 137.6, 135.0, 129.9, 128.1 (2C), 127.4, 123.9 (2C), 120.9, 119.6, 117.3 (2C), 114.6, 112.4, 98.1, 52.6 (2C), 50.7 (2C); HPLC-MS (APCI/ESI): Purity = 98%, t_R = 3.179 min, *m/z* $[M+H]^+$ = 422.2.

1-(4-(4-(methylsulfonyl)phenyl)piperazin-1-yl)-3-(trifluoromethyl)benzo[4,5]imidazo[1,2-*a*]pyridine-4-carbonitrile (22)

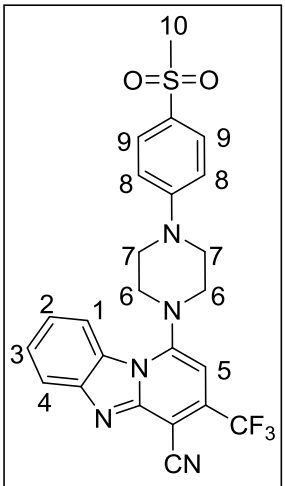

22

$C_{24}H_{20}F_3N_5O_2S$

Exact Mass: 499.13

Mwt: 499.51

Obtained from **III-a** as a yellow solid (0.88 g, 88%); m.p. 260 – 262 °C; R_f (MeOH: DCM, 0.5:9.5) 0.45; ^{1}H NMR (400 MHz, DMSO-d_6) δ 8.44 (dd, *J* = 8.5, 1.0 Hz, 1H, H^1), 8.01 (dd, *J* = 8.4, 1.1 Hz, 1H, H^4), 7.69 (ddd, *J* = 8.4, 7.2, 1.0 Hz, 1H, H^3), 7.56 (ddd, *J* = 8.6, 7.1, 1.4 Hz, 1H, H^2), 7.21 (d, *J* = 8.0 Hz, 2H, H^8), 7.04 (d, *J* = 8.1 Hz, 2H, H^9), 6.90 (s, 1H, H^5), 3.42 - 3.36 (m, 4H, H^7), 3.26 (s, 3H, H^{10}), 3.12 - 3.04 (m, 4H, H^6); ^{13}C NMR (101 MHz, DMSO-d_6) δ 157.9, 149.6, 145.9, 138.9, 137.2, 135.6, 130.7, 128.4 (2C), 127.1, 123.6 (2C), 120.3, 119.5, 117.2 (2C), 115.1, 113.4, 97.9, 52.7 (2C), 51.1 (2C), 49.1; HPLC-MS (APCI/ESI): Purity = 98%, t_R = 2.911 min, *m/z* $[M+H]^+$ = 500.1.

1-(4-(pyridin-2-yl)piperazin-1-yl)-3-(trifluoromethyl)benzo[4,5]imidazo[1,2-*a*]pyridine-4-carbonitrile (23)

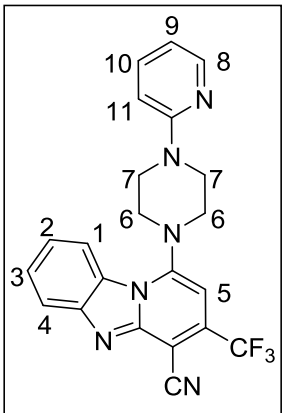

23

$C_{22}H_{17}F_3N_6$

Exact Mass: 422.15

Mwt: 422.42

Obtained from **III-a** as a yellow solid (0.91 g, 91%); m.p. 275 – 277 °C; R_f (EtOAc: Hex, 1:1) 0.32; ^{1}H NMR (400 MHz, DMSO-d_6) δ 8.45 (dd, *J* = 8.4, 1.0 Hz, 1H, H^1), 8.18 (dd, *J* = 8.1, 1.1 Hz, 1H, H^8), 8.01 (dd, *J* = 8.5, 1.1 Hz, 1H, H^4), 7.70 (ddd, *J* = 8.0, 7.2, 1.1 Hz, 1H, H^{10}), 7.61 (ddd, *J* = 8.3, 7.1, 1.0 Hz, 1H, H^3), 7.55 (ddd, *J* = 8.6, 7.1, 1.4 Hz, 1H, H^2), 6.99 (ddd, *J* = 8.1, 7.1, 1.2 Hz, 1H, H^9), 6.92 (dd, *J* = 8.0, 1.2 Hz, 1H, H^{11}), 6.89 (s, 1H, H^5), 3.47 - 3.40 (m, 4H, H^7), 3.22 - 3.18 (m, 4H, H^6); ^{13}C NMR (101 MHz, DMSO-d_6) δ 159.9, 157.7, 150.6, 147.6, 145.8, 138.6, 135.7, 131.1, 129.1, 127.6, 123.1 (2C), 121.2, 119.9, 117.4, 115.2, 105.8, 98.8, 52.8 (2C), 51.2 (2C); HPLC-MS (APCI/ESI): Purity = 97%, t_R = 2.916 min, *m/z* $[M+H]^+$ = 423.2.

1-(4-(pyridin-4-yl)piperazin-1-yl)-3-(trifluoromethyl)benzo[4,5]imidazo[1,2-*a*]pyridine-4-carbonitrile (24)

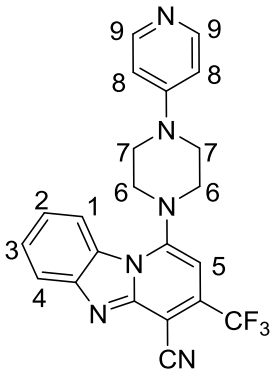

24

$C_{22}H_{17}F_3N_6$
Exact Mass: 422.15
Mwt: 422.42

Obtained from **III-a** as a yellow solid (0.90 g, 90%); m.p. 274 – 276 °C; R_f (EtOAc: Hex, 2:3) 0.50; ^{1}H NMR (400 MHz, DMSO-d_6) δ 8.45 (dd, *J* = 8.5, 1.0 Hz, 1H, H^1), 8.32 (d, *J* = 8.2 Hz, 2H, H^9), 8.01 (dd, *J* = 8.2, 1.0 Hz, 1H, H^4), 7.71 (ddd, *J* = 8.3, 7.1, 1.0 Hz, 1H, H^3), 7.56 (ddd, *J* = 8.4, 7.1, 1.2 Hz, 1H, H^2), 7.17 (d, *J* = 8.4 Hz, 2H, H^8), 6.92 (s, 1H, H^5), 3.69 - 3.65 (m, 4H, H^7), 3.19 - 3.14 (m, 4H, H^6); ^{13}C NMR (101 MHz, DMSO-d_6) δ 159.6, 157.5, 151.6 (2C), 147.6, 145.8, 136.4, 131.7, 129.1, 127.2, 123.8 (2C), 121.3, 119.4, 116.8, 105.8 (2C), 98.8, 52.8 (2C), 51.2 (2C); HPLC-MS (APCI/ESI): Purity = 97%, t_R = 2.588 min, *m/z* $[M+H]^+$ = 423.2.

1-(4-(pyrazin-2-yl)piperazin-1-yl)-3-(trifluoromethyl)benzo[4,5]imidazo[1,2-*a*]pyridine-4-carbonitrile (25)

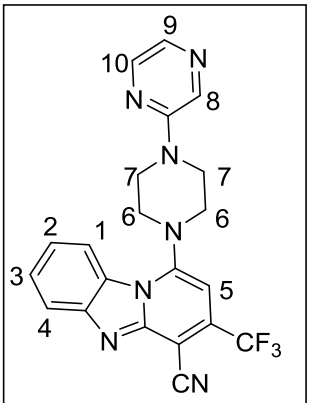

25

$C_{21}H_{16}F_3N_7$
Exact Mass: 423.14
Mwt: 423.40

Obtained from **III-a** as a yellow solid (0.63 g, 63%); m.p. 256 – 258 °C; R_f (EtOAc: Hex, 2:3) 0.50; ^{1}H NMR (600 MHz, DMSO-d_6) δ 8.39 (dd, *J* = 8.3, 1.0 Hz, 1H, H^1), 8.18 (d, *J* = 8.0 Hz, 1H, H^{10}), 8.14 - 8.11 (m, 2H, $H^{8,9}$), 8.01 (dd, *J* = 8.3, 1.1 Hz, 1H, H^4), 7.94 (ddd, *J* = 8.3, 7.1, 1.0 Hz, 1H, H^3), 7.70 (ddd, *J* = 8.2, 7.1, 1.0 Hz, 1H, H^2), 6.94 (s, 1H, H^5), 3.69 - 3.58 (m, 4H, H^7), 3.18 - 3.08 (m, 4H, H^6); ^{13}C NMR (151 MHz, DMSO-d_6) δ 159.6, 157.5, 151.6, 147.6, 145.8, 136.4, 134.8, 132.1, 130.7, 128.9, 126.8, 122.9 (2C), 121.4, 117.1, 113.8, 98.6, 52.8 (2C), 51.6 (2C); HPLC-MS (APCI/ESI): Purity = 98%, t_R = 3.008 min, *m/z* $[M+H]^+$ = 424.1.

1-(3-oxopiperazin-1-yl)-3-(trifluoromethyl)benzo[4,5]imidazo[1,2-*a*]pyridine-4-carbonitrile (26)

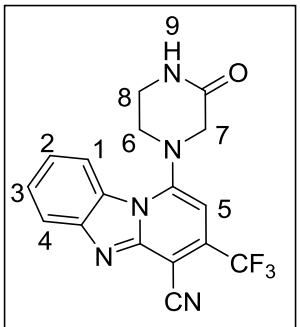

26

$C_{17}H_{12}F_3N_5O$
Exact Mass: 359.10
Mwt: 359.31

Obtained from **III-a** as a yellow solid (0.79 g, 79%); m.p. 263 – 265 °C; R_f (MeOH: DCM, 0.5:9.5) 0.45; ^{1}H NMR (300 MHz, DMSO-d_6) δ 8.30 (dd, *J* = 8.3, 1.0 Hz, 1H, H^1), 8.18 (dd, *J* = 8.2, 1.1 Hz, 1H, H^4), 7.69 (ddd, *J* = 8.3, 7.1, 1.1 Hz, 1H, H^3), 7.54 (ddd, *J* = 8.4, 7.1, 1.2 Hz, 1H, H^2), 6.83 (s, 1H, H^5), 4.08 (s, 2H, H^7), 3.33 - 3.27 (m, 2H, H^8), 3.16 - 3.09 (m, 2H, H^6). ^{13}C NMR (101 MHz, DMSO-d_6) δ 158.8, 155.9, 147.7, 144.9, 128.9, 126.8, 123.1 (2C), 122.2, 119.7, 115.7, 113.3, 112.1, 98.0, 58.7, 56.8, 39.6; HPLC-MS (APCI/ESI): Purity = 98%, t_R = 2.588 min, *m/z* $[M+H]^+$ = 360.1.

1-(4-(4-chlorophenyl)piperazin-1-yl)-3-(trifluoromethyl)benzo[4,5]imidazo[1,2-*a*]pyridine-4-carbonitrile (27)

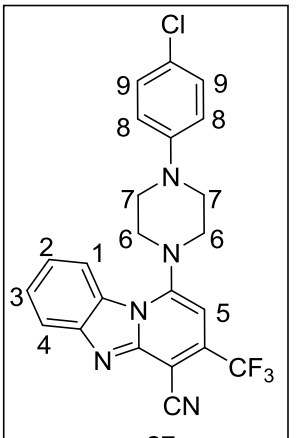

27

$C_{23}H_{17}ClF_3N_5$
Exact Mass: 455.11
Mwt: 455.87

Obtained from **III-a** as a yellow solid (0.77 g, 77%); m.p. 265 – 267 °C; R_f (EtOAc: Hex, 2:3) 0.44; ^{1}H NMR (600 MHz, DMSO-d_6) δ 8.41 (dd, *J* = 8.4, 1.0 Hz, 1H, H^1), 8.01 (dd, *J* = 8.3, 1.1 Hz, 1H, H^4), 7.69 (ddd, *J* = 8.2, 7.0, 1.0 Hz, 1H, H^3), 7.56 (ddd, *J* = 8.4, 7.0, 1.2 Hz, 1H, H^2), 7.25 (d, *J* = 8.0 Hz, 2H, H^9), 7.07 (d, *J* = 8.1 Hz, 2H, H^8), 6.93 (s, 1H, H^5), 3.19 - 3.14 (m, 4H, H^7), 3.06 - 3.02 (m, 4H, H^6); ^{13}C NMR (151 MHz, DMSO-d_6) δ 156.9, 149.6, 147.1, 144.9, 141.2, 135.9, 128.7 (2C), 125.1, 123.8 (2C), 120.6, 119.4, 117.2, 115.5(2C), 114.6, 112.4, 97.9, 51.6 (2C), 49.1 (2C); HPLC-MS (APCI/ESI): Purity = 98%, t_R = 3.375 min, *m/z* $[M+H]^+$ = 456.1.

3-(trifluoromethyl)-1-(4-(5-(trifluoromethyl)pyridin-2-yl)piperazin-1-yl)benzo[4,5]imidazo [1,2-a]pyridine-4-carbonitrile (28)

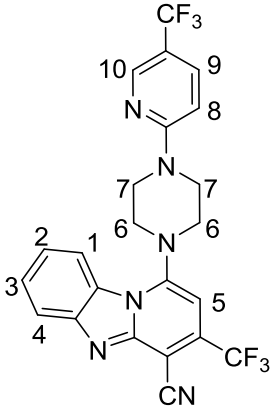

28

$C_{23}H_{16}F_6N_6$
Exact Mass: 490.13
Mwt: 490.41

Obtained from **III-a** as a yellow solid (0.65 g, 65%); m.p. 266 – 268 °C; R_f (EtOAc: Hex, 2:3) 0.43; ^{1}H NMR (400 MHz, DMSO-d_6) δ 8.50 (s, 1H, H^{10}), 8.46 (dd, *J* = 8.4, 1.0 Hz, 1H, H^1), 8.02 (d, *J* = 8.0 Hz, 1H, H^9), 7.89 (dd, *J* = 8.3, 1.1 Hz, 1H, H^4), 7.70 (ddd, *J* = 8.3, 7.1, 1.1 Hz, 1H, H^3), 7.56 (ddd, *J* = 8.4, 7.1, 1.2 Hz, 1H, H^2), 7.05 (d, *J* = 8.1 Hz, 1H, H^8), 6.94 (s, 1H, H^5), 3.28 - 3.25 (m, 4H, H^7), 3.22 - 3.16 (m, 4H, H^6); ^{13}C NMR (101 MHz, DMSO-d_6) δ 157.6, 154.6, 149.6, 145.8, 139.4, 137.4, 133.7, 128.4, 125.1, 123.2 (2C), 121.0, 120.4, 119.3, 117.8, 115.6, 113.8, 110.8, 98.8, 51.3 (2C), 50.1 (2C); HPLC-MS (APCI/ESI): Purity = 98%, t_R = 3.227 min, *m/z* $[M+H]^+$ = 491.1.

1-(4-(2,4-difluorophenyl)piperazin-1-yl)-3-(trifluoromethyl)benzo[4,5]imidazo[1,2-*a*]pyridine-4-carbonitrile (29)

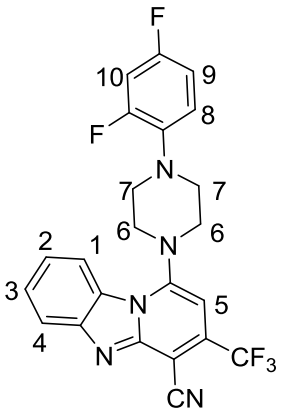

29

$C_{23}H_{16}F_5N_5$
Exact Mass: 457.13
Mwt: 457.41

Obtained from **III-a** as a yellow solid (0.84g, 84%); m.p. 270 – 272 °C; R_f (EtOAc: Hex, 2:3) 0.48; ^{1}H NMR (400 MHz, DMSO-d_6) δ 8.43 (dd, *J* = 8.4, 1.0 Hz, 1H, H^1), 8.02 (dd, *J* = 8.2, 1.0 Hz, 1H, H^4), 7.70 (ddd, *J* = 8.3, 7.1, 1.0 Hz, 1H, H^3), 7.60 (ddd, *J* = 8.4, 7.1, 1.1 Hz, 1H, H^2), 7.32 - 7.24 (m, 2H, $H^{8,9}$), 7.09 – 7.04 (m, 1H, H^{10}), 6.97 (s, 1H, H^5), 3.65 - 3.57 (m, 4H, H^7), 3.15 - 3.07 (m, 4H, H^6); ^{13}C NMR (101 MHz, DMSO-d_6) δ 158.9, 152.6, 150.5, 145.1, 144.6, 141.4, 136.7, 129.9, 123.8 (2C), 122.1, 121.3, 119.4, 117.1, 116.8, 113.5, 111.9, 105.8, 98.8, 52.8 (2C), 51.2 (2C); HPLC-MS (APCI/ESI): Purity = 98%, t_R = 3.188 min, *m/z* $[M+H]^+$ = 458.1.

1-(4-(1-methylpiperidin-4-yl)piperazin-1-yl)-3-(trifluoromethyl)benzo[4,5]imidazo[1,2-*a*]pyridine-4-carbonitrile (30)

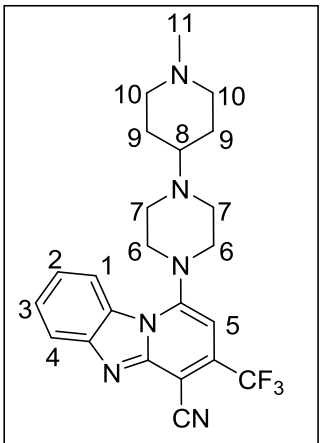

30

$C_{23}H_{25}F_3N_6$
Exact Mass: 442.21
Mwt: 442.49

Obtained from **III-a** as a yellow solid (0.67 g, 67%); m.p. 265 – 267 °C; R_f (EtOAc: Hex, 1:1) 0.28; ^{1}H NMR (400 MHz, DMSO-d_6) δ 8.31 (dd, *J* = 8.4, 1.0 Hz, 1H, H^1), 7.99 (dd, *J* = 8.2, 1.0 Hz, 1H, H^4), 7.72 (ddd, *J* = 8.3, 7.2, 1.1 Hz, 1H, H^3), 7.55 (ddd, *J* = 8.4, 7.1, 1.2 Hz, 1H, H^2), 6.84 (s, 1H, H^5), 3.26 - 3.19 (m, 4H, H^6), 3.16 - 3.11 (m, 1H, H^8), 3.07 - 3.01 (m, 4H, H^7), 2.76 - 2.62 (m, 4H, H^{10}), 2.34 (s, 3H, H^{11}), 1.74 - 1.65 (m, 4H, H^9); ^{13}C NMR (101 MHz, DMSO-d_6) δ 158.2, 149.7, 146.4, 138.8, 130.0, 123.9 (2C), 121.5, 120.8, 119.9, 116.6, 113.5, 100.7, 75.0, 53.9 (2C), 51.5 (2C), 48.9 (2C), 43.5, 29.1 (2C); HPLC-MS (APCI/ESI): Purity = 98%, t_R = 2.512 min, *m/z* $[M+H]^+$ = 443.2.

7,9-dichloro-1-(4-cyclohexylpiperazin-1-yl)-3-(trifluoromethyl)benzo[4,5]imidazo[1,2-*a*]pyridine-4-carbonitrile (31)

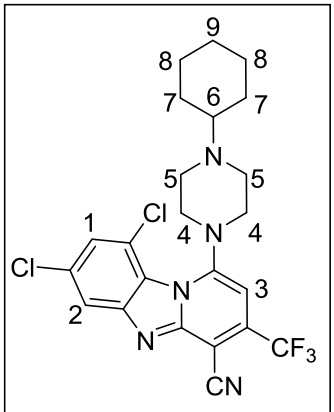

31

$C_{23}H_{22}Cl_2F_3N_5$
Exact Mass: 495.12
Mwt: 496.36

Obtained from **III-b** as a yellow solid (0.91 g, 91%); m.p. 269 – 271 °C; R_f (EtOAc: Hex, 2:3) 0.40; ^{1}H NMR (400 MHz, DMSO-d_6) δ 8.23 (d, *J* = 2.1 Hz, 1H, H^2), 7.96 (d, *J* = 2.0 Hz, 1H, H^1), 6.98 (s, 1H, H^3), 3.24 - 3.17 (m, 4H, H^4), 3.07 - 3.01 (m, 5H, $H^{5,6}$), 1.92 - 1.84 (m, 4H, H^7), 1.65 - 1.57 (m, 2H, H^9), 1.38 - 1.31 (m, 4H, H^8); ^{13}C NMR (101 MHz, DMSO-d_6) δ 157.8 148.4, 146.5, 142.6, 133.0, 127.9, 124.0, 122.8, 121.2, 119.0, 117.6, 114.5, 100.0, 63.0, 50.9 (2C), 48.0 (2C), 29.0(2C), 26.3, 25.6 (2C); HPLC-MS (APCI/ESI): Purity = 98%, t_R = 3.204 min, *m/z* $[M+H]^+$ = 496.1.

7,9-dichloro-1-(4-((5-fluoropyridin-2-yl)methyl)piperazin-1-yl)-3-(trifluoromethyl)benzo [4,5]imidazo[1,2-*a*]pyridine-4-carbonitrile (32)

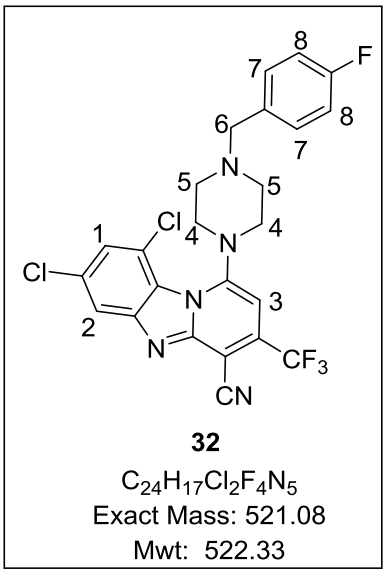

32

$C_{24}H_{17}Cl_2F_4N_5$

Exact Mass: 521.08

Mwt: 522.33

Obtained from **III-b** as a yellow solid (0.76 g, 76%); m.p. 273 – 275 °C; R_f (EtOAc: Hex, 2:3) 0.44; ^{1}H NMR (400 MHz, DMSO-d_6) δ 8.23 (d, *J* = 2.1 Hz, 1H, H^2), 7.92 (d, *J* = 2.1 Hz, 1H, H^1), 7.61 (dd, *J* = 8.6, 5.3 Hz, 2H, H^7), 7.23 (dd, *J* = 9.8, 8.6 Hz, 2H, H^8), 6.85 (s, 1H, H^3), 3.63 (s, 2H, H^6), 3.54 - 3.47 (m, 4H, H^4), 2.78 - 2.72 (m, 4H, H^5). Yellow solid (0.82 g, 82%); ^{13}C NMR (101 MHz, DMSO-d_6) δ 158.9, 154.6, 148.4, 145.7, 144.1, 135.5, 132.2, 129.9, 128.1, 127.3 (2C), 122.9, 120.3, 116.6, 115.8 (2C), 115.5, 113.1, 98.8, 61.4, 51.6 (2C), 46.5 (2C); HPLC-MS (APCI/ESI): Purity = 98%, t_R = 3.498 min, *m/z* $[M+H]^+$ = 522.0.

1-(4-cyclohexylpiperazin-1-yl)-7,8-difluoro-3-(trifluoromethyl)benzo[4,5]imidazo[1,2-*a*]pyridine-4-carbonitrile (33)

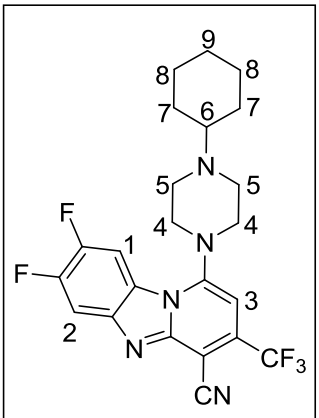

33

$C_{23}H_{22}F_5N_5$

Exact Mass: 463.18

Mwt: 463.46

Obtained from **III-d** as a yellow solid (0.74 g, 74%); m.p. 254 – 256 °C; R_f (EtOAc: Hex, 2:3) 0.33; ^{1}H NMR (400 MHz, DMSO-d_6) δ 8.49 (dd, *J* = 11.0, 7.4 Hz, 1H, H^1), 7.70 (dd, *J* = 10.8, 7.2 Hz, 1H, H^2), 6.71 (s, 1H, H^3), 3.77 - 3.56 (m, 4H, H^4), 3.31 - 3.24 (m, 5H, $H^{5,6}$), 1.94 - 1.88 (m, 4H, H^7), 1.67 - 1.56 (m, 2H, H^9), 1.33 - 1.20 (m, 4H, H^8); ^{13}C NMR (101 MHz, DMSO-d_6) δ 158.2, 147.8 (2C), 145.4, 141.6, 136.0, 131.9, 121.8, 119.0, 117.6, 107.7 (2C), 98.8, 69.0, 50.6 (2C), 48.5 (2C), 29.0 (2C), 26.3, 25.6 (2C); HPLC-MS (APCI/ESI): Purity = 98%, t_R = 2.946 min, *m/z* $[M+H]^+$ = 464.2.

7,8-difluoro-1-(4-(4-fluorobenzyl)piperazin-1-yl)-3-propylbenzo[4,5]imidazo[1,2-*a*]pyridine-4-carbonitrile (34)

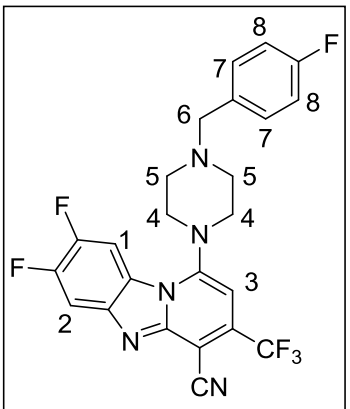

34

$C_{24}H_{17}F_6N_5$
Exact Mass: 489.14
Mwt: 489.43

Obtained from **III-d** as a yellow solid (0.73 g, 73%); m.p. 274 – 276 °C; R_f (EtOAc: Hex, 2:3) 0.40; ^{1}H NMR (400 MHz DMSO-d_6) δ 8.48 (dd, *J* = 10.8, 7.4 Hz, 1H, H^1), 7.78 (dd, *J* = 10.8, 7.3 Hz, 1H, H^2), 7.57 (dd, *J* = 8.5, 5.3 Hz, 2H, H^7), 7.28 (dd, *J* = 10.0, 8.5 Hz, 2H, H^8), 6.65 (s, 1H, H^3), 3.65 (s, 2H, H^6), 3.84 - 3.76 (m, 4H, H^4), 3.62 - 3.39 (m, 4H, H^5); ^{13}C NMR (101 MHz, DMSO-d_6) δ 159.9, 155.2, 145.8 (2C), 146.3, 143.8, 134.5, 131.2, 128.9, 127.9 (2C), 120.3, 116.6, 115.7 (2C), 113.6, 105.6 (2C), 98.1, 67.8, 51.9 (2C), 47.7 (2C); HPLC-MS (APCI/ESI): Purity = 98%, t_R = 2.904 min, *m/z* $[M+H]^+$ = 490.1.

Methyl 4-((4-(4-cyano-3-(trifluoromethyl)benzo[4,5]imidazo[1,2-*a*]pyridin-1-yl)piperazin-1-yl)methyl)benzoate (35)

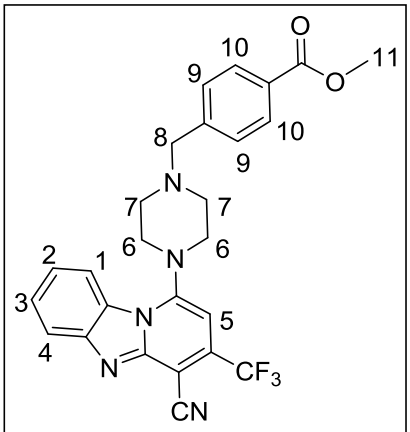

35

$C_{26}H_{22}F_3N_5O_2$
Exact Mass: 493.17
Mwt: 493.49

Obtained from **III-a** as a yellow solid (0.60 g, 60%); m.p. 265 – 267 °C; R_f (EtOAc: Hex, 2:3) 0.40; ^{1}H NMR (400 MHz, DMSO-d_6) δ 8.54 (dd, *J* = 8.3, 1.0 Hz, 1H, H^1), 8.34 (d, *J* = 8.2 Hz, 2H, H^{10}), 7.98 (dd, *J* = 8.2, 1.1 Hz, 1H, H^4), 7.90 (ddd, *J* = 8.3, 7.1, 1.1 Hz, 1H, H^3), 7.68 (ddd, *J* = 8.3, 7.2, 1.4 Hz, 1H, H^2), 7.55 (d, *J* = 8.1 Hz, 2H, H^9), 6.86 (s, 1H, H^5), 3.87 (s, 3H, H^{11}), 3.77 (s, 2H, H^8), 3.29 - 3.19 (m, 4H, H^6), 3.16 - 2.94 (m, 4H, H^7); ^{13}C NMR (101 MHz, DMSO-d_6) δ 159.7, 157.2, 146.8, 145.3, 143.6, 140.1, 138.3, 134.5 (2C), 131.9 (2C), 128.1 (2C), 127.8, 124.6, 121.2, 119.6, 116.6, 113.6, 98.3, 64.2, 55.5 (2C), 51.2, 49.9 (2C); HPLC-MS (APCI/ESI): Purity = 97%, t_R = 2.985 min, *m/z* $[M+H]^+$ = 494.1.

1-(4-(4-(methylsulfonyl)benzyl)piperazin-1-yl)-3-(trifluoromethyl)benzo[4,5]imidazo[1,2-*a*]pyridine-4-carbonitrile (36)

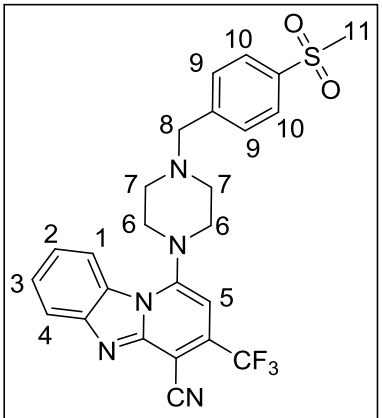

36

$C_{25}H_{22}F_3N_5O_2S$

Exact Mass: 513.14

Mwt: 513.54

Obtained from **III-a** as a yellow solid (0.73 g, 73%); m.p. 260 – 262 °C; R_f (EtOAc: Hex, 2:3) 0.40; ^{1}H NMR (400 MHz, DMSO-d_6) δ 8.35 (dd, *J* = 8.3, 1.0 Hz, 1H, H^1), 8.00 (dd, *J* = 8.2, 1.1 Hz, 1H, H^4), 7.90 (d, *J* = 8.2 Hz, 2H, H^{10}), 7.70 (d, *J* = 8.1 Hz, 2H, H^9), 7.65 (ddd, *J* = 8.3, 7.1, 1.0 Hz, 1H, H^3), 7.54 (ddd, *J* = 8.3, 7.2, 1.4 Hz, 1H, H^2), 6.86 (s, 1H, H^5), 3.56 (s, 2H, H^8), 3.42 - 3.36 (m, 4H, H^7), 3.20 (s, 3H, H^{11}), 3.12 - 2.97 (m, 4H, H^6); ^{13}C NMR (101 MHz, DMSO-d_6) δ 156.7, 145.6, 142.9, 139.9, 138.3, 135.6, 130.7, 128.4(2C), 127.1, 123.6 (2C), 120.3, 119.5, 117.2 (2C), 115.1, 113.4, 97.9, 66.5, 53.9 (2C), 48.2 (2C), 47.8; HPLC-MS (APCI/ESI): Purity = 98%, t_R = 2.990 min, *m/z* $[M+H]^+$ = 514.1.

6.2.3 Pharmacological Activity

6.2.3.1 *In vitro* Antiplasmodium activity

The test samples were tested in triplicate on one occasion against chloroquine-sensitive NF54 strain of *Plasmodium falciparum*. Continuous *in vitro* cultures of asexual erythrocyte stages of *P. falciparum* were maintained using a modified version of the Trager and Jensen method.[1] Quantitative assessment of antiplasmodium activity *in vitro* was determined using the parasite lactate dehydrogenase assay.[2] The test samples were prepared to a 20 mg/ml stock solution in 100% DMSO. Samples were tested as suspensions if not completely dissolved. Stock solutions were stored at -20 °C pending further dilution on the day of the experiment. Chloroquine (CQ) and artesunate served as reference drugs in all experiments. A full dose-response was performed for all test compounds to determine the concentration inhibiting 50% of parasite growth to give the IC_{50} value. Test compounds were initially tested at a concentration of 100 µg/ml, which was then serially diluted 2-fold to give 10 concentrations; 0.2 µg/ml being the lowest one. The same dilution technique was used for all samples. Reference drugs were tested at a starting concentration of 1000 ng/ml. The highest concentration of solvent to which the parasites were exposed had no measurable effect on parasite viability. The IC_{50} values were obtained using a non-linear dose-response curve fitting analysis using GraphPad Prism v.4.0 software.

6.2.3.2 *In vitro* Antischistosomal activity

6.2.3.2.1 Screening on Newly Transformed Schistosomula (NTS)

S. mansoni cercariae were mechanically transformed to NTS.[3] Snails were exposed to light to encourage cercarial shedding and the cercarial suspension was then collected. The cercariae were rinsed (x 3) with cold HBSS to detach the tails from the heads. The NTS were incubated overnight in culture medium and employed the following day. The test compounds and controls were dissolved in DMSO to a concentration of 10 mM. One hundred NTS were incubated in a 96-well plate with culture medium and the test compound to make up a final well volume of 250 µL. The culture medium was comprised of a mixture of medium 199 supplemented with 5% fetal calf serum and 1% penicillin/streptomycin. The

test compounds were assessed in triplicate at a concentration of 10 µM with NTS incubated in ≤ 1% DMSO serving as a control. The NTS were incubated at 37 °C and 5% CO_2 for up to 72 h. Thereafter, the effects of the compounds on NTS were evaluated microscopically using a scale from 3 (normal activity and morphological alteration) to 0 (dead).

6.2.3.2.2 Adult *S. mansoni* Worms

The adult schistosomes were obtained by subcutaneously infecting mice with 80−100 cercariae. After 7 – 8 weeks, mice were euthanized with CO_2 and the worms collected from the hepatic portal and mesenteric veins. In each well of the 24-well plate comprised of two pairs of adult worms incubated with 2 mL culture medium and the test compound. The culture medium was made up of RPMI 1640 supplemented with 5% fetal calf serum and a 1% penicillin/streptomycin mixture. Test compounds with > 70% activity against NTS were tested against adult worms at 10 µM with incubation at < 1% DMSO used as a control. The worms were incubated at 37 °C and 5% CO_2 for up to 72 h. Thereafter, the effects of the compounds on adult worms were evaluated microscopically using a scale from 3 (normal activity and morphological alteration) to 0 (dead).

6.2.3.3 Gametocytocidal Activity

The luciferase reporter assay was employed for accurate, reliable and quantifiable evaluation of the stage-specific action of gametocytocidal compounds against both the early and late gametocyte marker cell line NF54-PfS16-GFP-Luc. Drug assays were carried out on day 5 and 10 (representing > 90% of either early stage I/II/III or mature stage IV/V gametocytes, respectively). In each case, assays were set up using a 2 to 3% gametocytaemia, 1.5% haematocrit culture and 48 h drug pressure in a gas chamber (90% N_2, 5% O_2, and 5% CO_2) at 37 °C. Luciferase activity was determined in 30 µl parasite lysates by adding 30 µl luciferin substrate (Promega Luciferase Assay System) at room temperature and detection of resultant bioluminescence at an integration constant of 10 s with the GloMax® Explorer Detection System with Instinct® Software. Methylene blue and MMV390048 are the controls whose % inhibitions of gametocyte viability were assessed at 1 µM.

6.2.4 β-Hematin inhibition activity

Stock solutions of controls and test compounds were prepared using DMSO to make up 20 mM. A solution composed of water/305.5 µM NP40/DMSO at a v/v ratio of 70%/20%/10%, respectively was added to every well in columns 1-11 while 140 µL of water and 40 µL of 305.5 µM NP40 were added to column 12 to mediate the formation of β-haematin. 20 µL of the 20 mM test compounds were added to column 12 and 100 µL of this solution was serially diluted to column 2, with column 1 left as a blank (0 µM of compound). Hematin suspension was prepared by adding 178.8 µL aliquot of hematin stock to 20 ml of 1 M acetate buffer, pH 4.9 and 100 µL of the suspension was added into each well. 36

Plates were then incubated for ±5 h at 37 °C after which 32 µL of pyridine solution (20% water, 20% acetone, 10% 2M HEPES buffer (pH 7.4), 50% pyridine) was added. A volume of 60 µL of acetone was added to all the wells, plates were read at 405 nm and IC50 values were plotted using GraphPad.

6.2.5 Turbidimetric Solubility

Target compounds were dissolved in appropriate volumes of DMSO to make 10 mM stock solutions. Serial dilutions were then prepared on 96-well plates from a concentration range of 0.25 mM to 10 mM, with a blank well of 0 mM included as a reference. This was repeated three times for each sample on the pre-dilution plate. From each pre-dilution well, secondary dilutions of the samples in DMSO and 0.01 M phosphate-buffered saline (PBS, pH 7.4) were then prepared on a second 96-well plate, the turbidimetric assay plate. This plate set up was also done in triplicate. The samples on the turbidimetric plate were prepared such that the final sample concentrations ranged from 0 to 200 µM.

The turbidimetric assay plate was incubated for 2 h at room temperature. After incubation, absorbance at 620 nm was determined using a SpectraMax 340 PC384 microplate reader. Absorbance from the wells containing 100% DMSO and 2% v/v PBS in DMSO were blank readings. The absorbance versus concentration curves were plotted giving the solubility of the different test compounds. This is evident on the graph where the PBS curve deviates from the DMSO curve (baseline) due to an increase in absorbance readings.

6.3 References

(1) Trager, W.; Jensen, J. B. Human Malaria Parasites in Continuous Culture. *Science* **1976**, *193* (4254), 673-675.

(2) Makler, M. T.; Ries, J. M.; Williams, J. A.; Bancroft, J. E.; Piper, R. C.; Gibbins, B. L.; Hinrichs, D. J. Parasite Lactate Dehydrogenase as an Assay for Plasmodium Falciparum Drug Sensitivity. *Am. J. Trop. Med. Hyg.* **1993**, *48* (6), 739-741.

(3) Manneck, T.; Haggenmüller, Y.; Keiser, J. Morphological Effects and Tegumental Alterations Induced by Mefloquine on Schistosomula and Adult Flukes of Schistosoma Mansoni. *Parasitology* **2010**, *137* (1), 85−98.